Electrochemical Energy Production Using Fuel Cell Technologies

Viola Birss, Ehab El Sawy, Sanaz Ketabi, Parastoo Keyvanfar, Xiaoan Li, and Jason Young

Abstract

Fuel cells are highly efficient and environmentally friendly energy conversion devices that are receiving increasing attention and are steadily moving toward commercialization. Fuel cells deliver electricity and heat, based on the spontaneous electrochemical oxidation of fuels at the anode and the reduction of oxygen at the cathode, without combustion. In many ways, fuel cells are similar to batteries, although they do not require recharging and operate as long as fuel continues to be provided. There are four leading types of fuels reviewed in this chapter, proton exchange membrane fuel cells (PEMFCs) operating on clean hydrogen, direct alcohol (primarily methanol) fuel cells (DAFCs), solid oxide fuel cells (SOFCs), and molten carbonate fuel cells (MCFCs). PEMFCs and DAFCs normally operate at below 100 °C and are targeted primarily for transportation and mobile applications, while SOFCs and MCFCs, which run at temperatures above 600 °C, can run on a wide variety of fuels and are intended mostly for stationary combined heat and power applications. This review is focused primarily on a description of each of these technologies, with an emphasis on the materials used in the electrodes, the electrolyte that separates them, and the current collectors.

Keywords

Proton exchange membrane fuel cells • Direct alcohol fuel cells • Methanol fuel cells • Ethanol fuel cells • Solid oxide fuel cells • Molten carbonate fuel cells • Fuel oxidation • Oxidation • Reduction • Carbon • Ceramics • Molten salts • Electrochemistry • Electrodes • Electrolytes • Efficiency • Oxygen reduction • Catalyst • Electrocatalyst

V. Birss (✉) • E. El Sawy • S. Ketabi • P. Keyvanfar
X. Li • J. Young
Department of Chemistry, University of Calgary,
Calgary, AB, Canada T2N 1N4
e-mail: birss@ucalgary.ca

J.A. Kent et al. (eds.), *Handbook of Industrial Chemistry and Biotechnology*,
DOI 10.1007/978-3-319-52287-6_32

Introduction to Fuel Cells

Fuel cells are clean and highly efficient devices that can convert the chemical energy of fuels, such as methane, alcohols, diesel, syngas, and H_2, and oxidants such as air (or oxygen), directly into electrical energy, without combustion (burning). In addition to their very high efficiency (fuel cells are not limited by the Carnot cycle, but rather involve direct electricity production without combustion, with their efficiency defined as $\Delta G_{rx}/\Delta H_{rx}$) [1, 2], these devices are environmentally friendly in terms of pollutant emissions, with no NO_x or particulates released and only small amounts of SO_x produced under some circumstances. As increasing energy demand is one of the world's major concerns, fuel cell technology represents a safe, highly efficient, and green energy source that is a good replacement for combustion-based technologies.

Fuel cells convert chemical energy to electricity through electrochemical processes, very similar to what occurs in a battery. In both cases, an oxidation process occurs at the anode, a reduction reaction takes place at the cathode, the electron(s) move through an external circuit from anode to cathode, and the electrolyte between the anode and cathode transports a specific ion from one electrode to the other to balance the charge. In a battery, these reactions occur until all of the electrochemically active materials at the electrodes are consumed, and the battery then needs recharging, a process that can take a significant period of time. In contrast, in a fuel cell, the reactants at both electrodes (fuels at the anode and oxygen at the cathode) are continuously supplied, and thus the fuel cell will continue to operate as long as the fuel (at the anode) and the oxidant (at the cathode) are present, similar to how energy is supplied in our existing combustion-based infrastructure.

There are some common requirements in all fuel cells. First, the electrolyte must be dense to minimize fuel or oxygen crossover to the opposite electrode, electron-blocking, so that electrons move only through the external circuit, ion conducting, and unreactive with the electrodes. In contrast, the electrodes must be porous to ensure a high active surface area and to expedite the transport of fuel and air to the reaction sites and remove the reaction products away from them, electrocatalytic toward the reactions of interest, and chemically stable under either fuel or air conditions and when in contact with the electrolyte. A key overarching driver is that these critical components of all fuel cells must be as low in cost and as durable as possible.

The performance of all fuel cells is commonly described by a plot of cell voltage (V) vs. cell current (I), as shown in Fig. 1, with the product, $V \times I$, being the fuel cell power, which can range from mW to MW. The cell voltage under equilibrium (no current flowing) is often termed the open circuit voltage (OCV) of the equilibrium voltage, obtained using the Nernst equation for the full fuel cell reaction. Once current begins to flow, various processes cause a loss of voltage, which ultimately results in a maximum in the power delivered at a particular combination of V and I (Fig. 1).

All electrodes suffer from activation losses, which are related to the intrinsic kinetics of the fuel oxidation and oxygen reduction reactions and defined by the activation energy barrier and the reaction mechanisms [1, 2]. The more catalytic the electrodes are and the higher their real surface areas, the lower the activation losses will

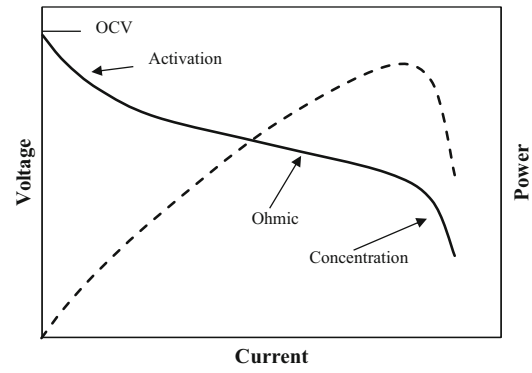

Fig. 1 Fuel cell performance plot, showing the three sources of losses and the resulting power plot (voltage: *solid line*; power, *dashed line*)

be. At low currents, activation losses will dominate the fuel cell power output, although reaction kinetics will contribute to the cell performance at all currents. It will be shown in the sections below that significant research has been undertaken to identify the best catalysts for fuel oxidation and oxygen reduction, with oxygen reduction normally being the more sluggish process. Also, major efforts have been made to increase the dispersion of electrocatalysts to ensure the maximum active surface area.

All cells also suffer from ohmic losses, arising from the resistance of the electrolyte (separator), related to its intrinsic ionic conductivity and thickness, as well as from the resistance of electrode contacts and interfaces within the cell. Thus, efforts have been focused on identifying new electrolytes with higher ionic conductivities and on improved current collectors that do not form an oxide at the interface with the electrodes. Higher temperatures normally serve to lower the ohmic losses.

Finally, at high current densities, all fuel cells can suffer from transport losses, termed "concentration overpotentials" or "concentration losses." This is due to limitations in the mass transport of oxygen, most typically, or fuel to the active sites, products away from the electrodes, or ion transport within the electrode structure. Once again, higher temperatures and concentrations of the reactants serve to increase the limiting currents and thus minimize concentration or diffusion losses in operating fuel cells.

In order to produce high power outputs, single cells are connected in series with each other to construct fuel cell stacks. The current collection from each cell is achieved by using carbon or metallic current collectors at both sides of the cell, known as interconnects, bipolar plates, or current collectors.

In order to maximize fuel cell performance and its associated power output, research and development efforts have been focused heavily on minimizing the losses shown in Fig. 1. This includes the careful selection of the most catalytic electrode materials under the specific conditions of operation of the fuel cell (type of fuel, temperature, etc.) and optimizing the porosity of the electrode structures to minimize mass transport effects and to maximize active surface areas. Also, new electrolyte materials are being developed that have a high ionic conductivity to minimize ohmic losses, while nanoengineering is being utilized to make electrolyte layers as thin as possible and yet durable. Therefore, this review is focused primarily on recent developments in the fuel cell material area.

Fuel cells are commonly divided into five different categories, based on the identity of the electrolyte. These are polymer electrolyte (sometimes referred to as proton exchange) membrane fuel cells (PEMFCs), solid oxide fuel cells (SOFCs), molten carbonate fuel cells (MCFCs), phosphoric acid fuel cells (PAFCs), and alkaline fuel cells (AFCs). However, PAFCs and AFCs are not presently being commercially developed, and thus they are not included in the present review. Furthermore, PEMFCs can be subdivided into H_2-fueled PEMFCs and those operated on alcohols (methanol, ethanol), which are called direct alcohol fuel cells (DAFCs), systems that are actively being researched and developed. For this reason, this review is focused only on PEMFCs operated on H_2 fuels (section "H_2-Fueled Polymer Electrolyte Membrane Fuel Cells (PEMFCs)"), DAFCs (section "Proton Exchange Membrane-Based Direct Alcohol Fuel Cells (PEM-DAFCs)"), SOFCs (section "Solid Oxide Fuel Cells (SOFCs)"), and MCFCs (section "Molten Carbonate Fuel Cells").

H_2-Fueled Polymer Electrolyte Membrane Fuel Cells (PEMFCs)

Introduction

Polymer electrolyte membrane fuel cells (PEMFCs) are also known as proton exchange membrane fuel cells, devices that run at 60–100 °C and are able to convert the chemical energy of H_2 and O_2 to electricity with electrical efficiencies up to 60% in practice. H_2 is used as the fuel for PEMFCs because of its high energy

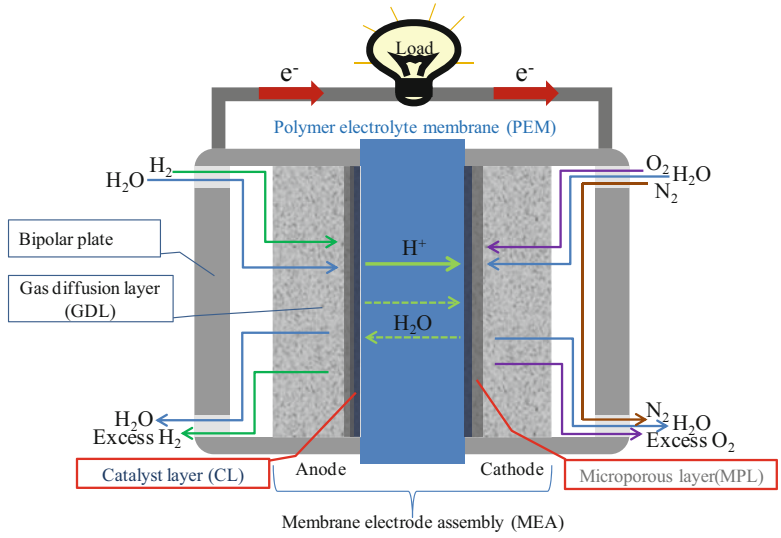

Fig. 2 Cross section of an H_2–air polymer electrolyte membrane fuel cell (PEMFC), labelling each component on the anode side (the same layers are present at the cathode)

density of 33 kWh/kg and also as hydrocarbon fuels are not suitable for PEMFCs. Further, the product of a conventional PEMFC, running on H_2 and air, is environmentally friendly, being water, which can also be regenerated in an electrolysis cell, running on renewable energy.

Similar to all fuel cells and as shown in Fig. 2, a typical state-of-the-art PEMFC consists of three layers, two catalyst layers (CLs), and a polymer electrolyte membrane (PEM) separator, which separates the two CLs. On the other side, each CL is attached to a microporous layer (MPL) which is connected to a gas diffusion layer (GDL) and then to a bipolar plate (bipolar plates are used when multiple single fuel cells are stacked in series). Without including the flow/bipolar plates, these components (PEM, CLs, MPLs, and GDLs) are collectively referred to as the membrane electrode assembly (MEA), which is the core component of a PEMFC (Fig. 2). During operation, humidified H_2 flows through the channels of the bipolar plate, diffusing through the anode GDL and MPL and then the anode catalyst layer (ACL), while humidified O_2 or air flows through the GDL and MPL at the cathode side and then into the cathode catalyst layer (CCL).

At the anode catalyst layer (ACL), hydrogen is oxidized, according to the electrochemical half reaction (1):

$$2H_2 \rightarrow 4H^+ + 4e^- \quad E^0 = 0V \qquad (1)$$

The generated protons (hydrated) are transported through the electrolyte membrane to the cathode catalyst layer (CCL), where they react with oxygen (Fig. 2) and the electrons released by reaction (1) (and passed through the external circuit) to form water, as shown in Reaction (2):

$$O_2 + 4H^+ + 4e^- \rightarrow 2H_2O \quad E^0 = 1.23V \qquad (2)$$

When H_2 and O_2 are consumed in a PEMFC, electrical power, heat, and pure water are generated, with the overall reaction given in Reaction (3):

$$2H_2 + O_2 \rightarrow 2H_2O \qquad (3)$$

The H_2O formed at the cathode is removed either via the cathode flow channels by excess O_2 or air, or through the PEM (Nafion) membrane to the anode side, and is then carried out of the cell by the excess H_2 flow (Fig. 2).

Polymer Electrolyte Membrane Separator

Nafion®

Various polymer electrolyte materials have been developed for PEMFCs to satisfy the need for both high ionic conductivity and chemical and electrochemical stability under PEMFC operating conditions [3]. The separator must also serve as a pinhole-free gas separator between the anode and cathode, preventing the mixing of the fuel and oxidant.

The most common material used in PEMFCs today is poly(perfluorosulfonic acid) (PFSA), which exhibits very high proton conductivity. Nafion® is the most commonly known commercial brand, with its molecule structure shown in Scheme 1. Nafion ionomers were developed by the E. I. du Pont Company, with Nafion 117 referring to a polymer film having an equivalent weight of 1100 and a nominal thickness of 0.007 in. (0.178 mm). Nafion is also a critical component in both the anode and cathode CLs, where it is mixed with the carbon-supported catalytic Pt nanoparticles in order to facilitate proton transport to/from the catalytic sites [4–9]. The cost of the Nafion membrane is estimated as being 11% of the total cost of PEMFC stack for the production of 500,000 systems/year [10].

Nafion consists of a polytetrafluoroethylene (PTFE) backbone with attached sulfonic acid functional groups (Scheme 1), giving it both hydrophilic and hydrophobic characteristics. The Teflon backbone also provides mechanical strength, while the sulfonic acid ($SO_3^-H^+$) chains provide charged sites for proton transport.

Proton transport in Nafion can take place by the Grotthus (i.e., hopping of protons via the water network) and vehicle (i.e., diffusion of H_3O^+ ions through the Nafion structure) mechanisms [11, 12]. It is generally believed that the probability of proton hopping in Nafion is higher when it is hydrated. The water in the swollen state is assumed to be more bulk like, and therefore H-bond breaking and formation between sulfonic groups and water can take place. However, with low water content, proton transport relies on the motion of water as well as the polymer side chain motion [13]. Thus, to maintain the high proton conductivity of Nafion, it must be fully hydrated with liquid water.

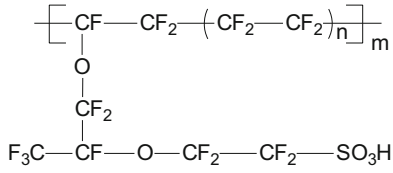

Scheme 1 Molecular structure of Nafion

The water content in Nafion, λ, is defined as the ratio of the number of water molecules absorbed to the number of charged sites ($SO_3^-H^+$). Based on experimental results, λ can vary from almost 0 (completely dehydrated Nafion) to 22 (full saturation under certain conditions) [13, 14]. Therefore, the water content in the membrane can be estimated by knowing the humidity conditions within the fuel. In general, the proton conductivity of Nafion follows a linear trend with water content and increases exponentially with temperature. Figure 3 shows the relationship between the ionic conductivity and the Nafion water content, showing that the proton conductivity of Nafion (up to ~0.1 S/cm) is highly dependent on water content (the relative humidity of the operating PEMFC) [2].

Since Nafion is the best candidate for PEMFCs, it is necessary to understand its

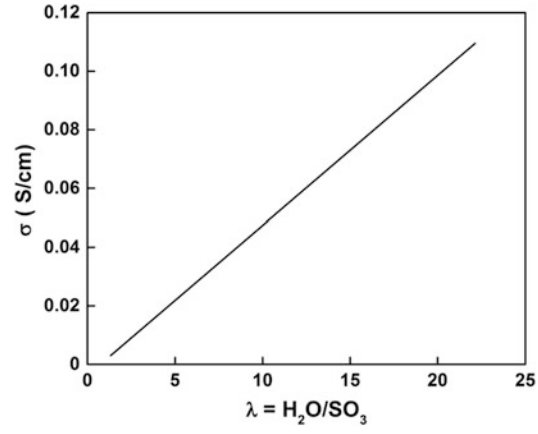

Fig. 3 Experimental data for ionic conductivity of Nafion vs. water content at 303 K [2]. Reprinted with permission of John Wiley and Sons

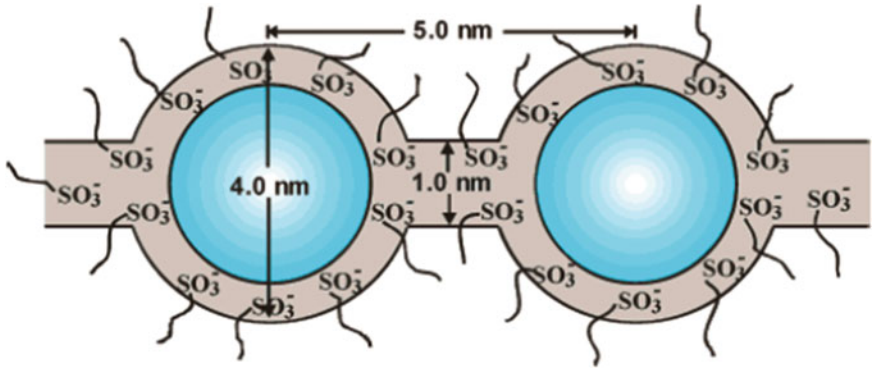

Fig. 4 Cluster-network model for the Nafion structure in hydrated state [15]. Reprinted with permission from Elsevier

morphology and structure in order to modify it for optimum performance. While there are many studies on characterizing the morphology of Nafion, a universal structure for Nafion has not yet been reported. This is due to the unique random chemical structure of this ionomer that is capable of organizing into ionic and crystalline domains with significant spatial distribution. Among the early concepts on the morphology of Nafion was the work of Gierke et al. [15] using small-angle X-ray scattering (SAXS) and wide-angle X-ray diffraction (WAXD). Based on their findings, the morphology of Nafion in the hydrated state is described by a cluster-network model, including ionic clusters that are approximately spherical in shape with a diameter of 4 nm. These ionic clusters are interconnected by narrow channels with a diameter of 1 nm, as shown in Fig. 4 [15–17].

Many other models have been proposed in the literature to describe the morphology of Nafion [18–23], with most agreeing that ionic groups form clusters in the polymer network that allow for significant swelling and efficient ion transport. However, further studies have suggested that structural reorganization occurs during swelling in order to keep constant the specific surface (area of polymer–water interface per polar head) with increasing cluster size [24].

As Nafion is one of the key components of the CLs, its morphology in the CLs, the thickness of Nafion covering the electrode material, and the optimum concentration for enhancing the ionic conductivity are critical factors to CL performance. The hydrophilic/hydrophobic characteristics of Nafion likely produce different adsorption modes and coverages of the catalyst particles under different operating conditions in PEMFCs [25]. PEM/catalyst interfaces were experimentally monitored using idealized layers of Nafion on glassy carbon and Pt surfaces [26], showing the presence of discrete hydrophobic and hydrophilic regions within the Nafion layer. Nafion's hydrophobic regions were shown to be preferentially oriented toward Pt, and a three-layer Nafion structure was observed in contact with glassy carbon. Since the nanostructure of the Nafion ionomer in the CL can differ from that in the bulk membrane, the proton conduction mechanism may also be different [27].

DuPont's Nafion® is the industry standard material for forming the ion permeable membranes used in PEMFCs. The description of the manufacturing process is based on patents and publicly available information [28]. The non-reinforced Nafion membranes are produced by extrusion cast and dispersion cast methods. The extrusion cast membranes are melt extruded from perfluorosulfonyl fluoride resins, followed by hydrolysis and acid exchange steps. Dispersion-cast films are formed directly from solutions of Nafion in water and alcohol by a coating process onto an inert PTFE backing film. These membranes are known to be the new generation products, formed at lower processing costs. The dispersion is casted on a polymer belt from which the film can be easily released (e.g., PTFE). The film is formed by

evaporating the liquid dispersion medium in two steps, heating at a temperature below the coalescence temperature, i.e., less than 100 °C, and then curing by heating to above the coalescence temperature [28].

Nafion is also a key component of the CLs in PEMFCs, serving to extend the region of proton transfer beyond the CL/Nafion separator interface. Nafion dispersions are available from both DuPont and Ion Power. The dispersions consist of PFSA polymer, water, and low-molecular weight alcohols. DuPont's product line includes 5, 10, and 20% PFSA with 34–90% water and 1–50% volatile organic compounds (VOCs) by weight (5 and 15% dispersions, by weight, are available from Ion Power). These PFSA solutions are typically further diluted and mixed with carbon-supported catalyst materials for the fabrication of the PEMFC CLs.

As mentioned earlier, the proton conductivity of Nafion depends on the relative humidity. This shortcoming limits the operating temperature of PEMFCs to temperatures below 80 °C, and humidification of inlet gases is required to ensure that the membrane remains fully hydrated. On the other hand, the pores of the CLs and the GDLs, as well as gas flow channels, may be flooded by excessive liquid water (i.e., from humidification and from the electrochemical production of water at the cathode), resulting in a higher mass transport resistance. Therefore, optimization of water management is essential to maintain a balance between membrane drying and water flooding to prevent fuel cell degradation [29].

The chemical degradation of Nafion under PEMFC-operating conditions is another problem, related to the formation of hydrogen peroxide during oxygen reduction, which can then generate active radicals ($OH^{\bullet}$, $OOH^{\bullet}$) in the presence of contaminating metal cations (e.g., Fe^{2+}, Pt^{2+}) [30]. A study of Nafion degradation under normal fuel cell conditions [31] showed that H_2O_2 exposure results in cleavage of the sulfonic groups from the side chain and may also crosslink the sulfonic sites on the side chains (S–O–S bond, SO_2–O–SO_2, and/or SO_2F) in the Nafion structure. In agreement with other studies, the exposure of Nafion to H_2O_2 may lower the H-bond strength between water molecules, water uptake [32], and conductivity of Nafion membranes. Metal cations, which are attracted to the sulfonic sites in the Nafion polymer and decrease its proton conductivity, can be generated from low concentrations of impurities in the gas stream or during cell preparation. The ionomer in the membrane separator appears to be more prone to degradation than the Nafion in the anode and cathode catalyst layers, initiating problems at the membrane–electrolyte interface [33, 34].

In recent years, chemically modified membranes have been developed by DuPont, which show lowered fluoride release rates and longer accelerated lifetimes [30]. In these modified polymers, the number of reactive end groups has been reduced by an alternative synthesis route. Also, it is reported that non-sulfonated aromatic membranes, such as polyether ether ketone (PEEK), are less prone to chemical attack by radicals, compared to sulfonated compounds [35].

During the MEA manufacturing process, pinholes and foreign materials can be introduced into the Nafion membrane, which can initiate cracks and lead to significantly reduced lifetimes [36]. Under operating conditions, nonuniform contact pressure [36], high differential initial gas pressure over the membrane, punctures, and fatigue from stresses occurring during temperature and humidity cycling [37, 38] can all lead to mechanical failure of the membrane.

While Nafion membranes meet the mechanical stability requirements in a PEMFC, a well-controlled manufacturing process is necessary, especially when using very thin membranes (25 μm). Reinforcement of the membrane with materials such as porous polyethylene or PTFE [38, 39] has been done to enhance the dimensional stability and lower the shrinkage stress in Nafion membranes during drying.

Some H_2 can diffuse through the Nafion membrane to the cathode, where it can be oxidized, releasing protons that are transported back to the anode, where they can be reduced to H_2. This current is directly proportional to the crossover

rate of H_2 through the membrane. For a Nafion 112 membrane (50 μm), a crossover current of 1 mA cm^{-2} at atmospheric conditions is reported for the beginning of life, corresponding to 2.6×10^{-13} mol H_2 cm^{-1} kPa^{-1} s^{-1}. End-of-life conditions are considered to correspond with values in the order of 13 mA cm^{-2} bar^{-1} [40]. The permeability of membranes for oxygen is usually half of the hydrogen permeability [36, 41].

Alternative Polymer Electrolytes

To overcome some of the limitations of Nafion, other commercially available perfluorinated sulfonic acid (PFSA) materials have also sometimes been used, such as Flemion® and Aciplex®. In addition, a number of new proton-conducting polymer electrolytes are being developed, e.g., sulfonated PEEK, sulfonated polyimide [42], and metal–organic framework materials [43], such as Na_3(2,4,6-trihydroxy-1,3,5-benzenetrisulfonate) [44], LaH_5(1,2,4,5-tetrakisphosphonomethylbenzene)$(H_2O)_4$ and $[Na_3$(2,4,6-trihydroxy-1,3,5-trisulfonate benzene)$]_{0.66}[Na_3$(1,3,5-benzenetriphosphonate)$]_{0.34}\cdot 0.75H_2O$ [43].

PFSA membranes similar to Nafion, but with modified and shorter chain lengths, have been developed for higher temperature PEMFC applications. Their improved performance is attributed to an increased crystallinity and a higher glass transition temperature [45, 46]. To allow higher temperature operation, sulfonated hydrocarbon polymers have been studied, including PEEK, an aromatic semicrystalline polymer with high thermal and chemical stability and good electrical and mechanical properties [47, 48].

Polybenzimidazole (PBI) has received much attention due to its ability to serve as a proton exchange membrane and as a host in phosphoric acid [49, 50]. Direct copolymerization of sulfonated monomers has been used to synthesize sulfonated PBIs, and a relatively high conductivity of 0.037 S cm^{-1} at 170 °C and 0% RH, and promising single-cell performance, was achieved [51].

Azole-containing and azole-functionalized polymer systems are another category of anhydrous proton-conducting membranes [52], while amphoteric nitrogen-containing heterocyclic structures, which can serve as a solvent for protons, were introduced by Kreuer [11, 53]. These proton solvents have been combined with acidic polymers to fabricate thin films, serving as a source of protons. Various types of azole-based polymer systems have also been developed, with a proton conductivity that depends on temperature and doping ratio [54–57]. To avoid leaching of the dopant out of the polymer membrane under operating conditions, these heterocycles have been immobilized in the polymeric network. As the azole groups are attached to the polymer chains, the flexibility and polymer chain movement become important factors in controlling proton conduction.

Modifying polymer membranes with materials that can increase thermal stability is another attractive approach being used. Composite membranes are prepared by incorporating filler materials into the polymer network [58]. These fillers can improve the water uptake and retention, leading to reasonable conductivity at high temperature and low humidification. Inorganic fillers, such as hygroscopic oxides (SiO_2, TiO_2, ZrO_2, Al_2O_3) [58, 59], clays (montmorillonite) [60], zeolites [61], and mineral acids (HCl, H_3PO_4) [58], have been used in these types of polymeric electrolytes. Recently, Nafion, doped with sulfonic acid-functionalized graphene oxide, has been shown to exhibit enhanced proton conductivity at 120 °C and 30% RH [62].

Despite these many efforts, however, none of these ionomeric materials have shown better cumulative properties as yet than Nafion. Thus, Nafion is still the leading material of use as separators and as the ionically conducting phase in the catalyst layers within PEMFCs.

Catalysts Used in PEMFC Anodes and Cathodes

In terms of large-scale commercialization of PEMFCs, the manufacturing of catalysts at high production rates, with high quality, and at low cost is a key consideration [63]. However, at both the anode and cathode, platinum (Pt), which is very costly, is still the material used to catalyze

the redox reactions (Reactions (1) and (2)) [64]. In order to decrease the cost and to increase its utilization, Pt is normally in the form of nanoparticles (2–6 nm, having a high mass-specific catalytic surface area), deposited on a carbon support, which has a relatively low cost as well as a high electronic conductivity, surface area, and porosity.

While hydrogen oxidation (HOR, Reaction (2)) at Pt is a very rapid process, the catalytic activity of Pt toward the oxygen reduction reaction (ORR, Reaction (2)) is still quite sluggish ($\sim 10^{-6}$ lower reaction rate) [64, 65]. Pt-based alloys, such as PtNi, PtCo, and PtCoMn, have been developed to improve the ORR activity by up to ten times higher in some cases [63, 64, 66]. The catalytic activity of Pt-based alloys is also dependent on the structure and/or morphology of the alloy nanoparticles. For example, core-shell nanoparticles are very promising, with the non-Pt metal normally going into the core, which influences the catalytic activity of the surrounding thin Pt shell in three possible ways, electronically, through strain effects, and via bifunctional mechanisms [63]. However, the dissolution (leaching) of the less noble metal from the core of these nanoparticles can deteriorate the performance of the fuel cell. Prior to loading into a PEMFC, de-alloying (or leaching) and/or annealing of the particles has been shown to be a successful approach to further enhancing both the activity and stability of Pt-alloy catalysts [63, 64, 67].

Challenges involved in the development and commercialization of high-performance PEMFCs include the need to lower the manufacturing costs and enhance the long-term durability [68–75]. In a PEMFC (Fig. 2), the Pt catalyst, used at both electrodes, is much more costly than all of the other components. Therefore, it is essential to cut down the usage of Pt in the CLs while also maintaining high power density, with the goal being to lower the Pt loading to 0.15 mg/cm^2 of the MEA and also simultaneously increase its power density to 0.8–0.9 W/cm^2 at a cell voltage of $\geq$0.65 V [76]. The US Department of Energy (DOE) has established technical targets for 2017 for the lowering of the total Pt group metal (PGM) loading to 0.125 mg_{PGM}/cm^2 of the MEA in PEMFCs or 0.125 g_{PGM}/kW (the same as the 2020 targets [77]), a significant decrease over current Pt loadings of 0.4–1.0 mg/cm^2 [78]. These targets can be realized by enhancing the utilization of the Pt-active surface area at high current densities.

The use of non-noble metal catalysts is also being developed in order to reduce the cost of PEMFC manufacturing [79, 80]. Examples of these electrocatalysts include non-pyrolyzed and pyrolyzed transition metal nitrogen-containing complexes, conductive polymer-based catalysts, transition metal oxides/carbides/nitrides/oxynitrides/carbonitrides, etc. [79]. These catalysts can be carbon supported or nonsupported. Of these, carbon-supported pyrolyzed transition metal nitrogen-containing complexes have shown promising ORR catalytic activity [79]. Even so, the catalytic activity of these electrocatalysts is still lower (<1/10) than that of commercially available Pt/C catalysts, and their long-term stability is another challenging issue for implementation in PEMFCs.

Catalyst Supports for PEMFCs

Carbon Support Materials

As mentioned in section "Catalysts Used in PEMFC Anodes and Cathodes," the most typical support used for the catalyst at both the anode and cathode in PEMFCs is carbon black, with Vulcan carbon XC-72R (VC), Black Pearls BP 2000, and Ketjen Black Intl, being the most widely used [81–83], due to their low cost and high availability. Carbon blacks are normally produced by the pyrolysis of hydrocarbons and have been used almost exclusively as catalyst supports in low-temperature PEMFCs [84]. VC is a typical example of a carbon black with a relatively high surface area, but it is microporous (<2 nm pore size) in nature. Thus, the loaded Pt nanoparticles are only present on the outer surface of the VC particles (size: ~30 nm) (Fig. 5a, b), making them unstable and prone to dislodgement and agglomeration [85]. As there is likely a

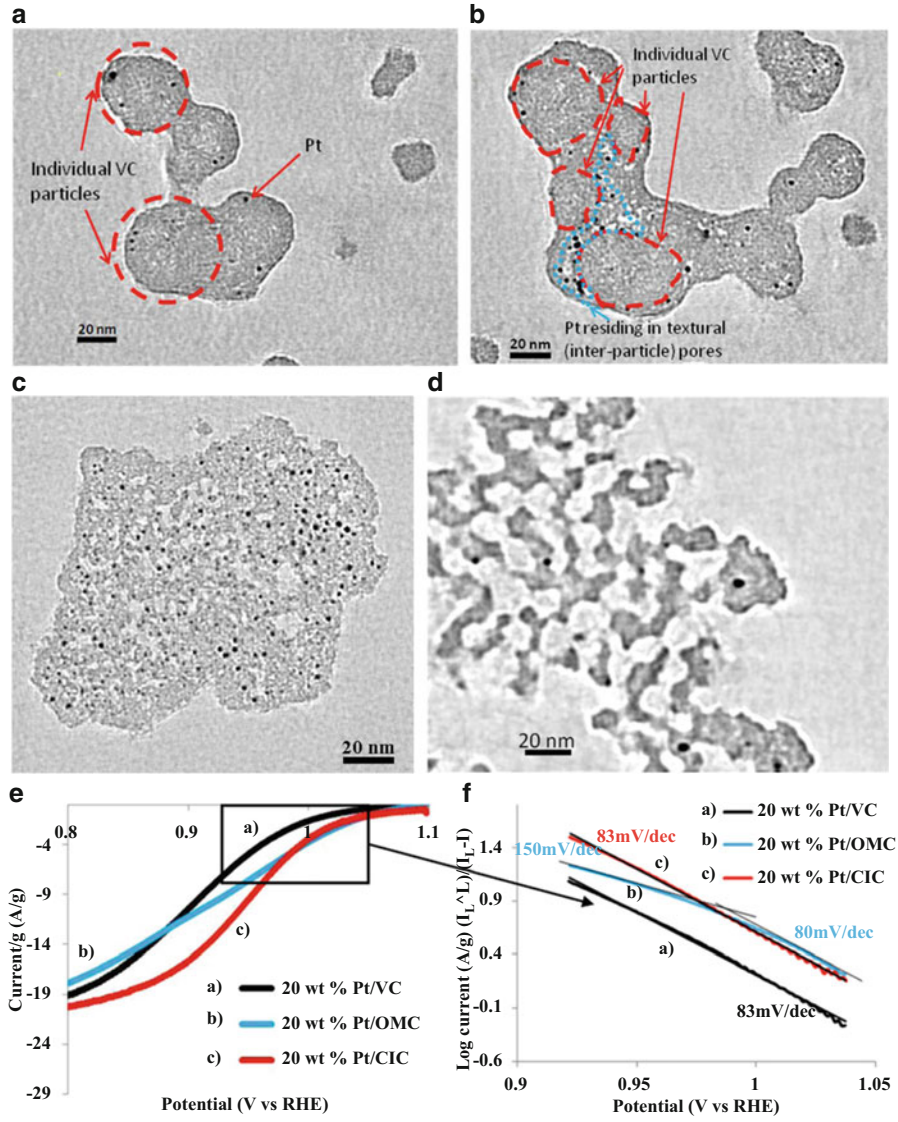

Fig. 5 Transmission electron microscopic (TEM) tomograms of 20% Pt-loaded (**a** and **b**) Vulcan carbon (VC), (**c**) ordered mesoporous carbon (OMC), and (**d**) colloid-imprinted carbon (CIC) and their (**e**) oxygen reduction activity and (**f**) Tafel plots in room temperature O_2-saturated 0.5 M H_2SO_4 at 10 mV/s and 1000 rpm. The red dash curves in (a and b) circled the cross section of individual VC particles, showing their outer surfaces reside the Pt nanoparticles, while Pt nanoparticles are well distributed in the pores of (**c**) OMC and (**d**) CIC [85]. Reprinted with permission of Elsevier

wide range of textural pores between the VC particles, any aggregation of the VC particles may bury some of the Pt nanoparticles and also block gases and protons from reaching them [86]. This will inevitably result in low utilization of the loaded Pt nanoparticles. Thus, a range of other carbon support materials have been explored.

Due to their high graphitic nature, carbon nanotubes (CNTs) are more stable and conductive than are carbon blacks. Wang et al. compared the electrochemical surface oxidation of Pt-loaded Vulcan carbon XC-72 (VC) to that of Pt-loaded multiwalled CNTs and found that CNT-supported Pt is more stable than VC-supported Pt [87]. However, due to their

nonpolar surfaces, CNTs may not be good for the binding of the Pt nanoparticles [84], leading to efforts to modify the CNT surface to improve the bonding to Pt [84] without affecting the conductivity and corrosion resistance of the CNTs [88]. In 2013, chemically modified single-wall CNTs were used to support Pt for use in both CLs of PEMFCs, resulting in a decrease in the Pt loading to 0.06 mg/cm^2 MEA, in accordance with the US DOE 2017 targets [78]. However, due to their unique shape, it may be difficult to control the nature of the pores between individual CNTs and retain optimal pathways for gas diffusion through the CLs [88].

Another class of carbon that has been investigated as a PEMFC catalyst support is ordered mesoporous carbon (OMC) [85, 86, 89, 90]. The high surface area of the OMCs promotes good dispersion of Pt nanoparticles, and the ordered mesopores (2–50 nm in size) could be a benefit electrochemically (Fig. 5c). Using hexagonal mesoporous silica (HMS) with different pore sizes, a series of OMCs with different carbon "nanostring" (wall) diameters were studied, showing that the thinner the nanostring, the poorer the ORR activity, attributed to ohmic losses [91]. At the same time, the OMC-supported catalysts (Pt/OMC) showed better ORR performance at lower overpotentials due to the smaller particle size of Pt on the OMCs, while, at higher overpotentials, the ORR performance of Pt/OMC was worse than Pt/Vulcan carbon (Fig. 5e, f), due to significant mass transport losses through the CL [85]. It was reported that OMC pores 3–8 nm in size may allow for the diffusion of reactants but restrict ionomer access to the Pt nanoparticles contained in the pores [84]. Therefore, for the use of the OMCs as catalyst supports in PEMFCs, larger pores and more conductive carbon walls would be required.

There are various methods used to fabricate mesoporous carbons [92–95], including colloid (e.g., silica) imprinting of various carbon precursors, including mesophase pitch (MP) [90, 96], followed by carbonization and then removal of the colloid. Colloid-imprinted carbons (CICs) formed in this way have a uniform pore size distribution and dense (thus very conductive) pore walls (Fig. 5d), making them promising catalyst supports [85, 90, 97, 98]. CICs with a range of pore sizes (15–80 nm) and varied pore depths have been demonstrated to be quite active for oxygen reduction in acidic solutions (e.g., Fig. 5e, f) [85, 90, 97, 98]. In addition to the high-surface area carbons discussed above, other types of carbon supports, such as carbon nanofibers [99, 100], carbon gels [84], metal oxides [100, 101], and so on [100], may be of use. Each of them has been shown to have advantages and disadvantages for PEMFC applications [84, 100, 102–104].

Other Catalyst Supports

A key problem of carbon is its propensity toward corrosion [105], which is thermodynamically feasible even at very low potentials and is thus a serious problem at the cathode, where potentials of up to 1.4 V vs. SHE can be reached [106]:

$$C + 2H_2O \; CO_2 + 4H^+ + 4e^- \quad E^0 = 0.207 \text{ V} \tag{4}$$

The corrosion of the carbon supports is believed to be accelerated in the presence of Pt and, in turn, carbon corrosion causes a loss of active Pt nanoparticle surface area, thus decreasing the ORR activity in the CCL [107]. Therefore, it is also important to enhance the corrosion resistance of the carbon supports, which can be realized by surface functionalization or doping with boron and phosphorous [108, 109], as well as by heat treatment [107, 110–112].

Because of the corrosion susceptibility of carbon supports, there is great interest in employing a range of metal oxides, which are thermodynamically more corrosion resistant than carbon samples [101]. Some of the metal oxides that are promising as catalyst supports in PEM fuel cells include titanium oxide (TiO_x), tungsten oxide (WO_x), molybdenum oxide (MoO_x), ruthenium oxide (RuO_x), tin oxide (SnO_x), cerium oxide (CeO_x), manganese oxide (MnO_x), and various mixed metal perovskite oxide (ABO_3) [101, 113, 114]. At the same time, metal oxides normally

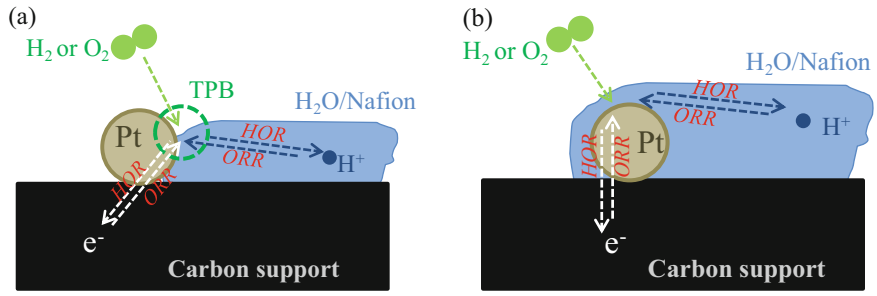

Fig. 6 (**a**) Cartoon of the triple phase boundary (TPB) and (**b**) the modified reaction zone in the catalyst layers of a PEMFC where the hydrogen oxidation reaction (HOR, Reaction (1)) and oxygen reduction reaction (ORR, Reaction (2)) occur

have a lower electric conductivity than do carbon supports. However, doping with other metal ions or generating oxygen vacancies can be used to increase the conductivity of insulating oxides, such as Ti_4O_7 (up to 1000 S/cm) and Nb-doped TiO_2 (up to 1.5 S/cm) [113].

Hybrid composites are also being considered in order to obtain property-optimized catalyst supports. For example, CeO_2 nanocubes/graphene oxide composites have been investigated as catalyst supports in PEMFCs [115], where CeO_2 serves as the radical scavenger to enhance the stability of the CLs. WO_3/VC, used as a support for Pd nanoparticles, was found to show good ORR activity [116], while ultrathin TiO_2-coated multiwalled carbon nanotubes (MWCNTs) show excellent conductivity and also enhance the ORR activity and stability of Pt nanoparticles [108].

Catalyst Layers (CLs)

The anode and cathode catalyst layers (CLs, Fig. 2) in PEMFCs contain a mixture of both the carbon-supported Pt catalyst and the electrolyte phase, typically Nafion, which is deposited on the surface of the Nafion membrane, followed by hot pressing, which allows the softened Nafion membrane surface to fuse into the CL. Notably, the specific Nafion content in the CL has a significant impact on the catalyst activity and thus on the fuel cell performance [6–9]. This is because, in a CL, the electrochemical reactions ((1) and (2)) can occur only when the gas (H_2 or O_2), liquid (water for H^+ transport), and electronically conducting and catalytic solid (e.g., Pt supported on carbon) are in direct contact, called the triple phase boundary (TPB) [6, 9, 70, 71].

As an example, Fig. 6a shows the normally accepted TPB model for a PEMFC cathode, where the TPB should be as long as possible. Figure 6b shows a schematic of the cathode CL that is probably closer to reality [117], where water or hydrated Nafion covers the hydrophilic catalyst surface. O_2, dissolved in the aqueous phase, can then reach the catalyst surface and react with the protons and electrons to form water (Reaction (2). Similarly, in the ACL, H_2 moves through the aqueous phase and reacts on the catalyst surface, forming protons, which are transferred to the cathode by the hydrated Nafion and electrons, conducted through the catalyst and carbon support to the cathode via the external circuit (Fig. 6).

In order to achieve high utilization of the Pt nanoparticles, the number of TPB sites (Fig. 6a), or reaction zones (Fig. 6b), must be maximized, realized through the high dispersion of Pt on the carbon support and of Nafion in the pores. Optimal water management is also required within the CLs, especially in the cathode CL, because too much water in the CLs could block the pathways for gases (O_2 in CCL), termed "flooding," while too little reduces the proton conductivity of Nafion. Thus, the surface wettability of the carbon supports used in PEMFC CLs is critical to all of these objectives.

Gas Diffusion Layer (GDL)

A GDL is present on each side of a single PEM fuel cell (Fig. 2). Normally, carbon fiber paper or carbon fiber cloth is used as the GDL material (Fig. 2) in order to support and protect the CL-coated membrane and to collect the electrons generated from the electrochemical reactions in each CL (Reactions (1) and (2)) [118, 119]. These carbon fiber-based materials contain pores that are tens to hundreds of micrometer-size pores, which facilitate the mass transport of humidified gases (Fig. 2) and provide good conductivity for current collection. These materials are normally treated with PTFE in order to increase their hydrophobicity, preventing water from being trapped within the pores and impeding gas transport [72, 120].

Microporous Layer (MPL)

In the last decade, a microporous layer (MPL), composed of carbon black or graphite particles and PTFE beads, has often been placed between the GDL and CL (at each electrode) in order to improve mass transport and current collection between these two layers. MPLs are also believed to play an important role in maintaining the water balance within the catalyst layers. Recent research has shown that Nafion can also be used as the binder in the MPL, replacing PTFE, resulting in improved performance [121]. In some manifestations, the MPL is considered to be part of the GDL, and thus the GDL (composed of carbon fiber paper/cloth) is sometimes called a macroporous layer to distinguish these two layers [120]. MPLs are commercially available as a component of MPL-coated GDLs.

Bipolar Plates

The bipolar plates (Fig. 2) are typically composed of polymeric graphite or a metal, e.g., stainless steel, containing flow channels to provide the desired flow field of hydrogen and air at the anode and cathode, respectively [122, 123]. The bipolar plate also functions as a current collector and provides mechanical support to the MEA. In some cases, the flow channels may not be a part of the plate. For example, a three-dimensional (3D) fine mesh, made of carbon-coated titanium, is used as airflow field at the cathode side of the PEMFCs in the Toyota Mirai [124]. This novel design promotes O_2 diffusion and distribution within the GDL and CCL, also preventing flooding problems at the cathode.

Other Cell Components

During the operation of PEMFCs, ~40% or more of the fuel energy is released in the form of heat [2]. In order to maintain the temperature of PEMFCs and prevent overheating, a cooling plate, containing channels through which a coolant flows, is often added to each cell. In most cases, the channels are integrated with one or both of the anode or cathode bipolar plates, located on the side opposite to the reactant flow channels.

Sealing materials (edge-sealing gasket), such as polytetrafluoroethylene (PTFE) and silicone rubber, are also a critical component of PEMFCs. Sealing is essential for the prevention of reactant gas leakage (e.g., fuel emitted to the air environment) and is also critical for performance stability and enhanced lifetime [105, 125].

End plates are normally used in order to hold the fuel cell assembly (Fig. 2) or a stack of fuel cells together. As is commonly seen, the plates at the two ends are held together with nuts and bolts. These end plates also contain inlets and outlets for both the oxidant (O_2 or air) and fuel, while also serving as the electrical leads needed to connect the cells to the external circuit or load.

PEMFC Full System

As is the case for all fuel cell types, a complete PEMFC system requires numerous other components or subsystems in order to continuously provide electric power. These include a

fuel/oxidant supply, cooling subsystem, power control, online monitoring, and so on. A fuel supply subsystem includes, at a minimum, the fuel (H_2) tank, a flow control meter, a humidifier, a pump to recycle the exhaust fuel from the exit of fuel cell stack, as well as a tubing to connect these components, with the same requirements for the oxidant (O_2 or air) supply subsystem. If air is used, a pump is needed to compress air to flow through a control meter, a humidifier, and then into the fuel cell stack. If self-humidification within the cells is used, the humidifiers can be removed from the system, such as in the design used in the Toyota Mirai PEMFCs [124].

The cooling subsystem normally involves at least one pump to circulate the coolant as well as a heat exchanger/radiator. The power control system includes a DC/DC converter to maintain a prescribed output voltage and/or a DC/AC inverter to transform DC to AC power, depending on the needs of the external load. The complete full cell system is normally operated using a control system, which adjusts the operating parameters in order to generate the desired power output. A control system should have three main functioning components, sensors (monitoring the conditions of fuel cells), actuators (imposing changes to the fuel cell system, e.g., switches, valves, etc.), and a central control unit that mediates between the sensors and actuators, in order to maintain the PEMFC operating in a stable mode [2].

Proton Exchange Membrane-Based Direct Alcohol Fuel Cells (PEM-DAFCs)

Although H_2 is the preferred fuel for PEMFCs, primarily because of its higher energy density (32.7 Wh/g) and the high cell voltage that can theoretically be obtained (1.23 V at 25 °C), the use of H_2 is associated with complexity in storing, handling, production, and transportation. These are some of the factors that are driving the use of other fuels [126], including organic liquid fuels (OLFs). Of these, alcohols, such as methanol and ethanol, are currently the most promising, giving rise to direct alcohol fuel cells (DAFCs). Methanol and ethanol are liquid fuels of high volumetric energy density (Fig. 7) [127] and are easy to handle and transport, especially compared to compressed gases, such as H_2 or natural gas (NG).

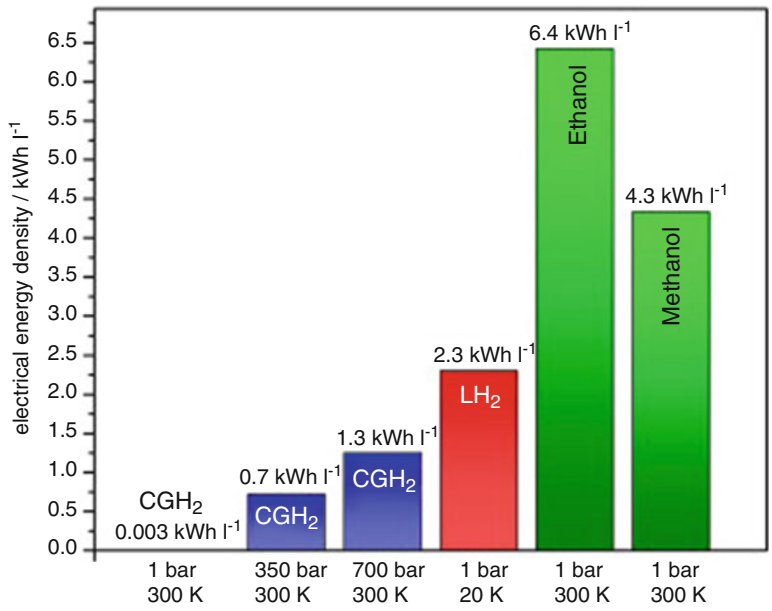

Fig. 7 Volumetric energy density in kWh/l for a range of fuels, multiplied by the thermodynamic efficiency of a fuel cell [127]. Reprinted with permission of Elsevier

Compared to gasoline or diesel, methanol and ethanol are available at a relatively non-fluctuating cost per unit of energy; they are not prone to ignition, have low volatility, and remain in the liquid state over a broad range of temperatures, from -98 to 65 °C for methanol [128, 129] and from -114 to 78 °C for ethanol [130]. Formic acid is also a promising nonflammable fuel that is miscible in water over a broad range of temperature (8–100 °C), with a high energy density (2.1 kWh L^{-1}), high theoretical cell voltage (1.48 V), and fast oxidation kinetics. A short discussion of direct formic acid fuel cells is included in section "Direct Formic Acid Fuel Cells (DFAFCs)."

Methanol can be prepared by the reduction of CO_2 or the oxidation of methane (NG). However, it is most typically obtained from fossil fuel-based syngas. It is believed that a long-range solution for efficient energy storage and overcoming global warming from the buildup of greenhouse gases could be achieved by the chemical recycling of CO_2 [128, 129, 131, 132]. In this process, H_2 obtained from water electrolysis reacts with atmospheric CO_2 that was captured in order to produce methanol. The limitation of this process is the absence of a low cost and efficient technology for atmospheric CO_2 capture. However, if methanol can be produced efficiently on a large scale during this process, it could replace oil and gas as both a fuel and as a starting material for polymers and other hydrocarbon-based products [128, 129, 131]. The conversion of NG to methanol is even more convenient in terms of fuel transportation and storage. The photocatalytic conversion of NG/CO_2 and O_2/H_2O to produce methane, methanol, and H_2 is a very promising technology that has attracted significant attention recently [131–134].

Methanol and ethanol can also be produced from renewable sources, such as biomass, although the technology associated with bioethanol production is more mature [135]. Bioethanol can be produced using sugarcane, corn, beetroot, wheat, soybean, low-grade widely available cellulose containing organic matter, woodchips, bagasse (dry pulpy residue left after the extraction of juice from sugar cane), waste from agro-industries, and organic fractions from municipal waste or forestry residues [136]. Although bioethanol can be easily produced from food crops by fermentation, the production of ethanol from non-edible lignocellulosic biomass feedstock, such as forest residues, industrial waste, and grass or trees grown specifically for this purpose, is gaining momentum [137].

Alcohol fuel can be used, either after onboard reformation or directly, in reformed alcohol fuel cells (RAFCs) or in direct alcohol fuel cells (DAFCs), respectively [138], as shown in Fig. 8. In comparison with combustion engines, onboard reformers operate at lower temperatures (250–300 °C), produce sulfur-free hydrogen with high efficiency (80–90%) [138], and have a low probability of formation of NO_x and SO_x.

In comparison with DAFCs, although RAFCs offer the use of small PEMFCs stacks that have a high efficiency and improved operation at low temperatures, they also have serious disadvantages. In RAFCs, the PEMFC stacks require a supply of H_2 with very low CO content (<20 ppm) in order to avoid poisoning of the anode catalyst. In order to purify the hydrogen, an array of fuel processors is necessary (Fig. 8) [139], which is a challenge for the production and design of a compact and user-friendly fuel cell [127, 139]. Moreover, since the reformers in RMFCs operate at higher temperatures, the RMFCs require heat management and insulation. In the case of DAFCs, the direct feed of the alcoholic fuel to the PEMFC stacks cuts out the reformer cost, heat management, and design problems, which makes DAFCs more favorable, especially for portable applications. In 2004, 15 companies were engaged in the development of DMFCs [140], with more companies participating in DAFC development in the last decade.

Components and Reactions in Direct Alcohol Fuel Cells

The overall structure and composition of a DAFC are essentially the same as in conventional PEMFCs (section "H_2-Fueled Polymer Electrolyte Membrane Fuel Cells (PEMFCs)"),

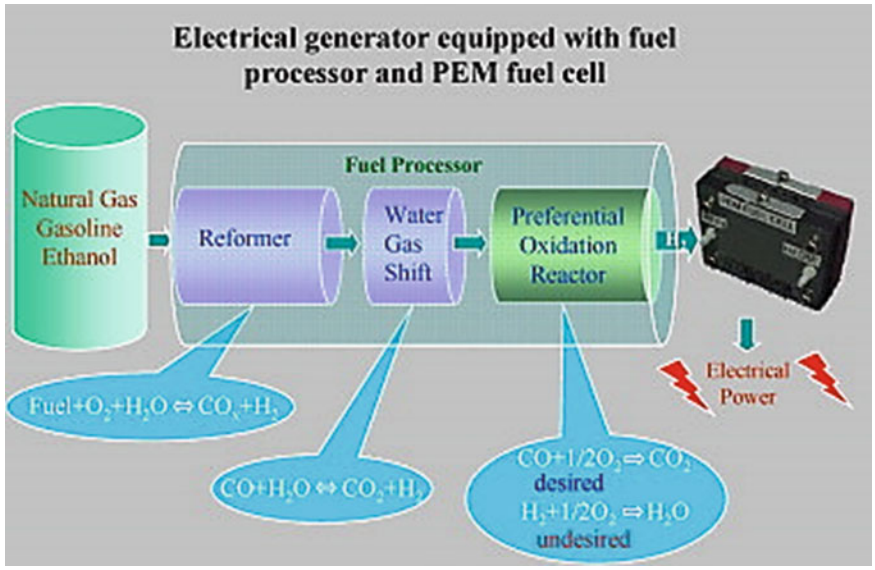

Fig. 8 Configuration of an electrical generator equipped with a liquid fuel processor and PEM fuel cell [139]. Reprinted with permission of Elsevier

and thus this will not be discussed again here. In general, DAFCs consist of a polymer electrolyte ion exchange membrane (e.g., Nafion) placed between the anode and cathode, with each electrode consisting of a catalyst layer, CL (normally noble metal-based nanoparticles, supported on various forms of high-surface area carbon), a gas diffusion layer (GDL), and a backing layer, and typically operate in the 60–80 °C temperature range. As explained in section "Catalyst Layers (CLs)," the CLs are composed of a mixture of three components, the ionomer (ionic conductor, e.g., Nafion), carbon (electronic conductor and catalyst support), and the electrocatalyst (normally Pt-based materials). The diffusion layer is usually a mixture of carbon and polytetrafluoroethylene (Teflon®), since the hydrophobic properties of these materials are needed to remove water from the cathode, to transport O_2 to the catalytic sites and to facilitate the release of CO_2 from the anode [141], as discussed in section "Gas Diffusion Layer (GDL)." In DAFCs, alcohol/H_2O mixtures are fed directly to the anode. In the air-breathing membraneless micro-DMFC, an alcohol/H_2SO_4 (or phosphate buffer) mixture is fed to a channel in which the anode is at the base and the two cathodes are at the side of the channel [142].

The simplest alcohol, methanol, is oxidized at the anode in a direct methanol fuel cell (DMFC) to form carbon dioxide, protons, and electrons, according to the reactions shown in Fig. 9 [143]. In the case of direct ethanol fuel cells (DEFCs), the main oxidation products are acetaldehyde and acetic acid, due the low probability of C–C bond breakage at low temperatures [144].

As in PEMFCs, the protons generated at the anode pass through the proton exchange membrane (under the electric field) and combine with O_2 (from air) and electrons at the cathode, reducing O_2 to water. The overall reactions within a DMFC and DEFC, based on the complete oxidation of the fuel at the anode, are given in reactions (5) and (6) [136, 145].

$$CH_3OH + 3/2O_2 \rightarrow CO_2 + 2H_2O \quad [E_{cell} = 1.21\ V] \tag{5}$$

$$CH_3CH_2OH + 3O_2 \rightarrow 2CO_2 + 3H_2O \quad [E_{cell} = 1.14\ V] \tag{6}$$

As Fig. 9 shows, one problem in a DMFC is that methanol can cross the Nafion membrane,

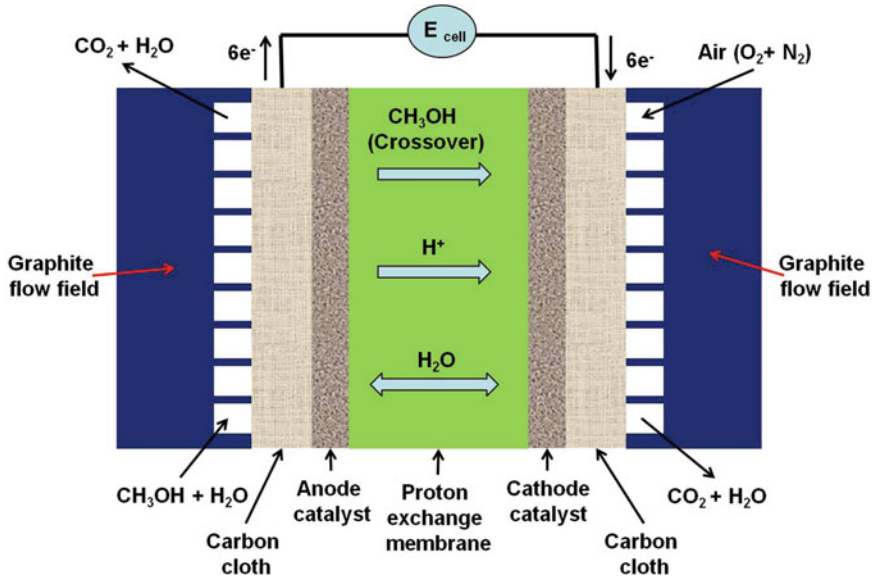

Fig. 9 Schematic drawing showing the operating principles of a DMFC

moving from the anode to cathode side, which leads to undesirable results, such as a lower (<0.8 V) open circuit potential (OCP), O_2 consumption by direct reaction with methanol, cathode catalyst poisoning by the CO intermediately generated, and a lower fuel utilization efficiency. In comparison with methanol, ethanol has a lower permeation rate through the Nafion membrane and thus exhibits lower crossover rates [146]. Section "Catalysts Used in PEMFC Anodes and Cathodes" shows a variety of cathode catalyst materials for PEMFCs, which are normally also suitable for DAFCs. In DAFC, the cathode catalysts are also expected to be tolerant to the fuel oxidation. Alcohol crossover in DAFCs depends on several factors, including the nature of the membrane material, its morphology, and its thickness; a detailed discussion of the membrane materials is given in section "Polymer Electrolyte Membrane Separator." Also, the extent of this problem depends on the fuel concentration, the fuel cell operating temperature, and the anode activity [146, 147].

Effect of DAFC Operating Conditions on Performance

DAFCs can be categorized as active or passive systems, according to the fuel delivery and handling process employed. In passive systems, very few external devices are needed for pumping methanol or blowing air into the cell, as oxygen diffuses into the cell by the air-breathing action of the cell, and the fuel diffuses from a feed container to the anode, driven only by concentration gradients [148, 149]. Even though passive systems would result in a minimum power loss and a smaller system volume, they exhibit lower performance and involve less control of the operating conditions (temperature, fuel flow rate, and concentrations) compared to active systems [148].

A very detailed study was carried out on the effect of cell temperature, fuel (methanol) concentration, cathode humidification temperature, fuel flow rate, and oxidant (air and pure O_2) flow rate on the performance of a single

DMFC [150]. Figure 10 shows the polarization curve obtained at various operating temperatures, while the other variables were fixed. Even though higher temperatures are known to increase the electrochemical kinetics of both the fuel oxidation and oxygen reduction reactions, there are some negative effects, such as a decrease in the oxygen partial pressure and an increase in the rate of fuel and water crossover from the anode to the cathode [150, 151]. The enhancement effect of temperature was found to be significant up to 70 °C, with no further enhancement at higher temperatures. The negative effect of increasing temperature was observed only at temperatures ≥70 °C, especially at high cell potentials (lower currents).

Our study, and others [149–152], showed that the optimum alcohol concentration is 1–2 M in water, especially when air is used at the cathode side. At concentration below 1 M, the anode experiences mass transport limitations (Fig. 11), while at concentrations >2 M, the sharp decrease in the cell performance was attributed to the high rate of methanol crossover. Figure 11 shows that when the airflow rate was increased from 600 to 1200 sccm, the drop in the cell performance with increasing methanol concentration (>2 M) became less severe [150]. By replacing air with pure oxygen, both at a flow rate of 600 sccm, the cell performance remained almost constant with a minimum effect of methanol crossover on the cell performance [150]. These results reveal that the problem of fuel crossover depends not only on the anode conditions (concentration and flow rate) but also on the cathode [150].

The fuel and oxidant flow rate also has a tremendous impact on DAFC performance. A higher fuel flow rate improves the performance by suppressing the fuel starvation (reaching limiting currents at low cell potentials), diffusion resistance, and accumulation of CO_2 gas bubbles [148, 150]. Similarly, on the other side of the cell (cathode), increasing the oxidant flow rate (air) can enhance the cell performance up to an optimum value (800 sccm), as a further increase of flow rate will negligibly change the oxygen concentration [150]. Also, the oxidant flow rate plays a crucial role in keeping the cathode side of the DMFC at an optimum hydration condition; as at low flow rates, the cathode can be flooded, while at high flow rates, it could dry out.

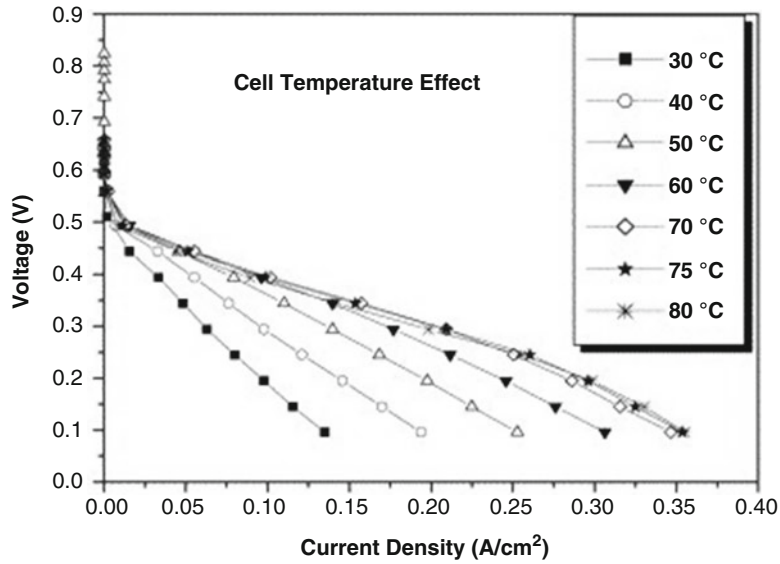

Fig. 10 Polarization curves at different fuel cell-operating temperatures at 3 M methanol concentration, 30 °C cathode humidification temperature, 4 mL/min methanol flow rate, and 600 sccm airflow rate [150]. Reprinted with permission of Elsevier

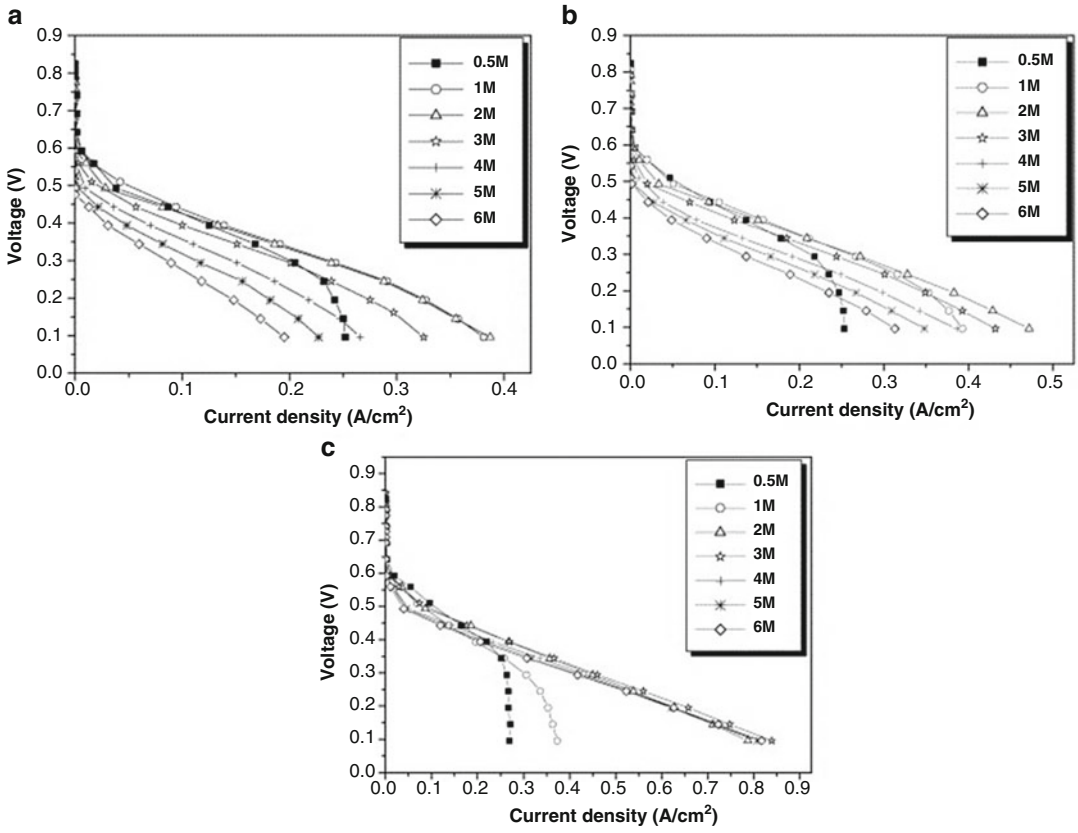

Fig. 11 Polarization curves at different methanol concentrations at (**a**) 600 sccm airflow rate, (**b**) 1200 sccm airflow rate, (**c**) 600 sccm pure oxygen flow rate, 70 °C cell temperature, 70 °C cathode humidification temperature, and 6 mL min^{-1} methanol flow rate [150]. Reprinted with permission of Elsevier

Methanol and Ethanol Oxidation Mechanism

In order to improve the performance of DAFCs, understanding the reaction mechanism is very important to help select and design the best catalytic materials at each electrode. Methanol oxidation is believed to follow a dual pathway mechanism on Pt catalysts [153–158]. One pathway proceeds *via* CO formation, followed by its subsequent oxidation to CO_2, as shown in Fig. 12 [156], whereas the second pathway proceeds through the formation of soluble intermediates, such as formaldehyde and formic acid, which can subsequently oxidize to form CO_2. Strongly adsorbed CO has been identified as the main poisoning species that blocks Pt sites from further adsorption of intermediates formed during methanol oxidation [159].

In order to improve the kinetics of the methanol oxidation reaction (MOR) on Pt, the electronic interactions between Pt and CO must be modified, including by weakening the CO adsorption energy or increasing the rate of CO oxidation [143]. The addition of a second element to Pt (e.g., Ru, Sn, Ni) should modify the Pt–CO electronic interaction and facilitate CO_{ads} electrooxidation [160–163]. This mechanism of improving the catalytic properties of Pt is called the electronic or ligand effect [164–169]. Also, CO, formed during methanol oxidation, can be removed by its oxidation to CO_2 when O-containing species are present at the electrode surface (bifunctional mechanism). The addition

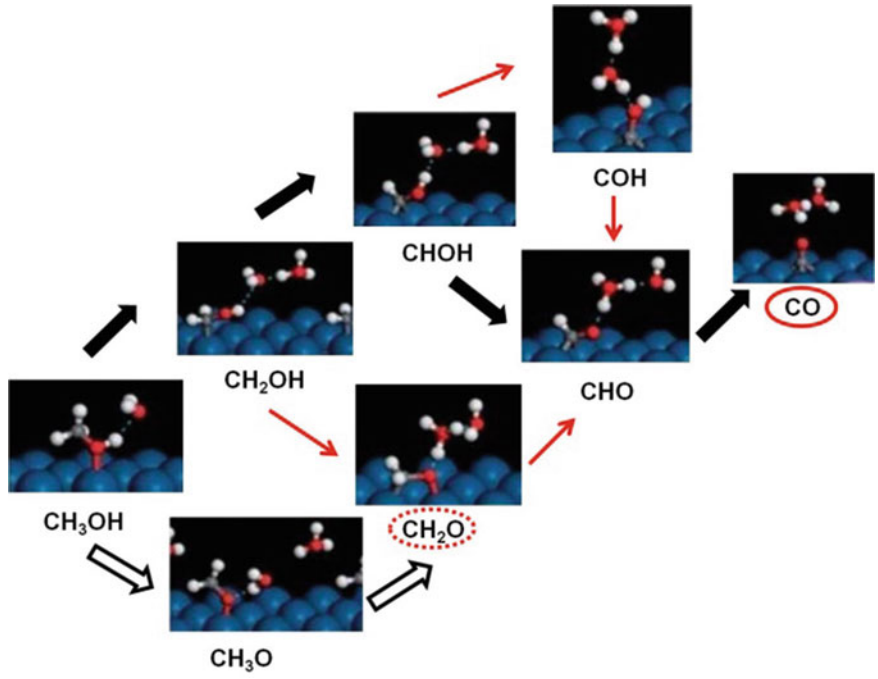

Fig. 12 Methanol decomposition pathways in the formation of CO and formaldehyde at Pt (111) at 0.5 V. The pathway that forms CO, shown in black arrows, is favored [158]. Reprinted with permission of the Royal Society of Chemistry

of other metals, e.g., Ru, that adsorb OH at lower potentials than Pt has been found to lead to more catalytic surfaces at which methanol oxidation occurs more rapidly [170, 171].

On the other hand, the methanol adsorption/dehydrogenation step in the MOR requires an ensemble of three adjacent Pt atoms in order to fully break all of the C–H bonds [172, 173]. According to this mechanism, the decrease in the Pt–Pt atomic distance could facilitate the breakage of C–H bonds during the methanol oxidation and result in an overall increase in the rate of the MOR. This compressive strain effect is known to cause a downshift in the *d*-band center of the Pt_{shell}, which results in weaker Pt-adsorbate interactions [174–176]. However, theoretical studies [176] have shown that the Pt_{shell} compression causes only a minor change in electronic properties compared to impact of the atomic interactions between the Pt and the second metal.

The complete oxidation of ethanol is more complicated, as it involves the splitting of a C–C bond (routes 1 and 4, Fig. 13) [177], a

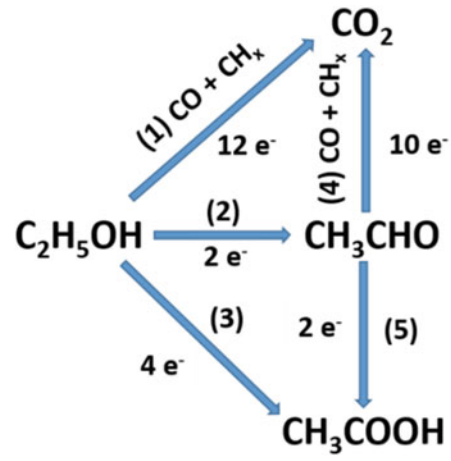

Fig. 13 Schematic representation of the various electrochemical pathways of ethanol oxidation

challenge that is not present during methanol oxidation. The high volumetric energy of ethanol (Fig. 7) assumes the complete oxidation of ethanol to CO_2 (12 e^-). Therefore, the incomplete oxidation of ethanol results in a loss in DEFC performance. All known electrocatalysts have

difficulty in breaking the C– C bond, even at temperatures as high as 90 °C, which leads to the incomplete oxidation of ethanol, forming either acetaldehyde (route 2, Fig. 13) or acetic acid (route 3 or route 2 plus 5, Fig. 13), which clearly lowers the DEFC performance [178]. The ratio between the amount of acetaldehyde and acetic acid formed depends strongly on the ethanol concentration [177], temperature [127], and catalyst composition [179].

According to routes 1 and 2 plus 4 (Fig. 13), ethanol decomposes into adsorbed CO and CH_x species on platinum, with adsorbed CH_x species being even more difficult to oxidize to CO_2 than CO. CO thus accumulates on the platinum surface, resulting in poisoning of the surface [144, 178–180]. Also, in order to increase the ethanol oxidation efficiency, the complete oxidation of acetaldehyde to acetic acid and/or CO_2 is a necessity. The oxidation of CO, CH_x species, and acetaldehyde requires the dissociation of water to produce adsorbed OH on the surface. Since OH formation starts at Pt at potentials >0.75 V [181, 182], the addition of other metals, such as Ru, Sn, and Rh, all of which can adsorb OH at lower potentials than at Pt, is crucial to obtaining high rates of ethanol oxidation [144, 178–180]. Another benefit of using Pt-based binary or tertiary alloys is the prevention of the formation of poisoning species, such as CO and CH_x, by suppressing C- C bond breaking. This is believed to take place by decreasing the required number of Pt atoms for the reaction to occur (ensemble effect) and/or changing the electronic properties of Pt [180, 183, 184].

Anode Catalysts Used in DAFCs

Pt–Ru-Based Catalysts

In 1987, Watanabe et al. [170] reported the preparation of highly dispersed Pt–Ru alloy nanoparticles on carbon powder, with Pt–Ru selected because the electronic effect between Pt and Ru atoms was thought to be important [141]. It was also shown that 40–60 atomic % Ru gives the optimum catalytic activity for methanol oxidation at unsupported, supported, and bulk Pt–Ru alloys [170, 185–188]. Lu et al. [189] applied cyclic voltammetry (CV), temperature programmed desorption (TPD), and radioactive labelling to probe the origin of MOR rate enhancement at Ru deposited on a Pt electrode surface. They found that changes in the Pt–CO bonding due to the electronic effect played only a minor role in enhancing CO tolerance, as the Ru bifunctional effect was found to be about four times larger than the electronic effect [189]. More recently, Yang et al. [190] employed in situ surface-enhanced Raman spectroscopy and showed that the addition of Ru to Pt surfaces does not change the Pt–CO stretching frequency, again suggesting that Ru has no significant electronic effect on Pt [190].

In other works [191], nanoparticles consisting of a Ru core covered with a 1–2 monolayers of Pt atoms gave high CO oxidation activity, significantly better than traditional Pt–Ru nano-alloys, mixtures of monometallic nanoparticles, or pure Pt particles [191]. Using DFT modelling, Alayoglu et al. [191] showed that the presence of subsurface Ru caused an enhancement of CO oxidation through modification of the electronic structure of the Pt surface, leading to a lower CO coverage. This provides a greater number of free active sites at which the reactants can be activated [191].

Although Pt–Ru is one of the best MOR anode catalyst materials, Zelenay et al. [192, 193] and others [194–197] have reported that Ru can dissolve in a DMFC, crossing-over to the cathode and inhibiting the oxygen reduction kinetics, while also degrading the membrane. Although Ru should be thermodynamically stable [198] under normal DMFC operating conditions, it is possible that hydrous Ru oxide species are formed at the anode at high potentials and that they then dissolve or leach out.

Pt–Sn-Based Catalysts

Pt–Sn has been studied for decades as an anode catalyst for the electrooxidation of methanol and other small hydrocarbon fuels [199], with mixed results [200], depending on the method of preparation [141]. A theoretical study by Liu et al. [169] showed that Pt_3Sn should be more active

toward CO electrooxidation than Pt or Pt–Ru, similar to the data reported by Schmidt [201]. It appears that Sn dissociates water (bifunctional effect) and also weakens the CO bond to nearby Pt sites (electronic effect), thus lowering the CO coverage. However, the electronic effect of Sn on Pt may also weaken methanol adsorption on Pt, which lowers the Pt–Sn MOR activity. It is also known that Sn is more susceptible to dissolution than is Ru in MFC condition [198]. However, Sn is 800 times less costly than Ru.

Other Pt-Based Catalysts for Both Methanol and Ethanol Oxidation Reactions

Similar to Sn, adsorbed oxygen on Ni helps to remove CO from Pt and promotes its oxidation at low potentials [202]. Consistent with this, Pt–Ni generally shows a higher activity for the MOR vs. Pt [203] but lower than at Pt–Ru [141], although Park et al. showed Pt–Ni to be a better catalyst than Pt–Ru [204]. A review by Antonlini et al. [202] showed that, at low Ni contents, the decreased MOR activity (vs. Pt–Ru) is due to the decrease in the Pt content on the surface, hindering methanol adsorption. At high Ni contents, the higher activity for the MOR is related to the electronic effects, the enhanced CO oxidation, and the presence of Ni oxide.

Pt–Ir has been proposed as a promising alternative to Pt–Ru, as Ir is more resistant to dissolution than Ru and shows very good MOR activity [205–208]. Also, contrary to Pt–Ru, Pt–Ir is reported to have a high catalytic activity toward the ORR [207, 209]. Therefore, if any Ir should be dissolved, the problems associated with this will be less than with Ru dissolution.

Pt–Ir NP synthesis and activity toward the MOR have been reported in a few previous studies. H. Tsaprailis et al. [205] prepared a Pt–Ir catalyst by mixing individual Pt and Ir sols together, aiming for a nanoparticulate binary mixture containing Pt and Ir in a controlled ratio. However, even though the sols were combined, a 1:1 Pt:Ir molar ratio, the bulk composition was found to be close to 2:1, using inductively coupled plasma atomic emission spectrophotometry (ICP-AES). Clearly, the mixing of these sols resulted in a different distribution of Pt and Ir at the molecular level. In another study [209], Pt–Ir alloy NPs (3–4 nm) were fabricated by the reduction of an alkaline mixture of H_2PtCl_6 and H_2IrCl_6 solutions at 80 °C. However, the predicted specific surface area (based on NP size, as determined by XRD measurements) was found to be 2–3 and 10–20 times the measured specific surface area determined by Brunauer–Emmett–Teller (BET) and electrochemical methods, respectively, revealing their low dispersion. In the same study [209], XPS showed that the surface composition of the Pt–Ir NPs matched their bulk composition. However, the Hupd (hydrogen underpotential deposition) peaks were similar to those at pure Pt NPs, suggesting Pt surface enrichment.

Pt-Based Core–Shell Methanol and Ethanol Oxidation Reactions

As it is known that the composition, size, and shape of nanoparticles are critical to their catalytic properties, recent work has focused on the fabrication of bimetallic nanoparticles having a "core–shell" structure, with one metal in the core of the particle and the second metal forming an outer shell around the core. Some of the core–shell architectures reported recently include $Pd_{core}@Pt_{shell}$ [210], $Cu_{core}–Pt_{shell}$ [211], $Rh_{core}–Pt_{shell}$ [212], $Ru_{core}–Pt_{shell}$ [191, 213–215], $Pt_{core}–Ru_{shell}$ [215, 216], $Ir_{core}–Pt_{shell}$ [206, 217], $Co_{core}–Pt_{shell}$ [174], $Au_{core}–Pt_{shell}$ [218], and $Ni_{core}–Pt_{shell}$ [93, 219]. For most of these systems, the core materials were prepared using glycol as a reducing agent and PVP (polyvinylpyrrolidone) as a stabilizer, followed by the addition and reduction of precursors to form the shell materials. Core–shell nanoparticles are highly catalytic toward CO oxidation [191, 210, 212], oxygen reduction [93, 215], and NO_x reduction [211]. However, only a few papers have been published on supported core–shell particles for methanol oxidation [174, 206, 218, 220–224].

In order to overcome the Ru dissolution problem, several studies have focused on $Ru_{core}–Pt_{shell}$ preparation and characterization [191, 216, 217, 220, 222–226], with several

groups examining the MOR activity at these materials [220, 222–224]. In some of this work [220, 222], the Ru_{core}–Pt_{shell} catalytic activity was judged based on the ratio between the forward and backward MOR peak currents (I_f/I_b), assuming that high I_f/I_b ratio indicates a higher CO tolerance and MOR activity. However, it has also been shown that I_f and I_b have the same chemical origin, and hence the I_f/I_b ratio does not predict the CO tolerance and catalytic activity for MOR [227]. Some of the factors that could influence the MOR activity of the Ru_{core}–Pt_{shell} NPs include the Pt shell strain (relaxation vs. compression), the Ru electronic effect on the Pt shell, and the bifunctional effect of exposed Ru when the Pt shell coverage is less than one monolayer. However, most prior studies do not involve a systematic investigation to distinguish which of these effects is playing the main role in determining the overall MOR catalytic activity.

Ni_{core}–Pt_{shell} and Co_{core}–Pt_{shell} NPs are attractive as alternatives to Ru_{core}–Pt_{shell} NPs, due to the low cost of the core material and their strong electronic effect on the shell material [174, 219]. Chen et al. [93] found that Ni_{core}–Pt_{shell} NPs exhibit characteristics of FCC Ni nanocrystals but with a slightly expanded lattice, even though the electrochemical properties of a Pt surface are also seen. Further, a significantly shortened Pt–Pt interatomic distance is seen in the shell layer, compared to a pure Pt NPs. The catalytic activity of Ni_{core}–Pt_{shell} NPs were examined in an alkaline medium and found to be highly active and more resistant to carbonaceous intermediate poisoning than is pure solid Pt [219]. However, the catalytic activity of Ni_{core}–Pt_{shell} NPs toward the MOR in acidic media needs to be further investigated. Similar to Ni_{core}–Pt_{shell} NPs, the Co_{core}–Pt_{shell} MOR catalytic activity, in an acidic medium, was found to arise from both electronic and strain effects of the Co_{core} on the Pt_{shell} [174]. Even though Pt–Ir catalysts have been reported to have a high catalytic activity toward the MOR [207, 228–230], very few of these studies have made efforts to determine what the origin is of the catalytic effect of Ir on Pt [229, 230].

Only a few reports have been published on Ir_{core}–Pt_{shell} NP synthesis, all using relatively complex procedures [206, 217]. A. U. Nilekar et al. reported that Ir_{core}–Pt_{shell} NPs have higher catalytic activity towards the preferential oxidation (PROX) of CO in H_2 feeds than Pt, Au_{core}–Pt_{shell}, or Pd_{core}–Pt_{shell} [217]. Also, K. S. Lee et al. prepared Ir_{core}–Pt_{shell} NPs (supported on Vulcan carbon) with different Pt_{shell} coverages, trying to correlate between the Pt_{shell} thickness and the catalytic activity of these catalysts toward the MOR but without a detailed investigation of the presence of a bifunctional or electronic effect of Ir on Pt [206]. Other core–shell NPs, such as Au_{core}–Pt_{shell} and PdCo–Pt [218, 221], were investigated as MOR catalysts and showed promising results, but further studies are needed to understand the reasons behind their good catalytic activity.

Direct Formic Acid Fuel Cells (DFAFCs)

A promising candidate for the organic liquid fuel cells is formic acid (FA). DFAFCs have the highest theoretical cell potential (1.48 V) among the other liquid fuels. Also, FA exhibits rapid oxidation kinetics and less chance for fuel crossover than methanol and ethanol [231–234]. Also, in contrast to methanol or ethanol, FA contributes to the proton conductivity in the anode, further extending the triple phase boundary and enhancing the cell performance [233].

Both methanol and ethanol have a high volumetric energy density in the pure form. However, due to the crossover problem, only low concentration (1–2 M) of these fuels can be used, as mentioned earlier. The small volumetric energy density (2104 Wh L^{-1}) of pure FA compared to methanol and ethanol could be seen as a disadvantage. However, due to the lower probability of FA crossover, a high concentration of formic acid can be used. Specifically, the methanol crossover current and the crossover flux were reported to be six times and two times, respectively, greater than that of FA [235]. Others have found the optimum FA concentration to be 10 M [234], as at higher concentrations, a significant

drop in the performance is observed, explained by the high rate of FA crossover. Also, due to the hygroscopic nature of FA, it is expected that the membrane will dry out at high FA concentrations, which could cause a substantial increase in the cell resistance [234].

Understanding the reaction mechanism of FA oxidation is again critical to help in the selection of the best electrocatalytic materials for use in DFAFCs. FA oxidation (FAO) through a dual pathway is the most commonly accepted mechanism, with a minor possibility for the formation of the bridged structure [158, 236, 237]. In the first pathway, FA oxidizes to CO_2 through direct dehydrogenation (direct pathway, reaction (7)), while in the second pathway, FA chemically dehydrates to form adsorbed CO (reaction (8)), which is oxidized to CO_2 (reaction (10)) at high potentials (>0.8 V vs. RHE, in the case of Pt) when water dissociation (reaction (9)) can take place at a suitable rate (indirect pathway) [231, 238]:

$$HCOOH \rightarrow CO_2 + 2H^+ + 2e^- \quad (7)$$

$$HCOOH \rightarrow CO_{ads} + H_2O \quad (8)$$

$$Pt + H_2O \rightarrow Pt - OH + H^+ + e^- \quad (9)$$

$$Pt - CO + Pt - OH \rightarrow CO_2 + H^+ + e^- \quad (10)$$

Pt- and Pd-based materials are the most common electrocatalysts employed to enhance the FAO rate. In the case of Pt, at low overpotentials, FAO takes place through the direct pathway. However, due to the continuous production of CO, the surface becomes blocked and the current drops dramatically with time. However, at high overpotentials, the indirect pathway dominates due to the ability of Pt to dissociate water [239]. In the case of Pd, the direct pathway prevails. However, Pd is known to deactivate with time due to the accumulation of inactive surface intermediates [238], likely CO, resulting from the reduction of the FA dehydrogenation product (CO_2) [240, 241].

The catalytic activity of Pt or Pd has been improved by preventing CO formation by blocking some fraction of the catalytic sites (third-body or ensemble effect) [242, 243], modifying electronic properties (electronic effect) [242], and changing the surface atomic distance (strain effect) [214]. These modifications have been achieved by adding a second metal to the surface of Pt (Pd) by irreversible adsorption or alloying [220, 242–245]. Also, core–shell structures [246], normally involving a Pt or Pd shell, have been examined, where the catalytic activity was altered by modifying either the core material or the shell coverage and thickness [214, 241].

The irreversible adsorption of Bi, Sb, or Pb (or as a second metal in an alloy) is known to dramatically enhance the Pt or Pd electrocatalytic activity through the third-body or ensemble effect, along with generating a selective FA adsorption orientation that enhances the kinetics of FA oxidation [231, 232, 238, 247]. Several other metals have been employed, such as Au, Ag, Cu, Ni, Co, Fe, Ir, Ru, and Sn, with the electronic and strain effects believed to be most relevant in altering the Pd or Pt FA oxidation activity [238].

Solid Oxide Fuel Cells (SOFCs)

As explained earlier, one of the most important features of fuel cells is their high-energy conversion efficiency, which can vary between 20 and 90%, depending on whether both electrical and thermal energy are used. SOFCs, which run at temperatures typically of 700–800 °C (but which could range from 600 to 900 °C), are one of the most efficient types of fuel cells with a theoretical electrical efficiency as high as 85%, recently reaching a practical efficiency close to 60% [248]. Moreover, SOFCs can be produced in a variety of sizes and therefore can cover the energy needs from kilowatts that can be suitable for individual residential needs to megawatts that can provide the energy needed for a small town. Another advantage of SOFCs is that they are fuel flexible, being able to reform hydrocarbon fuels internally, thus decreasing operation costs by removing expensive fuel processing systems. Furthermore, SOFCs are quiet and can thus be

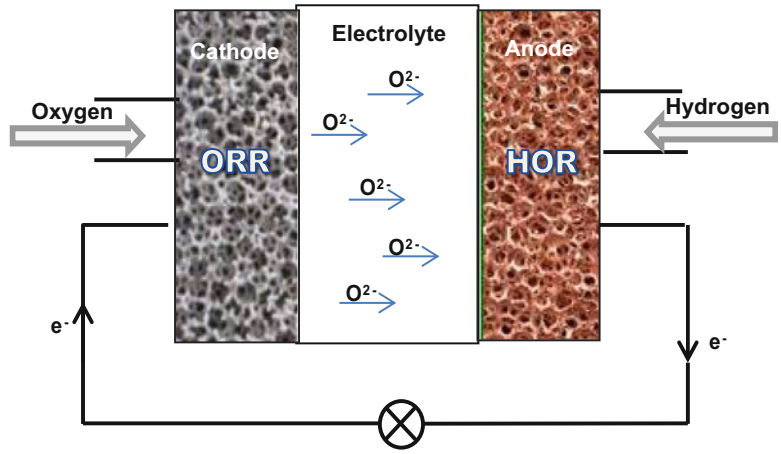

Fig. 14 Schematic diagram of an SOFC

placed near urban areas. At the time of writing this article, there is ca. 750 MW of installed SOFC capacity worldwide, used primarily for commercial/stationary applications.

The characteristic components of SOFCs include a dense, oxygen ion-conducting electrolyte, and, similar to PEMFCs and DAFCs, they also rely on porous solid electrodes (Fig. 14), but these materials must be active and stable under more aggressive conditions (temperatures between 650 and 1000 °C). At these temperatures, the electrode reactions are usually very rapid but material stability is a challenge.

In an SOFC, the oxidant (oxygen, as in PEMFCs and DAFCs) is pumped into the cathode where the O_2 reduction reaction (ORR) takes place:

$$\frac{1}{2}O_2 + 2e^- \rightarrow O^{-2} \qquad (11)$$

The dense electrolyte serves as a barrier to prevent gas leakage, but oxygen anions can pass through it and reach the anode, at which predominantly the hydrogen oxidation reaction (HOR) occurs (reaction (12)), as hydrocarbons and steam, fed into the system, are typically reformed quickly, generating H_2 and CO:

$$H_2 + O^{-2} \rightarrow H_2O + 2e^- \qquad (12)$$

As in all fuel cells, the electrons, produced at the anode, are transferred to the cathode through the external circuit. As fuel and oxygen ions are required as the reactants and electrons and water are the products, a porous structure, containing both an ionic conductor and electronic conductor, is again needed.

SOFCs typically run at ambient pressure, although efforts have been made to increase the operating pressure [249], which adds to the voltage of the cell. Air and fuel utilization can vary but is typically 15 and 70%, respectively [250].

SOFC Cell Designs

Because of the high temperature of operation of SOFCs (> 600 °C), all of the cell components must be chemically, morphologically, and dimensionally stable under these challenging conditions. A single cell within an SOFC can have various designs in terms of cell dimensions, as well as which layer serves as the mechanical support. The two most common SOFC cell designs are planar and tubular (Fig. 15). In the planar design, all of the cell components are thin and have a rectangular shape, often 10×10 cm^2 up to 25×25 cm^2 [251, 252]. Planar cells generally exhibit fewer ohmic and concentration losses as they are compact, although they show higher thermal gradients compared to tubular cells (Fig. 15).

The tubular cell configuration, developed originally by Westinghouse Corporation, was introduced as a shock resistant and easy to seal

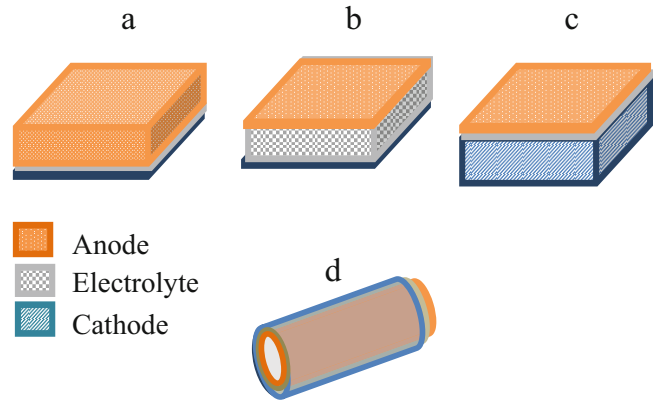

Fig. 15 Various SOFC cell designs including (**a**) a planar anode-supported, (**b**) planar electrolyte-supported, (**c**) planar cathode-supported cells, and (**d**) tubular cell

SOFC design. Michaela and Kendall [253], in the early 1990s, reported the first work on microtubular SOFCs. They demonstrated a thin-walled extruded YSZ tube (1–5 mm dia), which had reasonable performance and was surprisingly shock resistant. This latter characteristic allows a shorter start-up and shutdown time for the SOFC system. These tubular cells can be formed by conventional ceramic-forming methods, such as slip casting [254] and extrusion [255]. One of the benefits of the slip-casting technique of microtubular cell construction is that all of the cell components (anode, electrolyte, and cathode) can be fabricated at the same time, as each layer can be casted sequentially [254].

SOFC single cells can also be categorized in terms of which layer of the cell provides the mechanical support, including self-supported and externally supported cells. Self-supported cells can also be classified into three main categories, i.e., electrolyte supported, anode supported, and cathode supported, where the supported component is typically the thickest layer (Fig. 15). In externally supported cells, all of the cell components are deposited as thin layers on an additional porous support layer, such as a porous metal layer or a porous ceramic support. While metal-supported cells have received attention recently due to their low cost, robust, and shock-resistant characteristics, the metal support cannot tolerate very high temperatures compared to the ceramic cell components, thus limiting the selection of the other cell component materials [256]. For this reason, the maximum operating temperature is ca. 600 °C, as higher operating temperatures can severely limit their lifetime [257, 258]. In addition to difficulties in co-manufacturing of the metal support and the other ceramic cell components, Cr poisoning of the cathode is another challenge associated with this type of SOFC [258]. Recently, Ceres Power has developed a 1-kW metal-supported stack, based on a gadolinia-doped ceria $Ce_{0.9}Gd_{0.1}O_{1.95}$ (CGO10) electrolyte, displaying a degradation rate of 0.43%/kh [259].

The methods used to produce each SOFC cell depend on the materials used in each component, as well as which component is selected as the cell support. Tape casting and screen printing are the most commonly used manufacturing techniques for planar cell construction, due to their simplicity and cost-effectiveness and because they are amenable to mass production. For electrolyte-supported cells, the electrolyte can be pressed or tape-casted first and then the electrodes are deposited, typically using screen printing or tape-casting techniques [260, 261] or using tape calendaring and wet spraying [262]. For electrode-supported cells, the electrolyte is deposited using sputtering [263], physical vapor deposition (PVD) [264], pulsed laser deposition (PLD) [265], chemical vapor deposition (CVD) [266], slurry coating [267], or using sol–gel methods [268]. Plasma spraying has also been used to deposit each SOFC layer, especially

when the SOFC components cannot be co-sintered together because of their different melting points [269]. For tubular cells, the most common manufacturing techniques are extrusion [270, 271], slip casting [254, 272], and dip coating [273].

Typical SOFC Cell Materials

SOFC Electrolytes

In addition to demonstrating chemical stability at high temperatures and in both reducing and oxidizing atmospheres, SOFC electrolytes must have a high ionic conductivity to allow oxygen ions, produced at the cathode, to travel through and reach the anode. Yttria-stabilized zirconia (YSZ) is the most commonly used SOFC electrolyte material. The ionic conductivity of YSZ, when containing 8 mol% yttria (Y_2O_3), is about 0.01 S cm^{-1} at 800 °C [274]. By doping with yttria, the cubic structure of zirconia can be stabilized at high temperatures, and the ionic conductivity of zirconia is increased by the generation of additional oxygen anion vacancies. Further, YSZ has a very good mechanical strength and thus can serve as a structural component in SOFCs. Scandium (Sc) is another alternative dopant in zirconia, producing scandium-stabilized zirconia (SSZ), which has an even higher ionic conductivity than YSZ. The higher conductivity of SSZ is related to the smaller mismatch between the sizes of Zr^{+4} and Sc^{+3} compared with Zr^{4+} and Y^{+3}, resulting in better mobility of the O^{2-} ions [275].

Despite the excellent properties of zirconia-based materials as SOFC electrolytes, they have several disadvantages that limit their application as SOFC electrolytes. One problem is aging with time at SOFC operating temperatures, leading to a drop in conductivity [276]. Another limitation is the decrease in ionic conductivity of zirconia-based electrolytes at lower temperatures, making the application of these electrolytes at lower temperatures challenging. In addition, zirconia-based electrolyte can react with several anode and cathode materials, forming resistive interfaces, especially during cell preparation [277]. Therefore, electrolytes, such as doped ceria and $La_{1-x}Sr_xGa_yMg_{1-y}O_3$ (LSGM), have been introduced as alternatives to zirconia-based electrolytes.

Ceria and doped ceria are the most commonly used electrolytes for intermediate temperature SOFCs (550–650 °C) because of their higher O^{2-} conductivity than YSZ (0.1 S cm^{-1} at 800 °C) and also their compatibility with a number of perovskite-based anode and cathode materials, such as $La_{0.75}Sr_{0.25}Cr_{0.5}Mn_{0.5}O_{3-\delta}$ (LSCM) [278]. In order to increase the conductivity of ceria to values similar to that of YSZ, ceria can be doped. Gadolinia and samaria are the most common dopants for ceria (producing GDC and SDC, respectively), showing the highest conductivity among the doped ceria electrolytes [279]. However, Ce^{4+} can be reduced to Ce^{3+} at high temperatures (>500 °C) in reducing atmospheres, causing n-type electronic conductivity to develop in the electrolyte and therefore allowing some electronic leakage through the ceria and a loss in overall SOFC efficiency [280, 281]. However, GDC is an excellent electrolyte, even at low temperatures (<500 °C).

LSGM has a conductivity similar to GDC (0.1 S cm^{-1} at 800 °C), although, unlike ceria, LSGM does not contain a reducible metal ion in reducing atmospheres and at high temperatures and therefore is more stable to reduction. However, LSGM can react with several SOFC electrode materials through the interdiffusion of elements. Other materials that have been investigated as possible SOFC electrolyte include $Ba_{0.5}Sr_{0.5}Ce_{0.6}Zr_{0.2}Gd_{0.1}Y_{0.1}O_{3-\delta}$ (BSCZGY) and $BaZr_{0.1}Ce_{0.7}Y_{0.2}O_{3-\delta}$ (BZCY) [282].

SOFC Anode Materials

Ni/YSZ cermets (mixture of ceramic and metal) are the most common anode electrocatalysts used in SOFCs because of their low cost, chemical stability at high temperatures and in reducing atmospheres, very good activity for the HOR, and the good match of the thermal expansion coefficient of the cermet and the YSZ electrolyte [283, 284]. The melting point of pure Ni is about 1455 °C with a thermal expansion coefficient of

13.3×10^{-6} cm cm^{-1} k^{-1} and an electronic conductivity of 138×10^4 S cm^{-1} and 2×10^4 S cm^{-1} at 25 °C and 1000 °C, respectively [285]. In order to add ionic conductivity to the anode and to also enhance the structural strength of the anode at SOFC operating temperatures, ionically conducting YSZ has been added as a second component, roughly in a 1:1 mass (or 2 (YSZ):1 (Ni) volume) ratio. Additionally, as the thermal expansion coefficient of Ni is much higher than YSZ (10.5×10^{-6} cm cm^{-1} K^{-1}), the addition of YSZ makes the thermal expansion coefficient of the cermet more compatible with YSZ electrolytes.

Despite these advantages, Ni/YSZ anodes suffer from dimensional instability as a result of inadvertent air exposure, e.g., when the SOFC is being used in long-term operation, when the fuel supply is interrupted, or imperfect sealing is encountered, followed by reduction in H_2. Under the air-exposure conditions, the Ni component of the Ni/YSZ cermet is oxidized to form NiO, which is accompanied by an expansion of ~70% in solid volume [286–290]. This volume change causes mechanical stress at the anode/electrolyte interface and consequently results in damage and cell degradation [286].

Another problem can arise with the use of sulfur (H_2S) and/or hydrocarbon-containing fuels, in which undesired reactions of Ni bring about a loss in cell performance. With <100 ppm H_2S exposure, it is known that up to one monolayer of adsorbed sulfur forms on Ni [291], thus blocking the TPB sites for H_2 oxidation. However, it has been suggested that the addition of ceria can enhance the sulfur tolerance of Ni under normal operating conditions (>750 °C) [292]. Furthermore, it has been reported that ppm levels of H_2S can activate the H_2 oxidation reaction at lower temperatures (500–600 °C), thought to reflect the formation of small amounts of Ni sulfide at the Ni/YSZ TPB [293]. Hydrocarbons can be a problem because of the propensity of Ni to form coke, which builds up in the anode pores, causing mechanical stresses that ultimately lead to cell failure [294]. Coke formation at Ni-based anodes can be prevented by controlling the steam to carbon–fuel ratio (at ca 1.5), although, in practice, this ratio should be still larger [295].

When employing conventional two-phase anode materials (such as Ni/YSZ), the catalytically active area is limited to the TPB area. This is fully a function of the morphology of the anode, which is known to change with time in the case of Ni/YSZ anodes. To overcome these limitations in terms of changing and limiting TPB length, mixed ionic and electronic conductors (MIECs), possessing both ionic and electronic conductivity, have been developed. For these materials (primarily metal oxides having a perovskite or fluorite crystal structure), their entire surface area is active for fuel oxidation, thus lowering the anode polarization resistance [296].

As one example, ceria-based oxides have been investigated, especially as sulfur- and coke-tolerant anodes, also related to their high H_2 oxidation activity and their relatively low cost [297–299]. Ceria-based materials show mixed ionic and electronic conductivity in reducing atmospheres due to the presence of mixed Ce valencies (Ce^{+3} and Ce^{+4}), although doping with members of the lanthanide family can significantly increase their ionic conductivity [298]. Ceria-based materials can act as an oxidation catalyst for methane without coking, while cermets consisting of ceria mixed with a transition metal have been found to be effective even for hydrocarbon reforming [298, 299]. As stated above, ceria can serve as a sulfur-absorbing material and consequently can decrease the degree of sulfur poisoning of Ni [292, 300, 301]. However, GDC can react with the YSZ electrolyte during cell preparation at temperatures of ca. 1200 °C, forming interlayers with much lower conductivity that YSZ. In order to suppress the formation of this resistive layer, short-time sintering of YSZ and GDC has been suggested [302].

The most common family of mixed conducting anodes is the perovskite oxides, having the general chemical formula of ABO_3. The properties of perovskites can be modified by doping with various aliovalent metals in both the A (e.g., La, Sr, Ca, Pb, etc.) and B (e.g., Ti,

Cr, Ni, Fe, Co, Zr, etc.) sites. In recent years, several very promising perovskite materials have been developed for use as SOFC anodes. These include $SrTiO_3$-based materials, such as $La_{1-x}Sr_xTiO_{3+\delta}$ [303, 304] and $La_{0.7}Sr_{0.3}Cr_{0.8}Ti_{0.2}O_3$ [305]. Many other materials have been examined, including $La_{0.9}Sr_{0.1}Ga_{0.8}Mg_{0.2}O_{2.85}$ (LSGM) [306], $(La_{1-x}Sr_x)_{0.9}Cr_{0.5}Mn_{0.5}O_{3-\delta}$ [307], $Ba(Zr_{0.1}Ce_{0.7}Y_{0.2})O_{3-\delta}$ (BZCY) [308], and $BaZr_{0.1}Ce_{0.7}Y_{0.1}M_{0.1}O_{3-\delta}$ (M = Fe, Ni, Co, and Yb), the latter showing some sulfur tolerance and stability in CO_2-containing environments [309]. $La_{0.3}M_{0.7}Fe_{0.7}Cr_{0.3}O_{3-\delta}$ (M = Sr, Ca) is a newly reported, very active, sulfur-tolerant anode [310, 311], also being active as a cathode. Other promising anode materials include $Sr_2Mg_{1-x}Mn_xMoO_{6-\delta}$ [312] and $La_1Mn_{0.5}Cr_{0.5}O_{3\pm\delta}$ (LMC), the latter having superior stability, electronic conductivity, and catalytic activity [313] and multi-element-doped ceria, such as $Ce_{0.87}Y_{0.1}Mn_{0.01}M_{0.02}O_{2-\delta}$ (M = Ca, Mg), with a specific polarization resistance (ASR) in the range of 0.2–0.3 $\Omega\,cm^2$ [314].

Recently, an interesting method has been developed to increase the catalytic activity of perovskites, where the active catalyst is first doped into the B-site of the perovskite material (e.g., $La_{0.52}Sr_{0.28}Ni_{0.06}Ti_{0.94}O_3$) and then is partially exsolved out of the lattice at lower temperatures in reducing atmospheres [315]. In this way, a more active catalyst (transition or precious metal) is stabilized on the surface of the less-active perovskite materials [316]. Overall, MIEC anodes with improving characteristics are being developed. However, they still tend to display relatively low catalytic activity and chemical stability and also have a significantly higher electronic conductivity than ionic conductivity.

SOFC Cathode Materials

Similar to SOFC anodes, the materials used as SOFC cathodes must also be stable at high temperatures (>500 °C) but now in oxidizing atmospheres ($pO_2 > 0.2$). One of the first materials used as an SOFC cathode was the perovskite, $La_{0.7}Sr_{0.3}MnO_{3-x}$ (LSM). LSM is primarily an electronic conductor, and thus it is typically mixed with YSZ to add ionic conductivity and to extend its TPB length, similar to the development of the Ni/YSZ anode [317]. Furthermore, LSM has good catalytic activity for the oxygen reduction reaction and is also chemically compatible with YSZ. However, the electrocatalytic activity of this material decreases at lower SOFC operating temperatures, primarily due to its low oxygen ion conductivity ($\sim 10^{-7}$ S cm^{-1} at 900 °C) [318].

To overcome the limitations of LSM/YSZ, MIEC cathode materials, such as $La_{1-x}Sr_xCo_{1-y}Fe_yO_{3-\delta}$ (LSCF), having a higher ionic conductivity than LSM, have been developed. LSCF also has a lower thermal expansion coefficient ($13.8 \times 10^{-6}\,K^{-1}$), better compatibility with ceria-based electrolytes, and also considerably better oxygen reduction reaction (ORR) kinetics than does LSM [319, 320]. However, the LSCF perovskite can react with the YSZ electrolyte and form undesirable (resistive) interfaces [321], and thus a buffer layer, typically a ceria-based material (GDC), must be placed at the LSCF/YSZ interface [322]. A few other MIEC cathodes, such as $Ba_{0.5}Sr_{0.5}Co_{0.8}Fe_{0.2}O_{3-\delta}$ [323], $Pr_{1-x}Sr_xCo_{0.8}Fe_{0.2}O_{3-\delta}$ (PSCF) [324], and $La_{0.3}M_{0.7}Fe_{0.7}Cr_{0.3}O_{3-\delta}$ (M = Sr, Ca), the latter having the ability to be employed as both the fuel and air electrode in SOFCs, have recently been developed as highly active cathode materials [310, 325–327].

Interconnects

In order to produce higher power, single cells are connected in series with each other to construct SOFC stacks. The current collection from each cell is achieved by using ceramic or metallic current collectors (interconnects) at both sides of the cell (Fig. 16).

The interconnects play a key role in SOFC stack systems, as they electronically connect the anode of one single cell to the cathode of the next cell and also provide a physical barrier to gas crossover. Doped lanthanum chromite perovskites were the original interconnects used in SOFCs, running at up to 1000 °C, as they are relatively stable in both reducing and oxidizing atmospheres and have good electronic

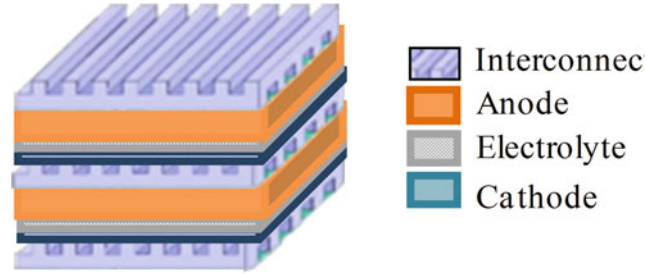

Fig. 16 SOFC stack with two cells

conductivity, although this is poorer in reducing conditions [328]. Therefore, metallic interconnects are now more common, including Cr, Fe, and Ni-based alloys. In general, metallic interconnects have the advantages of a higher electronic conductivity (which is not oxygen partial pressure dependent), a lower cost, and a less complex fabrication technique over ceramic interconnects. However, the thickening of a layer of Cr_2O_3 on the cathode side and Cr poisoning of cathodes are the main disadvantages of stainless steel interconnects [329].

In terms of new candidate interconnect materials, Crofer 22 APU (a low Si ferritic stainless steel with 20–24% Cr and additions of Mn and Ti and La) and Avesta 353 MA (austenitic Fe–Cr–Ni alloy, with 35% Ni and addition of Mn and Si) are two of the most promising [330, 331]. Crofer 22 APU is a high-temperature stainless steel that can form an electrically conducting layer of Cr–Mn oxide on its surface at SOFC operating temperatures, although during long-term exposure in the SOFC environment, Cr_2O_3 can again form, dropping the electrical conductivity of the alloy and lowering cell performance [331, 332].

As one solution, a protective layer can be applied on the surface of metallic interconnects [333–336]. The coating must have good electronic conductivity, a matching thermal expansion coefficient (TEC) with adjacent components, and chemical stability in oxidizing and reducing atmospheres, and more importantly, it should minimize Cr vaporization and prevent the formation of Cr_2O_3 on the cathode side. Various coating materials have been developed, including conductive perovskites, such as $(La,Sr)CrO_3$, $(La,Sr)CoO_3$, and $(La,Sr)MnO_3$, as perovskites generally have a high electronic conductivity and also a matching TEC with the interconnect alloy materials and the SOFC electrodes [333, 334]. However, the use of perovskite coatings is limited, primarily as a result of diffusion of Cr through the coating layer and also difficulties with densification of the coatings. In addition to perovskites, spinel protective coatings, such as $Mn_{1.5}Co_{1.5}O_4$, are also good candidates, as they can be a more effective barrier against Cr migration from the alloy to the cathode [335, 336].

SOFC Material Synthesis Methods

The development of new materials and synthesis methods is crucial in order to lower the SOFC working temperature (to minimize material degradation), to lower cost, and also to increase performance and lifetime. Solid state synthesis methods are the most frequently used techniques for SOFC material fabrication, as they involve inexpensive precursors and can easily be scaled up for mass production [337, 338]. This involves mixing together of ceramic precursor powders, such as metal oxides, carbonates, and/or sulfides, in the stoichiometric ratio of the desired catalysts, followed by calcination of the mixture at particular temperatures to form the desired phases. Despite the simplicity and cost-effectiveness of this approach, there are a number of disadvantages, such as poor compositional homogeneity, uncontrolled particle size, low surface area, and poor sinterability [339]. In order to optimize the properties of the materials used in SOFC components, especially in terms of purity and particle size distribution, other chemical

synthesis techniques have been introduced. These include solution combustion synthesis [340], coprecipitation [341], sol–gel [342], polymeric complexing [343], and hydrothermal methods, [344] all of which are generally more complex than solid state synthesis and rely on more costly precursors, as they require a higher purity level.

Recently, nanostructured SOFC electrocatalysts have been also investigated as highly active electrode materials. The nanoparticles are typically formed by precipitation and decomposition of one or a mixture of metal salts (such as metal nitrates) inside a porous pre-sintered backbone (e.g., of YSZ), using a technique termed infiltration [345–348]. As the produced nanoparticles have a higher active surface area than those produced by conventional methods, the cell performance is normally significantly better. In addition, SOFC electrocatalysts introduced by infiltration can be fired at much lower temperatures compared to those prepared using conventional fabrication techniques, such as mixed powder synthesis, to form the desired phase. This lower firing temperature is very beneficial in allowing the use of a variety of catalyst materials that cannot be sintered at high temperatures due to their low melting points (mostly for metallic catalysts) or their lack of chemical compatibility with other SOFC components.

Many anode and cathode catalysts have been fabricated using the infiltration technique. For anodes, metal-based catalysts, such as Ni, Co, and Cu, have been infiltrated into a pre-sintered scaffold (such as YSZ) [292, 349–352]. Infiltration of oxides, such as ceria-based materials [353] and also perovskites, such as $La_{0.8}Sr_{0.2}Cr_{0.5}Mn_{0.5}O_3$ (LSCM) [354] and $La_{0.3}Sr_{0.7}TiO_3$ (LST) [355], have also been studied. At the cathode, many catalyst layers have been synthesized using infiltration techniques, including the infiltration of $La_{0.65}Sr_{0.30}MnO_3$ (LSM) [356], $La_{0.6}Sr_{0.4}Co_{0.2}Fe_{0.8}O_{3-\delta}$ (LSCF) [357], and $Sm_{0.5}Sr_{0.5}CoO_{3-x}$ (SSC) [358], as well as various noble metals [359].

However, despite the advantages of infiltration techniques in terms of flexibility in the material choice and in the formation of higher surface area nanoparticles, the nanoparticles are often unstable at SOFC working temperatures, tending to grow in size (sinter) with time, resulting in a gradually deteriorating performance [349]. For this reason, efforts are underway to stabilize the infiltrated catalysts by employing a range of techniques, including the use of polymer-based vs. aqueous-based infiltration solutions [350, 360], exsolving of the infiltrated material from the substrate [349], and the use of a second ceramic phase to inhibit the growth of the infiltrated particles [361].

Molten Carbonate Fuel Cells

Molten carbonate fuel cells (MCFCs) utilize an alkali metal carbonate that is immobilized in a porous ceramic matrix (maintained by capillary forces), as the electrolyte. As such, the primary charge carrier in this case is the carbonate ion (CO_3^{2-}), making the electrode reactions unique among the various fuel cell types, as seen in Fig. 17. The primary cathode reaction (13) involves the reduction of O_2, which together with CO_2, which is also fed into the cathode compartment, forms carbonate ions, as follows:

$$\tfrac{1}{2}\,O_2 + CO_2 + 2e^- \rightarrow CO_3^{2-} \qquad (13)$$

At the anode (reaction (14)), H_2 is oxidized, forming water with an O^{2-} ion from the carbonate ion, thus releasing CO_2, as follows:

$$CO_3^{2-} + H_2 \rightarrow H_2O + CO_2 + 2e^- \qquad (14)$$

The requirement for CO_2 to be mixed with air at the cathode (13) creates some challenges, as CO_2 released at the anode must be recycled to the cathode. Significant materials and system design challenges result, since the gas should ideally remain at temperature in the journey from anode to cathode. However, if the CO_2 can be delivered to the cathode from the exhaust gas of a conventional combustion reaction, such as in a coal power plant, this requirement for CO_2 in the cathode gas becomes a distinct advantage of MCFCs. This is because the anode exhaust gas

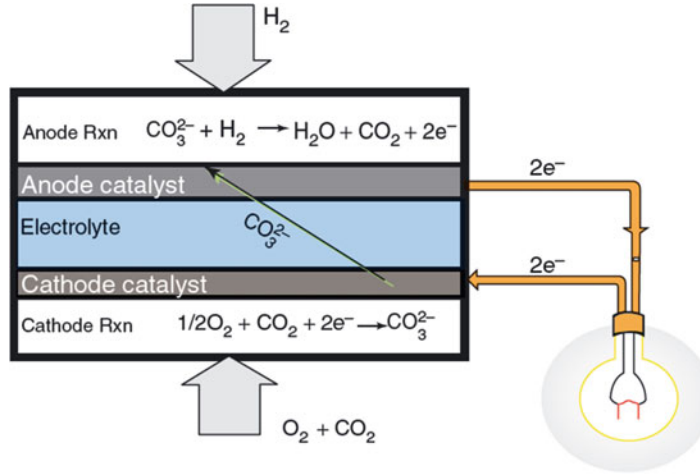

Fig. 17 Schematic diagram of a molten carbonate fuel cell showing electrode reactions. Reprinted from 362, with permission of John Wiley and Sons

contains primarily CO_2, H_2O (which is easily condensed out), and unreacted fuel, making CO_2 easily captured for subsequent storage. MCFCs therefore have the advantage that they can not only capture CO_2 through their own reactions, but they can also serve to concentrate CO_2 from the exhaust of other combustion processes. It is estimated that the capacity for CO_2 capture of a 1 MW MCFC is approximately 11,000 t/y of CO_2 fed to the cathode, excluding its own inherent CO_2 production [363, 364].

The electrical efficiency of MCFCs, which can be as high as 50% [363, 365], makes them additionally promising for stationary power generation, as an efficient alternative to coal-fired power plants and for backup power. Similar to SOFCs, these cells operate at high temperatures (600–650 °C), which results in fast kinetics (no precious metal catalysts are required) with no CO poisoning (CO is a fuel) and produces high-quality waste heat (cogeneration is possible). Notably, this temperature is still low enough to avoid significant NO_x production, and the majority of the NOx produced is destroyed within the fuel cell [362]. The production of heat by the MCFC can boost the overall efficiency of the system to between 85 and 90% [366], making MCFCs very attractive for distributed generation.

Because CO is a fuel, rather than a poison, in these systems, MCFCs (like SOFCs) can operate on a variety of gasified fuel feedstock, including H_2, CO, CH_4, etc. Thus, any hydrocarbon fuel (e.g., diesel [367]) from any source (e.g., biomass [368]) can be reformed to H_2 and CO and supplied to the anode. Further, the use of fuels that reform in the stack (e.g., CH_4) can serve to remove some of the excess heat of the reaction at the source and decrease the need for other stack-cooling measures (e.g., increased airflow rate at the cathode) that would lower the efficiency [369]. While there are technical issues (coking [368] and poisoning caused by sulfur, halogen, and siloxane gas contamination [362]), fuel flexibility is a key advantage that allows MCFCs (and SOFCs) to serve as a bridge between the use of the conventional fuels today and the hydrogen economy of the future, when H_2 prices are expected to decrease [363].

The primary difficulty with developing high temperature fuel cells, such as MCFCs, is that the materials must be compatible with each other (thermal expansion coefficients must match, and there should be no chemical reactions between adjacent layers), including at the relatively high operating temperatures (>500 °C) for >40,000 h. Also, although MCFCs are the furthest along in terms of commercialization, there are challenges with using an ionic melt

electrolyte. These include ensuring that there are no discontinuities of the electrolyte where air and fuel can intermix, and the electrolyte must be replaced as quickly as it vaporizes. The molten carbonate electrolyte is also very corrosive to the metals that are typically present in the stack (electrodes and interconnects), thus resulting in the dissolution (corrosion) of the components [370, 371]. In the case of NiO cathode dissolution, for example, the dissolved metal can precipitate within the electrolyte matrix as Ni metal and cause short circuiting between the anode and cathode [363, 371].

Ionic Melt Electrolytes

As discussed previously, the electrolyte is typically composed of a molten salt mixture suspended in an inert ceramic matrix between the anode and cathode by capillary forces. Pore equilibrium and capillary control models were developed for MCFCs in the 1970s [372], and this understanding has allowed the electrolyte ceramic matrix to remain filled and the electrodes to remain partially filled [362, 373]. The electrolyte is typically Li_2CO_3 (50–70 mol%) mixed with K_2CO_3 or Na_2CO_3, since it has low volatility, high ion conductivity, good wetting of the electrodes (especially the cathode), and good compatibility with the other cell and stack components at typical operating temperature of 650 °C [371]. $LiAlO_2$ is the primary material used as a support matrix for the electrolyte, since it can have high porosity (50–70%) with a narrow pore size distribution, good strength, and a high ohmic resistance [374–376].

As seen in Fig. 18, a period of constant degradation is typically followed by rapid and catastrophic degradation rates that lead to cell's end of life, which is caused by gas crossover and NiO dissolution at the cathode. Carbonate volatilization is a factor, but gas crossover is primarily caused by sintering of the ceramic $LiAlO_2$ matrix during long-term operation [377] [378, 379]. As the ceramic matrix sinters, the pore size increases, and the electrolyte material is lost as the capillary liquid electrolyte retention forces change [377]. NiO dissolution at the cathode causes significant problems because Ni^{2+} will migrate to the anode, reduce to Ni metal, and eventually short circuit the anode and cathode.

While these two processes (gas crossover and NiO dissolution) may not seem related, both have been shown to be related to the basicity of the carbonate melt [378]. $LiAlO_2$ sintering proceeds through a dissolution-precipitation mechanism that proceeds more rapidly as the basicity increases [379], and the dissolution of NiO at the cathode proceeds faster as the basicity decreases. The basicity of the melt has a strong

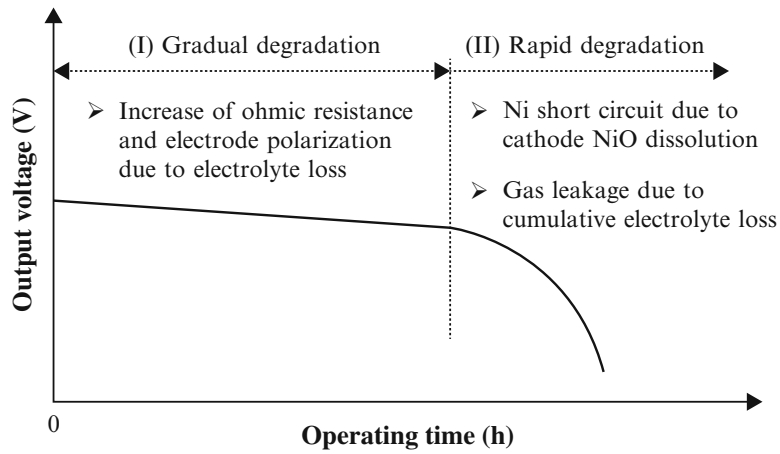

Fig. 18 Schematic representation of the typically observed MCFC degradation over time with a constant current. Reprinted from 380, with permission of Elsevier

relationship with the CO_2 content of the gas phase (in the anode and cathode compartments), decreasing as the CO_2 content increases. This relationship is typical in an oxyanion melt in which the oxide ion defines the acidity of the aqueous system. As such, NiO dissolves according to the following acid mechanism (reaction (15)), as an example [371]:

$$NiO(s) + CO_2(g) Ni^{2+}(l) + CO_3^{2-} \qquad (15)$$

For this reason, lowering the CO_2 pressure in the gas will increase the basicity of the carbonate melt, decrease the propensity for NiO dissolution, and increase the $LiAlO_2$ sintering rate. In addition, the basicity can be increased by increasing the Li_2CO_3 content or by substituting Na_2CO_3 for K_2CO_3 or by the addition of foreign cations, such as rare earth and alkaline earth cations [381]. However, Na_2CO_3 is not preferred as the electrolyte, as it has low oxygen solubility and high reactivity with the stainless steel components of the stack. The low oxygen solubility has a dramatic effect on cell performance, as the limiting current with a Li/K melt is three times higher than for Li/Na melts [371]. Current research emphasis is on the ternary Li/K/Na melts and on alternative cathode materials systems, discussed below.

Another significant issue related to the lifetime of the electrolyte is the very large thermal expansion mismatch between the $LiAlO_2$ matrix, which has a thermal expansion coefficient of 10×10^{-6} °C^{-1} and the solidified carbonate electrolyte, which can have a thermal expansion coefficient of 20×10^{-6} °C^{-1}. Many different approaches have therefore been taken to attempt to improve the mechanical strength of the $LiAlO_2$ matrix, including the addition of 1–6 vol% refractory metal alloys (e.g., Fe alloyed with Cr, Al, and Co) [382], the addition of large particles that relieve stress by forming tiny discontinuous cracks [383], and the addition of ceramic fibers, rods or particulates, or metal mesh [371]. Each of these attempts has been successful in making the matrix stronger. However, the stability of the materials after exposure to the carbonate melt is a key to long-term stability [371].

In recent years, it has been noted that improving the solubility of O_2 in the carbonate melt can increase the cathode performance in a MCFC [384, 385]. Oxygen solubility is typically on the order of 1 ppm mol/cm^3 at 650 °C, but with the addition of 3 mol% MgO and 0.5 mol% La_2O_3, the oxygen solubility increases to 6 ppm mol/cm [384, 386]. Nitrate anions can be added to increase oxidizing power [387] for chemical disposal applications, but there is negligible effect on oxygen solubility.

Anode Catalyst Materials

The current state-of-the-art MCFC anode is composed of Ni metal alloyed with Cr and/or Al to provide microstructural stability by forming interspersed oxides and intermetallics [363]. Mechanical creep of the Ni anode at operating temperatures can be substantial without these Cr/Al alloy additions, while endurance tests show good stability and performance for ~5 y. Ni–Cr has exhibited good performance as an anode because it has good wettability, due to Cr oxidation (forming small pores) and lithiation (forming $LiCrO_2$) [388].

To accelerate commercialization, however, research is focused on materials and alloy additions that will both improve performance and long-term stability and lower the costs associated with the current materials system. Ceramic additives, impregnation, and coating processes have all been investigated to this aim. CeO_2, doped CeO_2, TiO_2, YSZ, LSC, $LiAlO_2$, and Li_2TiO_3 have all been investigated as additives to the Ni-based anode to improve wettability, but LSC has shown the best improvement overall [389]. The addition of Zr, Cu, Ni_3Al, Al_2O_3, and $LiAlO_2$ to the Ni anode have all been shown to lower Ni creep, but long-term stability continues to be an issue for these materials [388, 390–393]. To lower cost, alternative anode materials have also been investigated, such as $LiFeO_2$ and Cu–Al [388]. $LiFeO_2$ and Cu–Al suffer from poor creep and electrochemical performance, and, further, Cu–Al suffers from rapid oxidation during the stack conditioning stage and system interruption. Ni additions to

the Cu–Al system have shown improvements in these areas, however [388].

Performance and endurance of MCFC anodes are influenced not only by the materials employed but also by the electrolyte fill level, pore structure, and wettability. The anode environment plays a role in anode wetting, for example, as it has been shown [388, 392] that the contact angle increases as the CO_2 partial pressure increases.

Cathode Catalyst Materials

As Reaction (13) shows, the cathode gas requires CO_2 to be present in addition to O_2 in order to recharge the carbonate ions that are consumed at the anode (Reaction (14)). Thus, a minimum of 2–3% CO_2 is required in order to prevent lowering of the cell performance due to insufficient electrolyte charge carriers being present [394]. The typical cathode gas used has a 15% content of CO_2 gas in order to replenish the carbonate ions that are consumed at the anode, and, due to mixing with the anode gas, the O_2 content is typically only 10% [395].

The state-of-the-art cathode in MCFCs is NiO that has been lithiated in situ by the Li_2CO_3 component of the electrolyte [396]. The conductivity of the NiO cathode is enhanced by Li doping because of an enrichment of Ni^{3+} cations, which enhances the intrinsic p-type conductivity of NiO [371]. Wetting of the cathode is much less of a problem in comparison with the anode, as lithiated NiO has very low contact angles with the Li_2CO_3-containing electrolyte [389].

As discussed above, a significant problem in MCFC cathodes is the chemical deterioration of NiO in the presence of molten salts and the CO_2 environment. Free Ni^{2+} ions are released into the solution (~15 mol ppm/cm^3 solubility), remaining in equilibrium with the cathode while moving toward the anode as a result of a concentration gradient. Once at the anode, Ni^{2+} is reduced, and, eventually, Ni metal forms Ni dendrites that can short circuit the electrodes [374]. To overcome the problem, the electrolyte basicity can be increased, or, alternatively, additives, coatings, and new materials can be used to mitigate the problem.

Other lithiated oxides have been investigated as cathodes, including $LiFeO_2$, $LiCoO_2$, and $LiMnO_2$, all of which have shown promise with good electrical conductivity and good stability [371]. $LiFeO_2$, for example, has a dissolution rate of zero, and $LiCoO_2$ has a dissolution rate that is an order of magnitude lower than what is seen with NiO. However, low mechanical strength, high manufacturing costs, and poor electrochemical performance hinder the use of these materials [397]. Co and Fe doping of lithiated NiO in a ternary system and coatings of $LiCoO_2$ on NiO have garnered recent attention. In the case of 20% Co doping of $LiFeO_2$ and NiO_2 (mixed in a 1:3 ratio), the electrochemical performance is almost as good as what is seen for commercially used NiO [398]. Alternative ceramic materials, such as Li_2MnO_3 and $La_{1-x}SrCoO_3$, have also been investigated, but their electrochemical performance is inadequate [399].

Manufacturing of MCFCs

Manufacturing costs of MCFCs can be significant, principally due to the large cell areas required in order to compensate for the very high cell resistance and low power output. The costs associated with the need for a large reactive area are typically mitigated by manufacturing large cells, as seen in Fig. 19. Pre-sintering of components, such as the electrolyte matrix, can also add significant cost to the MCFC. One method of avoiding any pre-sintering steps is to add between 3 and 45% Al to the raw $LiAlO_2$ powder and then precondition the electrolyte. In this way, Al reacts, as follows [400], and becomes a fully bonded matrix in situ.

$$2Al + Li_2CO_3 + 3/2O_2 \rightarrow 2LiAlO_2 + CO_2 \quad (16)$$

Fig. 19 Full size molten carbonate fuel cell and stack. Reprinted from [362], with permission of John Wiley and Sons

Aluminum acetylacetonate has also been investigated [401] as a sintering aid, and Li-containing materials have also been added so that the electrolyte is not depleted of Li_2CO_3 before operation [371].

Many manufacturing processes have been investigated in recent years for the production of anodes, including tape casting, dry doctoring, and screen printing. However, the cost of many of these processes, in addition to the sintering steps that are normally required, is generally high. At Fuel Cell Energy (the present-day world leader in MCFC development), anode tapes are typically produced by tape casting and then laminated to the porous $LiAlO_2$ electrolyte support. The anode is then sintered during the stack conditioning process in situ, which has greatly simplified and lowered the cost of the process [388, 402].

Direct Carbon (Molten Liquid) Fuel Cells (DCFCs)

Significant work is also being carried out to develop direct carbon fuel cells (DCFC), which are attractive, because solid carbon fuel has a very high energy density, as it is thought that the theoretical electrical efficiency could be as high as 72% for relatively small systems (<100 kW) [363, 403] and as the solid fuel source can be carbon [404, 405], coal [405, 406], coke, tar, or even biomass and organic waste [407, 408]. In addition, a very concentrated CO_2 by-product gas is produced, which can then be sequestered with little processing.

The electrolyte and electrode materials used in DCFCs can be quite diverse, since these fuel cells can utilize a molten carbonate, a molten hydroxide [403], or a solid ceramic yttria-stabilized zirconia (YSZ) electrolyte. In addition to the typically high-temperature material compatibility issues that are encountered in MCFCs and SOFCs, the DCFC has significant problems, primarily dealing with the high ash (inorganic) content present in most carbon sources, the carbon corrosion (i.e., consumption by the reverse Boudouard reaction), and the need for continuous fuel feeding [403].

There are two primary fuel feeding methods that are utilized in DCFCs. Fuel is fed in either by using a liquid carrier and a fluidized bed or using a batch process (e.g., fuel is periodically input during shutdown) to bring a constant supply of carbon into the anode chamber of the cell. The carrier fluid can be comprised of liquid Sb [407] or molten hydroxide/carbonate [408]. In a batch process, the carbon usually does not have direct contact with the anode. Instead, fuel containing a Fe-based catalyst (the Fe oxidation state does not affect the catalytic properties) is brought into the anode chamber prior to start-up [409], and residual oxygen from the loading reacts with carbon, producing CO. CO diffuses to the anode and reacts electrochemically to form CO_2, which then diffuses back to the fuel source and forms more CO by the reverse Boudouard reaction

(CO_2 + C↔2 CO). CO_2 containing some CO then exits through the exhaust as the pressure builds up [409].

Summary

Fuel cell technology, which is a clean and highly efficient alternative to combustion technologies, has been steadily moving toward commercialization over the last few years. Polymer electrolyte membrane fuel cells (PEMFCs) are making significant inroads into applications in the transportation sector and direct alcohol fuel cells (DAFCs) in mobile applications, and solid oxide fuel cells (SOFCs) and molten carbonate fuel cells (MCFCs) are being implemented into a variety of stationary applications.

Table 1 summarizes the current status of the five main fuel cell types, where DAFCs are represented by direct methanol fuel cells, which are among the furthest along in terms of commercialization. This table, which also includes alkaline fuel cells (not discussed in this chapter), provides a useful summary of the typical reactants used, the electrode materials, the average efficiency, target costs, and more, similar to (but updated) and relative to what has been shown in other reviews [10, 28, 410–413].

Table 1 Current status of fuel cell technologies [10, 28, 410–413]

	PEMFC	DMFC	AFC	SOFC	MCFC
Fuel	H_2	Alcohol, e.g., methanol, ethanol	H_2	H_2, CO, CH_4, etc.	H_2, CO, CH_4, etc.
Oxidant	O_2, air	O_2, air	O_2	O_2, air	O_2, air (+ CO_2)[e]
Electrolyte	Polymer electrolyte (membrane), e.g., polyfluorosulfonic acid, Nafion	Polymer electrolyte (membrane), e.g., polyfluorosulfonic acid, Nafion	KOH	Zirconia or ceria based, perovskites	Molten carbonate (Li_2CO_3, Na_2CO_3, K_2CO_3)
Anode catalyst	Pt- or Pt alloy-loaded carbon (e.g., PtNi, PtCo)	PtRu alloy-loaded carbon	Pt, other transition metals	Ni + yttria-stabilized zirconia (YSZ); ceria, perovskites	Ni–Cr, Ni–Al
Cathode catalyst	Pt- or Pt alloy-loaded carbon (e.g., PtNi, PtCo)	Pt- or Pt alloy-loaded carbon (e.g., PtNi, PtCo)	Pt, other transition metals	LaSrMn oxide perovskite + YSZ, LaSrCoFe perovskite, other mixed oxides	Lithiated NiO
Anode reaction	$2H_2 \rightarrow 4H^+ + 4e^-$	$CH_3OH + H_2O \rightarrow 6H^+ + CO_2 + 6e^-$	$2H_2 + 4OH^- \rightarrow 2H_2O + 4e^-$	$H_2 + O^{2-} \rightarrow H_2O + 2e^-$	$H_2 + CO_3^{2-} \rightarrow H_2O + CO_2 + 2e^-$
Cathode reaction	$O_2 + 4H^+ + 4e^- \rightarrow 2H_2O$	$O_2 + 4H^+ + 4e^- \rightarrow 2H_2O$	$O_2 + 2H_2O + 4e^- \rightarrow 4OH^-$	$½O_2 + 2e^- \rightarrow O^{2-}$	$½O_2 + CO_2 + 2e^- \rightarrow CO_3^{2-}$
Current collector	Carbon or graphite, transition metals (Ti, stainless steel, etc.)	Carbon, transition metals (Ti, stainless steel, etc.)	Carbon, metal	Ni, ceramic, steel	Ni, stainless steel
End plate/ lead to ext. circuit	Carbon or graphite, metal	Carbon or graphite, metal	metal	Ni, stainless steel	Ni, stainless steel
Operating temp (°C)	~ 80, 20–120	~ 80, 20–120	65–220	500–1000	600–800
Power density (mW/cm^2)	100–2500	50–500	100–400	200–800	100–300

(continued)

Table 1 (continued)

	PEMFC	DMFC	AFC	SOFC	MCFC
Power range	0.1 W–100 MW	2 W–250 W[b]	1–100 kW	1 W–100 MW	1 kW–100 MW
Electrical efficiency (%)	40–60	40	50	50–60	45–55
Operation hours	5000–50,000	1500–5000	–	>40,000	50,000
Interferences in fuel stream	CO, H_2S	CO, H_2S	CO	H_2S, halides, siloxanes	H_2S, halides, siloxanes
Cost	55 ($/kW)[a] (2013)	150–15 ($/W)[b] (2011)	–	$7000/kW[c]	2500 ($/kW)
Target cost	40 ($/kW)[a] (2020)	70–5 ($/W)[b] (2015)	–	<$800/kWe[d]	<1000 ($/kW)

[a]Projected to high-volume transportation fuel cell system cost (2014 DOE Annual Merit Review and Peer Evaluation Meeting)
[b]Portable power methanol fuel cells systems (2012 DOE Technical Targets)
[c]Bloom energy (2010)
[d]DOE's SECA program target
[e]CO_2 must be supplied at the cathode to replenish the carbonate ion in the melt

References

1. Srinivasan S (2006) Fuel cells: from fundamentals to applications. Springer, New York
2. O'Hayre R, Cha S-W, Colella W, Prinz FB (2009) Fuel cell fundamentals, 2nd edn. Wiley, New York
3. Hickner MA, Ghassemi H, Kim YS, Einsla BR, McGrath JE (2004) Alternative polymer systems for proton exchange membranes (PEMs). Chem Rev 104:4587–4612
4. Hayashi A, Notsu H, Kimijima KI, Miyamoto J, Yagi I (2008) Preparation of Pt/mesoporous carbon (MC) electrode catalyst and its reactivity toward oxygen reduction. Electrochim Acta 53:6117–6125
5. Ticianelli EA, Derouin CR, Redondo A, Srinivasan S (1988) Methods to advance technology of proton-exchange membrane fuel-cells. J Electrochem Soc 135:2209–2214
6. Do J-S, Liou B-C (2011) A mixture design approach to optimizing the cathodic compositions of proton exchange membrane fuel cell. J Power Sources 196:1864–1871
7. Gode P, Jaouen F, Lindbergh G, Lundblad A, Sundholm G (2003) Influence of the composition on the structure and electrochemical characteristics of the PEFC cathode. Electrochim Acta 48:4175–4187
8. Passalacqua E, Lufrano F, Squadrito G, Patti A, Giorgi L (2001) Nafion content in the catalyst layer of polymer electrolyte fuel cells: effects on structure and performance. Electrochim Acta 46:799–805
9. Wang QP, Eikerling M, Song DT, Liu ZS (2004) Structure and performance of different types of agglomerates in cathode catalyst layers of PEM fuel cells. J Electroanal Chem 573:61–69
10. James BD, Baum KN, Spisak AB (2012) Mass production cost estimation of direct H2 PEM fuel cell systems for automotive applications: 2011 update; AGB-0-40628-01; Strategic Analysis Inc.: Arlington, 5 Sept 2012
11. Kreuer KD, Fuchs A, Ise M, Spaeth M, Maier J (1998) Imidazole and pyrazole-based proton conducting polymers and liquids. Electrochim Acta 43:1281–1288
12. Lott KF, Ghosh BD, Ritchie JE (2005) Measurement of anion diffusion and transference numbers in an anhydrous proton conducting electrolyte. Electrochem Solid-State Lett 8:A513–A515
13. Zawodzinski TA, Derouin C, Radzinski S, Sherman RJ, Smith VT, Springer TE, Gottesfeld S (1993) Water-uptake by and transport through Nafion® 117 membranes. J Electrochem Soc 140:1041–1047
14. Springer TE, Zawodzinski TA, Gottesfeld S (1991) Polymer electrolyte fuel-cell model. J Electrochem Soc 138:2334–2342
15. Hsu WY, Gierke TD (1983) Ion transport and clustering in nafion perfluorinated membranes. J Membr Sci 13:307–326
16. Gierke TD, Munn GE, Wilson FC (1981) The morphology in nafion perfluorinated membrane products, as determined by wide- and small-angle x-ray studies. J Polym Sci Polym Phys Ed 19:1687–1704
17. Hsu WY, Gierke TD (1982) Elastic theory for ionic clustering in perfluorinated ionomers. Macromolecules 15:101–105
18. Fujimura M, Hashimoto T, Kawai H (1981) Small-angle x-ray scattering study of perfluorinated ionomer membranes. 1. Origin of two scattering maxima. Macromolecules 14:1309–1315
19. Fujimura M, Hashimoto T, Kawai H (1982) Small-angle x-ray scattering study of perfluorinated ionomer membranes. 2. Models for ionic scattering maximum. Macromolecules 15:136–144

20. Dreyfus B, Gebel G, Aldebert P, Pineri M, Escoubes M, Thomas M (1990) Distribution of the "micelles" in hydrated perfluorinated ionomer membranes from SANS experiments. J Phys 51:1341–1354
21. Litt M (1997) A reevaluation of Nafion® morphology. Abstracts of Papers of the American Chemical Society 213, 33-POLY
22. Haubold HG, Vad T, Jungbluth H, Hiller P (2001) Nano structure of NAFION: a SAXS study. Electrochim Acta 46:1559–1563
23. Rubatat L, Rollet AL, Gebel G, Diat O (2002) Evidence of Elongated Polymeric Aggregates in Nafion. Macromolecules 35:4050–4055
24. Gebel G (2000) Structural evolution of water swollen perfluorosulfonated ionomers from dry membrane to solution. Polymer 41:5829–5838
25. Andersen SM, Borghei M, Dhiman R, Ruiz V, Kauppinen E, Skou E (2014) Adsorption behavior of perfluorinated sulfonic acid ionomer on highly graphitized carbon nanofibers and their thermal stabilities. J Phys Chem C 118:10814–10823
26. Wood DL, Chlistunoff J, Majewski J, Borup RL (2009) Nafion structural phenomena at platinum and carbon interfaces. J Am Chem Soc 131:18096–18104
27. Paul DK, Fraser A, Karan K (2011) Towards the understanding of proton conduction mechanism in PEMFC catalyst layer: conductivity of adsorbed Nafion films. Electrochem Commun 13:774–777
28. Carlson EJ, Kopf P, Sinha J, Sriramulu S, Yang Y (2005) Cost analysis of PEM fuel cell systems for transportation; NREL/SR-560-39104; U.S. Department of Energy, Cambridge, 30 Sept 2005
29. Ji M, Wei Z (2009) A review of water management in polymer electrolyte membrane fuel cells. Energies 2:1057
30. Curtin DE, Lousenberg RD, Henry TJ, Tangeman PC, Tisack ME (2004) Advanced materials for improved PEMFC performance and life. J Power Sources 131:41–48
31. Hongsirikarn K, Mo X, Goodwin JG Jr, Creager S (2011) Effect of H2O2 on Nafion® properties and conductivity at fuel cell conditions. J Power Sources 196:3060–3072
32. Qiao JL, Saito M, Hayamizu K, Okada T (2006) Degradation of perfluorinated ionomer membranes for PEM fuel cells during processing with H2O2. J Electrochem Soc 153:A967–A974
33. Chen C, Levitin G, Hess DW, Fuller TF (2007) XPS investigation of Nafion® membrane degradation. J Power Sources 169:288–295
34. Mittal VO, Kunz HR, Fenton JM (2006) Is H2O2 involved in the membrane degradation mechanism in PEMFC? Electrochem Solid-State Lett 9:A299–A302
35. Roziere J, Jones DJ (2003) Non-fluorinated polymer materials for proton exchange membrane fuel cells. Annu Rev Mater Res 33:503–555
36. LaConti AB, Hamdan M, McDonald RC (2010) Mechanisms of membrane degradation. In: Handbook of fuel cells. Wiley, New York
37. Escobedo G, Raiford K, Nagarajan GS, Schwiebert KE (2006) Strategies for mitigation of PFSA polymer degradation in PEM fuel cells. ECS Trans 1 (8):303–311
38. Stone C, Calis GHM (2006) 2006 Fuel Cell Seminar Abstracts, Hawaii. Courtesy Associates, Hawaii
39. Liu W, Ruth K, Rusch G (2001) Membrane durability in PEM fuel cells. J New Mater Electrochem Syst 4:227–232
40. Cleghorn SJC, Mayfield DK, Moore DA, Moore JC, Rusch G, Sherman TW, Sisofo NT, Beuscher U (2006) A polymer electrolyte fuel cell life test: 3 years of continuous operation. J Power Sources 158:446–454
41. Zhang J, Litteer BA, Gu W, Liu H, Gasteiger HA (2007) Effect of hydrogen and oxygen partial pressure on pt precipitation within the membrane of PEMFCs. J Electrochem Soc 154:B1006–B1011
42. Borup R, Meyers J, Pivovar B, Kim YS, Mukundan R, Garland N, Myers D, Wilson M, Garzon F, Wood D (2007) Scientific aspects of polymer electrolyte fuel cell durability and degradation. Chem Rev 107:3904–3951
43. Ramaswamy P, Wong NE, Shimizu GKH (2014) MOFs as proton conductors—challenges and opportunities. Chem Soc Rev 43:5913–5932
44. Hurd JA, Vaidhyanathan R, Thangadurai V, Ratcliffe CI, Moudrakovski IL, Shimizu GKH (2009) Anhydrous proton conduction at 150 °C in a crystalline metal–organic framework. Nat Chem 1:705–710
45. Stassi A, Gatto I, Passalacqua E, Antonucci V, Arico AS, Merlo L, Oldani C, Pagano E (2011) Performance comparison of long and short-side chain perfluorosulfonic membranes for high temperature polymer electrolyte membrane fuel cell operation. J Power Sources 196:8925–8930
46. Rikukawa M, Sanui K (2000) Proton-conducting polymer electrolyte membranes based on hydrocarbon polymers. Prog Polym Sci 25:1463–1502
47. Kaliaguine S, Mikhailenko SD, Wang KP, Xing P, Robertson G, Guiver M (2003) Properties of SPEEK based PEMs for fuel cell application. Catal Today 82:213–222
48. Robertson GP, Mikhailenko SD, Wang K, Xing P, Guiver MD, Kaliaguine S (2003) Casting solvent interactions with sulfonated poly(ether ether ketone) during proton exchange membrane fabrication. J Membr Sci 219:113–121
49. Asensio JA, Borros S, Gomez-Romero P (2002) Proton-conducting polymers based on benzimidazoles and sulfonated benzimidazoles. J Polym Sci A Polym Chem 40:3703–3710
50. Wainright JS, Wang JT, Weng D, Savinell RF, Litt M (1995) Acid-doped polybenzimidazoles—a new polymer electrolyte. J Electrochem Soc 142:L121–L123

51. Sheng L, Xu H, Guo X, Fang J, Fang L, Yin J (2011) Synthesis and properties of novel sulfonated polybenzimidazoles from disodium 4,6-bis (4-carboxyphenoxy)benzene-1,3-disulfonate. J Power Sources 196:3039–3047
52. Bozkurt A, Meyer WH (2001) Proton-conducting poly(vinylpyrrolidone)–polyphosphoric acid blends. J Polym Sci B Polym Phys 39:1987–1994
53. Kreuer KD (1997) On the development of proton conducting materials for technological applications. Solid State Ionics 97:1–15
54. Erdemi H, Bozkurt A, Meyer WH (2004) PAMPSA–IM based proton conducting polymer electrolytes. Synth Met 143:133–138
55. Sevil F, Bozkurt A (2004) Proton conducting polymer electrolytes on the basis of poly (vinylphosphonic acid) and imidazole. J Phys Chem Solids 65:1659–1662
56. Günday ST, Bozkurt A, Meyer WH, Wegner G (2006) Effects of different acid functional groups on proton conductivity of polymer-1,2,4-triazole blends. J Polym Sci B Polym Phys 44:3315–3322
57. Göktepe F, Bozkurt A, Günday ŞT (2008) Synthesis and proton conductivity of poly(styrene sulfonic acid)/heterocycle-based membranes. Polym Int 57:133–138
58. Dupuis A-C (2011) Proton exchange membranes for fuel cells operated at medium temperatures: Materials and experimental techniques. Prog Mater Sci 56:289–327
59. Zhengbang W, Tang H, Mu P (2011) Self-assembly of durable Nafion/TiO2 nanowire electrolyte membranes for elevated-temperature PEM fuel cells. J Membr Sci 369:250–257
60. Xing D, He G, Hou Z, Ming P, Song S (2011) Preparation and characterization of a modified montmorillonite/sulfonated polyphenylether sulfone/PTFE composite membrane. Int J Hydrog Energy 36:2177–2183
61. Sancho T, Soler J, Pina MP (2007) Conductivity in zeolite–polymer composite membranes for PEMFCs. J Power Sources 169:92–97
62. Zarrin H, Higgins D, Jun Y, Chen ZW, Fowler M (2011) Functionalized graphene oxide nanocomposite membrane for low humidity and high temperature proton exchange membrane fuel cells. J Phys Chem C 115:20774–20781
63. Debe MK (2012) Electrocatalyst approaches and challenges for automotive fuel cells. Nature 486:43–51
64. Holton OT, Stevenson JW (2013) The role of platinum in proton exchange membrane fuel cells evaluation of platinum's unique properties for use in both the anode and cathode of a proton exchange membrane fuel cell. Platin Met Rev 57:259–271
65. O'Hayre R, Cha S-W, Colella W, Prinz FB (2009) Fuel cell fundamentals, 2nd edn. Wiley, New York, pp 95–96
66. Stamenkovic VR, Fowler B, Mun BS, Wang G, Ross PN, Lucas CA, Marković NM (2007) Improved oxygen reduction activity on Pt3Ni(111) via increased surface site availability. Science 315:493–497
67. Mistry H, Varela AS, Kühl S, Strasser P, Cuenya BR (2016) Nanostructured electrocatalysts with tunable activity and selectivity. Nat Rev Mater 1:16009
68. Bi W, Gray GE, Fuller TF (2007) PEM fuel cell Pt/C dissolution and deposition in nafion electrolyte. Electrochem Solid-State Lett 10:B101–B104
69. Borup RL, Davey JR, Garzon FH, Wood DL, Inbody MA (2006) PEM fuel cell electrocatalyst durability measurements. J Power Sources 163:76–81
70. Das PK, Li X, Liu Z-S (2010) Analysis of liquid water transport in cathode catalyst layer of PEM fuel cells. Int J Hydrog Energy 35:2403–2416
71. Li A, Chan SH, Nguyen N-t (2009) Anti-flooding cathode catalyst layer for high performance PEM fuel cell. Electrochem Commun 11:897–900
72. Li H, Tang Y, Wang Z, Shi Z, Wu S, Song D, Zhang J, Fatih K, Zhang J, Wang H, Liu Z, Abouatallah R, Mazza A (2008) A review of water flooding issues in the proton exchange membrane fuel cell. J Power Sources 178:103–117
73. Lim C, Wang CY (2004) Effects of hydrophobic polymer content in GDL on power performance of a PEM fuel cell. Electrochim Acta 49:4149–4156
74. Lin GY, Van Nguyen T (2005) Effect of thickness and hydrophobic polymer content of the gas diffusion layer on electrode flooding level in a PEMFC. J Electrochem Soc 152:A1942–A1948
75. Stevens DA, Hicks MT, Haugen GM, Dahn JR (2005) Ex situ and in situ stability studies of PEMFC catalysts. J Electrochem Soc 152:A2309–A2315
76. Gasteiger HA, Kocha SS, Sompalli B, Wagner FT (2005) Activity benchmarks and requirements for Pt, Pt-alloy, and non-Pt oxygen reduction catalysts for PEMFCs. Appl Catal B Environ 56:9–35
77. US-DRIVE. Fuel cell technical team roadmap http://energy.gov/sites/prod/files/2014/02/f8/fctt_roadmap_june2013.pdf. Accessed 22 Mar
78. Jha N, Ramesh P, Bekyarova E, Tian X, Wang F, Itkis ME, Haddon RC (2013) Functionalized single-walled carbon nanotube-based fuel cell benchmarked against US DOE 2017 technical targets. Sci Rep 3:2257
79. Chen Z, Higgins D, Yu A, Zhang L, Zhang J (2011) A review on non-precious metal electrocatalysts for PEM fuel cells. Energy Environ Sci 4:3167–3192
80. Othman R, Dicks AL, Zhu Z (2012) Non precious metal catalysts for the PEM fuel cell cathode. Int J Hydrog Energy 37:357–372
81. Liu Z, Gan LM, Hong L, Chen W, Lee JY (2005) Carbon-supported Pt nanoparticles as catalysts for proton exchange membrane fuel cells. J Power Sources 139:73–78
82. Moreira J, del Angel P, Ocampo AL, Sebastián PJ, Montoya JA, Castellanos RH (2004) Synthesis,

characterization and application of a Pd/Vulcan and Pd/C catalyst in a PEM fuel cell. Int J Hydrog Energy 29:915–920
83. Litster S, McLean G (2004) PEM fuel cell electrodes. J Power Sources 130:61–76
84. Antolini E (2009) Carbon supports for low-temperature fuel cell catalysts. Appl Catal B Environ 88:1–24
85. Banham D, Feng F, Fürstenhaupt T, Pei K, Ye S, Birss V (2011) Effect of Pt-loaded carbon support nanostructure on oxygen reduction catalysis. J Power Sources 196:5438–5445
86. Chang H, Joo SH, Pak C (2007) Synthesis and characterization of mesoporous carbon for fuel cell applications. J Mater Chem 17:3078–3088
87. Wang X, Li W, Chen Z, Waje M, Yan Y (2006) Durability investigation of carbon nanotube as catalyst support for proton exchange membrane fuel cell. J Power Sources 158:154–159
88. Zhang W, Sherrell P, Minett AI, Razal JM, Chen J (2010) Carbon nanotube architectures as catalyst supports for proton exchange membrane fuel cells. Energy Environ Sci 3:1286–1293
89. Joo SH, Choi SJ, Oh I, Kwak J, Liu Z, Terasaki O, Ryoo R (2001) Ordered nanoporous arrays of carbon supporting high dispersions of platinum nanoparticles. Nature 412:169–172
90. Pei K, Banham D, Feng F, Fuerstenhaupt T, Ye S, Birss V (2010) Oxygen reduction activity dependence on the mesoporous structure of imprinted carbon supports. Electrochem Commun 12:1666–1669
91. Banham D, Feng F, Pei K, Ye S, Birss V (2013) Effect of carbon support nanostructure on the oxygen reduction activity of Pt/C catalysts. J Mater Chem A 1:2812–2820
92. Lee J, Kim J, Hyeon T (2006) Recent progress in the synthesis of porous carbon materials. Adv Mater 18:2073–2094
93. Liang C, Li Z, Dai S (2008) Mesoporous carbon materials: synthesis and modification. Angew Chem Int Ed Engl 47:3696–3717
94. Chuenchom L, Kraehnert R, Smarsly BM (2012) Recent progress in soft-templating of porous carbon materials. Soft Matter 8:10801–10812
95. Lee J, Han S, Hyeon T (2004) Synthesis of new nanoporous carbon materials using nanostructured silica materials as templates. J Mater Chem 14:478–486
96. Li ZJ, Jaroniec M (2001) Colloidal imprinting: a novel approach to the synthesis of mesoporous carbons. J Am Chem Soc 123:9208–9209
97. Banham D, Feng F, Furstenhaupt T, Ye S, Birss V (2012) First time investigation of Pt nanocatalysts deposited inside carbon mesopores of controlled length and diameter. J Mater Chem 22:7164–7171
98. Banham DWH (2012) Design and optimization of nanoporous carbon for electrochemical applications. PhD thesis, The University of Calgary, Calgary
99. Lee K, Zhang J, Wang H, Wilkinson DP (2006) Progress in the synthesis of carbon nanotube- and nanofiber-supported Pt electrocatalysts for PEM fuel cell catalysis. J Appl Electrochem 36:507–522
100. Sharma S, Pollet BG (2012) Support materials for PEMFC and DMFC electrocatalysts—a review. J Power Sources 208:96–119
101. Huang S-Y, Ganesan P, Park S, Popov BN (2009) Development of a titanium dioxide-supported platinum catalyst with ultrahigh stability for polymer electrolyte membrane fuel cell applications. J Am Chem Soc 131:13898–13899
102. Yu X, Ye S (2007) Recent advances in activity and durability enhancement of Pt/C catalytic cathode in PEMFC: Part II: degradation mechanism and durability enhancement of carbon supported platinum catalyst. J Power Sources 172:145–154
103. Yu X, Ye S (2007) Recent advances in activity and durability enhancement of Pt/C catalytic cathode in PEMFC: Part I. Physico-chemical and electronic interaction between Pt and carbon support, and activity enhancement of Pt/C catalyst. J Power Sources 172:133–144
104. Shao Y, Liu J, Wang Y, Lin Y (2009) Novel catalyst support materials for PEM fuel cells: current status and future prospects. J Mater Chem 19:46–59
105. de Bruijn FA, Dam VAT, Janssen GJM (2008) Review: durability and degradation issues of PEM fuel cell components. Fuel Cells 8:3–22
106. Shao Y, Wang J, Kou R, Engelhard M, Liu J, Wang Y, Lin Y (2009) The corrosion of PEM fuel cell catalyst supports and its implications for developing durable catalysts. Electrochim Acta 54:3109–3114
107. Shao Y, Yin G, Gao Y (2007) Understanding and approaches for the durability issues of Pt-based catalysts for PEM fuel cell. J Power Sources 171:558–566
108. Akalework NG, Pan C-J, Su W-N, Rick J, Tsai M-C, Lee J-F, Lin J-M, Tsai L-D, Hwang B-J (2012) Ultrathin TiO2-coated MWCNTs with excellent conductivity and SMSI nature as Pt catalyst support for oxygen reduction reaction in PEMFCs. J Mater Chem 22:20977–20985
109. Park M-S, Lee J, Lee J-W, Kim KJ, Jo Y-N, Woo S-G, Kim Y-J (2013) Tuning the surface chemistry of natural graphite anode by H3PO4 and H3BO3 treatments for improving electrochemical and thermal properties. Carbon 62:278–287
110. Shao Y, Zhang S, Kou R, Wang X, Wang C, Dai S, Viswanathan V, Liu J, Wang Y, Lin Y (2010) Noncovalently functionalized graphitic mesoporous carbon as a stable support of Pt nanoparticles for oxygen reduction. J Power Sources 195:1805–1811
111. Shanahan PV, Xu L, Liang C, Waje M, Dai S, Yan YS (2008) Graphitic mesoporous carbon as a durable fuel cell catalyst support. J Power Sources 185:423–427

112. Lv H, Cheng N, Mu S, Pan M (2011) Heat-treated multi-walled carbon nanotubes as durable supports for PEM fuel cell catalysts. Electrochim Acta 58:736–742
113. Zhang Z, Liu J, Gu J, Su L, Cheng L (2014) An overview of metal oxide materials as electrocatalysts and supports for polymer electrolyte fuel cells. Energy Environ Sci 7:2535–2558
114. Tripković V, Abild-Pedersen F, Studt F, Cerri I, Nagami T, Bligaard T, Rossmeisl J (2012) Metal oxide-supported platinum overlayers as proton-exchange membrane fuel cell cathodes. ChemCatChem 4:228–235
115. Lei M, Wang ZB, Li JS, Tang HL, Liu WJ, Wang YG (2014) CeO2 nanocubes-graphene oxide as durable and highly active catalyst support for proton exchange membrane fuel cell. Sci Rep 4:7415
116. Zhang Z, Wang X, Cui Z, Liu C, Lu T, Xing W (2008) Pd nanoparticles supported on WO3/C hybrid material as catalyst for oxygen reduction reaction. J Power Sources 185:941–945
117. Kongkanand A, Mathias MF (2016) The priority and challenge of high-power performance of low-platinum proton-exchange membrane fuel cells. J Phys Chem Lett 7:1127–1137
118. Cindrella L, Kannan AM, Lin JF, Saminathan K, Ho Y, Lin CW, Wertz J (2009) Gas diffusion layer for proton exchange membrane fuel cells—a review. J Power Sources 194:146–160
119. Benziger J, Nehlsen J, Blackwell D, Brennan T, Itescu J (2005) Water flow in the gas diffusion layer of PEM fuel cells. J Membr Sci 261:98–106
120. Dai W, Wang H, Yuan X-Z, Martin JJ, Yang D, Qiao J, Ma J (2009) A review on water balance in the membrane electrode assembly of proton exchange membrane fuel cells. Int J Hydrog Energy 34:9461–9478
121. Ahn M, Cho Y-H, Cho Y-H, Kim J, Jung N, Sung Y-E (2011) Influence of hydrophilicity in microporous layer for polymer electrolyte membrane fuel cells. Electrochim Acta 56:2450–2457
122. Middelman E, Kout W, Vogelaar B, Lenssen J, de Waal E (2003) Bipolar plates for PEM fuel cells. J Power Sources 118:44–46
123. Li XG, Sabir M (2005) Review of bipolar plates in PEM fuel cells: flow-field designs. Int J Hydrog Energy 30:359–371
124. Konno N, Mizuno S, Nakaji H, Ishikawa Y (2015) Development of compact and high-performance fuel cell stack. SAE Int J Altern Powertrains 4:123–129
125. Wu J, Yuan XZ, Martin JJ, Wang H, Zhang J, Shen J, Wu S, Merida W (2008) A review of PEM fuel cell durability: degradation mechanisms and mitigation strategies. J Power Sources 184:104–119
126. Viswanathan B, Scibioh MA (2007) Fuel cells: principles and applications. Universities Press (India) Private Limited, Hyderabad, p 494
127. Friedl J, Stimming U (2013) Model catalyst studies on hydrogen and ethanol oxidation for fuel cells. Electrochim Acta 101:41–58
128. Olah GA, Goeppert A, Prakash GKS (2009) The "Methanol Economy": general aspects. In: Olah GA, Goeppert A, Surya Prakash GK (eds) Beyond oil and gas: the methanol economy. Wiley-VCH Verlag GmbH & Co. KGaA, Weinheim, pp 179–184
129. Olah GA (2005) Beyond Oil and Gas: The Methanol Economy. Angew Chem Int Ed 44:2636–2639
130. Gutmann V, Resch G (1995) Water and alcohols. In: Gutmann V, Resch G (eds) Lecture notes on solution chemistry. World Scientific, Singapore, pp 117–128
131. Olah GA, Goeppert A, Prakash GKS (2009) Production of methanol: from fossil fuels and bio-sources to chemical carbon dioxide recycling. In: Olah GA, Goeppert A, Surya Prakash GK (eds) Beyond oil and gas: the methanol economy. Wiley-VCH Verlag GmbH & Co. KGaA, Weinheim, pp 233–278
132. Izumi Y (2013) Recent advances in the photocatalytic conversion of carbon dioxide to fuels with water and/or hydrogen using solar energy and beyond. Coord Chem Rev 257:171–186
133. Foster NR (1985) Direct catalytic-oxidation of methane to methanol—a review. Appl Catal 19:1–11
134. Gesser HD, Hunter NR, Prakash CB (1985) The direct conversion of methane to methanol by controlled oxidation. Chem Rev 85:235–244
135. Xuan J, Leung MKH, Leung DYC, Ni M (2009) A review of biomass-derived fuel processors for fuel cell systems. Renew Sust Energ Rev 13:1301–1313
136. Badwal SPS, Giddey S, Kulkarni A, Goel J, Basu S (2015) Direct ethanol fuel cells for transport and stationary applications—a comprehensive review. Appl Energy 145:80–103
137. Sanchez OJ, Cardona CA (2008) Trends in biotechnological production of fuel ethanol from different feedstocks. Bioresour Technol 99:5270–5295
138. Olah GA, Goeppert A, Prakash GKS (2009) Methanol and dimethyl ether as fuels and energy carriers. In: Olah GA, Goeppert A, Surya Prakash GK (eds) Beyond oil and gas: the methanol economy. Wiley-VCH Verlag GmbH & Co. KGaA, Weinheim, pp 185–231
139. Avgouropoulos G, Ioannides T, Kallitsis JK, Neophytides S (2011) Development of an internal reforming alcohol fuel cell: concept, challenges and opportunities. Chem Eng J 176–177:95–101
140. Apanel G, Johnson E (2004) Direct methanol fuel cells—ready to go commercial? Fuel Cells Bull 2004:12–17
141. Liu H, Zhang J (2009) Electrocatalysis of direct methanol fuel cells: from fundamentals to application. Wiley-VCH Verlag GmbH & Co. KGaA, Weinheim, p 582
142. Tominaka S, Ohta S, Obata H, Momma T, Osaka T (2008) On-chip fuel cell: micro direct methanol fuel cell of an air-breathing, membraneless, and monolithic design. J Am Chem Soc 130:10456–10457
143. Lamy C, Leger J-M, Srinivasan S (2001) Direct methanol fuel cells: from a 20th century electrochemist's dream to a 21st century emerging technology. In: Bockris JO, Conway BE, White RE

(eds) Modern aspects of electrochemistry, vol 34. Kluwer Academic Publishers, New York, p 53
144. Wang H, Jusys Z, Behm RJ (2006) Ethanol electrooxidation on carbon-supported Pt, PtRu and Pt3Sn catalysts: a quantitative DEMS study. J Power Sources 154:351–359
145. Sarma LS, Taufany F, Hwang B-J (2009) Electrocatalyst Characterization and Activity validation—fundamentals and methods. In: Liu H, Zhang J (eds) Electrocatalysis of direct methanol fuel cells. Wiley-VCH Verlag GmbH & Co. KGaA, Weinheim, pp 115–163
146. Ling J, Longtin G, Savadogo O (2009) Comparison of ethanol and methanol crossover through different MEA components and structures by cyclic voltammetry. Asia Pac J Chem Eng 4:25–32
147. Ahmed M, Dincer I (2011) A review on methanol crossover in direct methanol fuel cells: challenges and achievements. Int J Energy Res 35:1213–1228
148. Kamarudin SK, Achmad F, Daud WRW (2009) Overview on the application of direct methanol fuel cell (DMFC) for portable electronic devices. Int J Hydrog Energy 34:6902–6916
149. Pereira JP, Falcão DS, Oliveira VB, Pinto AMFR (2014) Performance of a passive direct ethanol fuel cell. J Power Sources 256:14–19
150. Ge J, Liu H (2005) Experimental studies of a direct methanol fuel cell. J Power Sources 142:56–69
151. Narayanan SR, Kindler A, Jeffries-Nakamura B, Chun W, Frank H, Smart M, Valdez TI, Surampudi S, Halpert G, Kosek J, Cropley C (1996) Recent advances in PEM liquid-feed direct methanol fuel cells. In: Battery Conference on Applications and Advances, 1996, Eleventh Annual, 9–12 Jan 1996, pp 113–122
152. Oedegaard A, Hentschel C (2006) Characterisation of a portable DMFC stack and a methanol-feeding concept. J Power Sources 158:177–187
153. Herrero E, Chrzanowski W, Wieckowski A (1995) Dual path mechanism in methanol electrooxidation on a platinum-electrode. J Phys Chem 99:10423–10424
154. Batista EA, Malpass GRP, Motheo AJ, Iwasita T (2003) New insight into the pathways of methanol oxidation. Electrochem Commun 5:843–846
155. Batista EA, Malpass GRP, Motheo AJ, Iwasita T (2004) New mechanistic aspects of methanol oxidation. J Electroanal Chem 571:273–282
156. Cao D, Lu GQ, Wieckowski A, Wasileski SA, Neurock M (2005) Mechanisms of methanol decomposition on platinum: a combined experimental and ab initio approach. J Phys Chem B 109:11622–11633
157. Cohen JL, Volpe DJ, Abruna HD (2007) Electrochemical determination of activation energies for methanol oxidation on polycrystalline platinum in acidic and alkaline electrolytes. Phys Chem Chem Phys 9:49–77
158. Neurock M, Janik M, Wieckowski A (2009) A first principles comparison of the mechanism and site requirements for the electrocatalytic oxidation of methanol and formic acid over Pt. Faraday Discuss 140:363–378
159. Beden B, Lamy C, Bewick A, Kunimatsu K (1981) Electrosorption of methanol on a platinum electrode. IR spectroscopic evidence for adsorbed co species. J Electroanal Chem Interfacial Electrochem 121:343–347
160. Iwasita T, Nart FC, Vielstich W (1990) An FTIR study of the catalytic activity of a 85:15 platinum-ruthenium alloy for methanol oxidation. Ber Bunsen Ges 94:1030–1034
161. McBreen J, Mukerjee S (1995) In situ x-ray absorption studies of a Pt-Ru electrocatalyst. J Electrochem Soc 142:3399–3404
162. Mukerjee S, McBreen J (1997) Electrocatalysis of methanol and CO oxidation: an in situ XAS study. Proc—Electrochem Soc 97–13:36–51
163. Mukerjee S, McBreen J (1997) Effect of Ru and Sn additions to Pt on the electrocatalysis of methanol oxidation: an in-situ XAS investigation. In: New Materials for Fuel Cell and Modern Battery Systems II, Proceedings of the International Symposium on New Materials for Fuel Cell and Modern Battery Systems, 2nd, Montreal, July 6–10, 1997, pp 548–559
164. Krausa M, Vielstich W (1994) Study of the electrocatalytic influence of Pt/Ru and Ru on the oxidation of residues of small organic molecules. J Electroanal Chem 379:307–314
165. Frelink T, Visscher W, van Veen JAR (1995) On the role of Ru and Sn as promotors of methanol electrooxidation over Pt. Surf Sci 335:353–360
166. Buatier de Mongeot F, Scherer M, Gleich B, Kopatzki E, Behm RJ (1998) CO adsorption and oxidation on bimetallic Pt/Ru(0001) surfaces—a combined STM and TPD/TPR study. Surf Sci 411:249–262
167. Watanabe M, Zhu YM, Igarashi H, Uchida H (2000) Mechanism of CO tolerance at Pt-alloy anode catalysts for polymer electrolyte fuel cells. Electrochemistry 68:244–251
168. Camara GA, Giz MJ, Paganin VA, Ticianelli EA (2002) Correlation of electrochemical and physical properties of PtRu alloy electrocatalysts for PEM fuel cells. J Electroanal Chem 537:21–29
169. Liu P, Logadottir A, Nørskov JK (2003) Modeling the electro-oxidation of CO and H2/CO on Pt, Ru, PtRu and Pt3Sn. Electrochim Acta 48:3731–3742
170. Watanabe M, Uchida M, Motoo S (1987) Preparation of highly dispersed Pt + Ru alloy clusters and the activity for the electrooxidation of methanol. J Electroanal Chem 229:395–406
171. Ye S (2008) CO-tolerant catalysts. In: Zhang J (ed) PEM fuel cell electrocatalysts and catalyst layers: fundamentals and applications. Springer, London, pp 759–834

172. Gasteiger HA, Markovic N, Ross PN, Cairns EJ (1993) Methanol electrooxidation on well-characterized platinum-ruthenium bulk alloys. J Phys Chem 97:12020–12029
173. Yuan D, Gong X, Wu R (2008) Decomposition pathways of methanol on the PtAu(111) bimetallic surface: A first-principles study. J Chem Phys 128:5
174. Zhang XT, Wang H, Key JL, Linkov V, Ji S, Wang XL, Lei ZQ, Wang RF (2012) Strain effect of Core-Shell Co@Pt/C nanoparticle catalyst with enhanced electrocatalytic activity for methanol oxidation. J Electrochem Soc 159:B270–B276
175. Strasser P, Koh S, Anniyev T, Greeley J, More K, Yu C, Liu Z, Kaya S, Nordlund D, Ogasawara H, Toney MF, Nilsson A (2010) Lattice-strain control of the activity in dealloyed core-shell fuel cell catalysts. Nat Chem 2:454–460
176. Schlapka A, Lischka M, Gross A, Kasberger U, Jakob P (2003) Surface strain versus substrate interaction in heteroepitaxial metal layers: Pt on Ru (0001). Phys Rev Lett 91:016101
177. Camara GA, Iwasita T (2005) Parallel pathways of ethanol oxidation: the effect of ethanol concentration. J Electroanal Chem 578:315–321
178. Wang H, Abruña HD (2011) Electrocatalysis of direct alcohol fuel cells: quantitative DEMS studies. In: Bocarsly A, Mingos PDM (eds) Fuel cells and hydrogen storage. Springer, Berlin, pp 33–83
179. Lamy C, Coutanceau C, Leger J-M (2009) The direct ethanol fuel cell: a challenge to convert bioethanol cleanly into electric energy. In: Barbaro P, Bianchini C (eds) Catalysis for sustainable energy production. Wiley-VCH Verlag GmbH & Co. KGaA, Weinheim, pp 1–46
180. Antolini E (2007) Catalysts for direct ethanol fuel cells. J Power Sources 170:1–12
181. Tilak BV, Conway BE, Angerstein-Kozlowska H (1973) The real condition of oxidized pt electrodes: part III. Kinetic theory of formation and reduction of surface oxides. J Electroanal Chem 48:1–23
182. Li N-H, Sun S-G, Chen S-P (1997) Studies on the role of oxidation states of the platinum surface in electrocatalytic oxidation of small primary alcohols. J Electroanal Chem 430:57–67
183. Rousseau S, Coutanceau C, Lamy C, Leger JM (2006) Direct ethanol fuel cell (DEFC): electrical performances and reaction products distribution under operating conditions with different platinum-based anodes. J Power Sources 158:18–24
184. Alcala R, Shabaker JW, Huber GW, Sanchez-Castillo MA, Dumesic JA (2005) Experimental and DFT studies of the conversion of ethanol and acetic acid on PtSn-based catalysts. J Phys Chem B 109:2074–2085
185. Chu D, Gilman S (1996) Methanol electro-oxidation on unsupported Pt-Ru alloys at different temperatures. J Electrochem Soc 143:1685–1690
186. Park K-W, Choi J-H, Ahn K-S, Sung Y-E (2004) PtRu Alloy and PtRu-WO3 nanocomposite electrodes for methanol electrooxidation fabricated by a sputtering deposition method. J Phys Chem B 108:5989–5994
187. Gasteiger HA, Markovic N, Ross JPN, Cairns EJ (1994) Temperature-dependent methanol electro-oxidation on well-characterized Pt-Ru alloys. J Electrochem Soc 141:1795–1803
188. Jusys Z, Kaiser J, Behm RJ (2002) Composition and activity of high surface area PtRu catalysts towards adsorbed CO and methanol electrooxidation—: a DEMS study. Electrochim Acta 47:3693–3706
189. Lu C, Rice C, Masel RI, Babu PK, Waszczuk P, Kim HS, Oldfield E, Wieckowski A (2002) UHV, electrochemical NMR, and electrochemical studies of platinum/ruthenium fuel cell catalysts. J Phys Chem B 106:9581–9589
190. Yang H, Yang Y, Zou S (2007) In situ surface-enhanced raman spectroscopic studies of co adsorption and methanol oxidation on Ru-modified Pt surfaces. J Phys Chem C 111:19058–19065
191. Alayoglu S, Nilekar AU, Mavrikakis M, Eichhorn B (2008) Ru-Pt core-shell nanoparticles for preferential oxidation of carbon monoxide in hydrogen. Nat Mater 7:333–338
192. Piela P, Eickes C, Brosha E, Garzon F, Zelenay P (2004) Ruthenium crossover in direct methanol fuel cell with Pt-Ru black anode. J Electrochem Soc 151: A2053–A2059
193. Zelenay P (2006) Performance durability of direct methanol fuel cells. ECS Trans 1:483–495
194. Sarma LS, Chen C-H, Wang G-R, Hsueh K-L, Huang C-P, Sheu H-S, Liu D-G, Lee J-F, Hwang B-J (2007) Investigations of direct methanol fuel cell (DMFC) fading mechanisms. J Power Sources 167:358–365
195. Chung Y, Pak C, Park G-S, Jeon WS, Kim J-R, Lee Y, Chang H, Seung D (2008) Understanding a degradation mechanism of direct methanol fuel cell using TOF-SIMS and XPS. J Phys Chem C 112:313–318
196. Gancs L, Hakim N, Hult B, Mukerjee S (2006) Dissolution of Ru from PtRu electrocatalysts and its consequences in DMFCs. ECS Trans 3:607–618
197. Antolini E (2011) The problem of Ru dissolution from Pt-Ru catalysts during fuel cell operation: analysis and solutions. J Solid State Electrochem 15:455–472
198. Pourbaix M (1974) Atlas of electrochemical equilibria in aqueous solutions. National Association of Corrosion Engineers, Houston, pp 343–349
199. Gonzalez MJ, Hable CT, Wrighton MS (1998) Electrocatalytic oxidation of small carbohydrate fuels at Pt-Sn modified electrodes. J Phys Chem B 102:9881–9890
200. Honma I, Toda T (2003) Temperature dependence of kinetics of methanol electro-oxidation on PtSn alloys. J Electrochem Soc 150:A1689–A1692
201. Schmidt TJ, Gasteiger HA, Behm RJ (1999) Electro-oxidation of H-2 and CO/H-2-mixtures on a carbon-

supported Pt3Sn catalyst. J New Mater Electrochem Syst 2:27–32
202. Antolini E, Salgado JRC, Gonzalez ER (2006) The methanol oxidation reaction on platinum alloys with the first row transition metals: the case of Pt-Co and -Ni alloy electrocatalysts for DMFCs: a short review. Appl Catal B Environ 63:137–149
203. Wang Z-C, Ma Z-M, Li H-L (2008) Functional multi-walled carbon nanotube/polysiloxane composite films as supports of PtNi alloy nanoparticles for methanol electro-oxidation. Appl Surf Sci 254:6521–6526
204. Park K-W, Choi J-H, Kwon B-K, Lee S-A, Sung Y-E, Ha H-Y, Hong S-A, Kim H, Wieckowski A (2002) Chemical and electronic effects of Ni in Pt/Ni and Pt/Ru/Ni alloy nanoparticles in methanol electrooxidation. J Phys Chem B 106:1869–1877
205. Tsaprailis H, Birss VI (2004) Sol-gel derived Pt-Ir mixed catalysts for DMFC applications. Electrochem Solid-State Lett 7:A348–A352
206. Lee K-S, Yoo SJ, Ahn D, Jeon T-Y, Choi KH, Park I-S, Sung Y-E (2011) Surface structures and electrochemical activities of Pt overlayers on Ir nanoparticles. Langmuir 27:3128–3137
207. Holt-Hindle P, Yi Q, Wu G, Koczkur K, Chen A (2008) Electrocatalytic activity of nanoporous Pt-Ir materials toward methanol oxidation and oxygen reduction. J Electrochem Soc 155:K5–K9
208. Aramata A, Kodera T, Masuda M (1988) Electrooxidation of methanol on platinum bonded to the solid polymer electrolyte, Nafion. J Appl Electrochem 18:577–582
209. Ioroi T, Yasuda K (2005) Platinum-iridium alloys as oxygen reduction electrocatalysts for polymer electrolyte fuel cells. J Electrochem Soc 152:A1917–A1924
210. Wang Y, Toshima N (1997) Preparation of Pd-Pt bimetallic colloids with controllable core/shell structures. J Phys Chem B 101:5301–5306
211. Zhou SH, Varughese B, Eichhorn B, Jackson G, McIlwrath K (2005) Pt-Cu core-shell and alloy nanoparticles for heterogeneous NOx, reduction: anomalous stability and reactivity of a core-shell nanostructure. Angew Chem Int Ed 44: 4539–4543
212. Alayoglu S, Eichhorn B (2008) Rh-Pt bimetallic catalysts: synthesis, characterization, and catalysis of core-shell, alloy, and monometallic nanoparticles. J Am Chem Soc 130:17479–17486
213. El Sawy EN, El-Sayed HA, Birss VI (2014) Novel electrochemical fingerprinting methods for the precise determination of Pt shell coverage on Rucore nanoparticles. Chem Commun 50:11558–11561
214. El Sawy EN, El-Sayed HA, Birss VI (2015) Clarifying the role of Ru in methanol oxidation at Rucore@Ptshell nanoparticles. Phys Chem Chem Phys 17:27509–27519
215. Luo J, Wang L, Mott D, Njoki PN, Lin Y, He T, Xu Z, Wanjana BN, Lim IIS, Zhong CJ (2008) Core/shell nanoparticles as electrocatalysts for fuel cell reactions. Adv Mater 20:4342–4347
216. Alayoglu S, Zavalij P, Eichhorn B, Wang Q, Frenkel AI, Chupas P (2009) Structural and architectural evaluation of bimetallic nanoparticles: a case study of Pt-Ru core-shell and alloy nanoparticles. ACS Nano 3:3127–3137
217. Nilekar AU, Alayoglu S, Eichhorn B, Mavrikakis M (2010) Preferential CO oxidation in hydrogen: reactivity of core-shell nanoparticles. J Am Chem Soc 132:7418–7428
218. Yang L, Chen J, Zhong X, Cui K, Xu Y, Kuang Y (2007) Au@Pt nanoparticles prepared by one-phase protocol and their electrocatalytic properties for methanol oxidation. Colloids Surf A Physicochem Eng Asp 295:21–26
219. Fu XZ, Liang Y, Chen SP, Lin JD, Liao DW (2009) Pt-rich shell coated Ni nanoparticles as catalysts for methanol electro-oxidation in alkaline media. Catal Commun 10:1893–1897
220. Lu L, Shen L, Shi Y, Chen T, Jiang G, Ge C, Tang Y, Chen Y, Lu T (2012) New insights into enhanced electrocatalytic performance of carbon supported Pdâ€Cu catalyst for formic acid oxidation. Electrochim Acta 85:187–194
221. Wang R, Wang H, Wei B, Wang W, Lei Z (2010) Carbon supported Pt-shell modified PdCo-core with electrocatalyst for methanol oxidation. Int J Hydrog Energy 35:10081–10086
222. Chen T-Y, Lin T-L, Luo T-JM, Choi Y, Lee J-F (2010) Effects of Pt shell thicknesses on the atomic structure of Ru–Pt core–shell nanoparticles for methanol electrooxidation applications. ChemPhysChem 11:2383–2392
223. Bokach D, de la Fuente JLG, Tsypkin M, Ochal P, Endsjø IC, Tunold R, Sunde S, Seland F (2011) High-temperature electrochemical characterization of Ru core Pt shell fuel cell catalyst. Fuel Cells 11:735–744
224. Muthuswamy N, de la Fuente JLG, Tran DT, Walmsley J, Tsypkin M, Raaen S, Sunde S, Ronning M, Chen D (2013) Ru@Pt core-shell nanoparticles for methanol fuel cell catalyst: control and effects of shell composition. Int J Hydrog Energy 38:16631–16641
225. Hwang B-J, Sarma LS, Chen C-H, Bock C, Lai F-J, Chang S-H, Yen S-C, Liu D-G, Sheu H-S, Lee J-F (2008) Controlled synthesis and characterization of Ru core-Pt shell bimetallic nanoparticles. J Phys Chem C 112:19922–19929
226. Ochal P, Gomez de la Fuente JL, Tsypkin M, Seland F, Sunde S, Muthuswamy N, Ronning M, Chen D, Garcia S, Alayoglu S, Eichhorn B (2011) CO stripping as an electrochemical tool for characterization of Ru@Pt core-shell catalysts. J Electroanal Chem 655:140–146
227. Hofstead-Duffy AM, Chen D-J, Sun S-G, Tong YJ (2012) Origin of the current peak of negative scan in the cyclic voltammetry of methanol electro-

oxidation on Pt-based electrocatalysts: a revisit to the current ratio criterion. J Mater Chem 22:5205–5208
228. Hwang SJ, Yoo SJ, Jeon T-Y, Lee K-S, Lim T-H, Sung Y-E, Kim S-K (2010) Facile synthesis of highly active and stable Pt-Ir/C electrocatalysts for oxygen reduction and liquid fuel oxidation reaction. Chem Commun 46:8401–8403
229. El Sawy EN, Handal HT, Thangadurai V, Birss VI (2013) Pt-Ir nanoparticles with controlled composition as promising DMFC anode catalyst. Power Sources (under preparation)
230. El Sawy EN, Molero HM, Birss VI (2013) Electrodeposited Pt-Ir thin films as promising DMFC anode materials. Electrochimica Acta (EAST13-0480)
231. Yu X, Pickup PG (2008) Recent advances in direct formic acid fuel cells (DFAFC). J Power Sources 182:124–132
232. Rees NV, Compton RG (2011) Sustainable energy: a review of formic acid electrochemical fuel cells. J Solid State Electrochem 15:2095–2100
233. Cai W, Liang L, Zhang Y, Xing W, Liu C (2013) Real contribution of formic acid in direct formic acid fuel cell: investigation of origin and guiding for micro structure design. Int J Hydrog Energy 38:212–218
234. Rejal SZ, Masdar MS, Kamarudin SK (2014) A parametric study of the direct formic acid fuel cell (DFAFC) performance and fuel crossover. Int J Hydrog Energy 39:10267–10274
235. Jeong K-J, Miesse CM, Choi J-H, Lee J, Han J, Yoon SP, Nam SW, Lim T-H, Lee TG (2007) Fuel crossover in direct formic acid fuel cells. J Power Sources 168:119–125
236. Gao W, Keith JA, Anton J, Jacob T (2010) Theoretical elucidation of the competitive electro-oxidation mechanisms of formic acid on Pt(111). J Am Chem Soc 132:18377–18385
237. Xu J, Yuan D, Yang F, Mei D, Zhang Z, Chen Y-X (2013) On the mechanism of the direct pathway for formic acid oxidation at a Pt(111) electrode. Phys Chem Chem Phys 15:4367–4376
238. Jiang K, Zhang H-X, Zou S, Cai W-B (2014) Electrocatalysis of formic acid on palladium and platinum surfaces: from fundamental mechanisms to fuel cell applications. Phys Chem Chem Phys 16:20360–20376
239. Okamoto H, Kon W, Mukouyama Y (2005) Five current peaks in voltammograms for oxidations of formic acid, formaldehyde, and methanol on platinum. J Phys Chem B 109:15659–15666
240. Wang J-Y, Zhang H-X, Jiang K, Cai W-B (2011) From HCOOH to CO at Pd electrodes: a surface-enhanced infrared spectroscopy study. J Am Chem Soc 133:14876–14879
241. Obradovic MD, Gojkovic SL (2013) HCOOH oxidation on thin Pd layers on Au: self-poisoning by the subsequent reaction of the reaction product. Electrochim Acta 88:384–389
242. El Sawy EN, Khan MA, Pickup PG (2016) Factors affecting the spontaneous adsorption of Bi(III) onto Pt and PtRu nanoparticles. Appl Surf Sci 364:308–314
243. Perales-Rondon JV, Ferre-Vilaplana A, Feliu JM, Herrero E (2014) Oxidation mechanism of formic acid on the bismuth adatom-modified Pt(111) surface. J Am Chem Soc 136:13110–13113
244. Vidal-Iglesias FJ, López-Cudero A, Solla-Gullón J, Feliu JM (2013) Towards more active and stable electrocatalysts for formic acid electrooxidation: antimony-decorated octahedral platinum nanoparticles. Angew Chem Int Ed 52:964–967
245. Yuan Q, Zhou Z, Zhuang J, Wang X (2010) Pd-Pt random alloy nanocubes with tunable compositions and their enhanced electrocatalytic activities. Chem Commun 46:1491–1493
246. Fang P-P, Duan S, Lin X-D, Anema JR, Li J-F, Buriez O, Ding Y, Fan F-R, Wu D-Y, Ren B, Wang ZL, Amatore C, Tian Z-Q (2011) Tailoring Au-core Pd-shell Pt-cluster nanoparticles for enhanced electrocatalytic activity. Chem Sci 2:531–539
247. Ferre-Vilaplana A, Perales-Rondon JV, Feliu JM, Herrero E (2015) Understanding the effect of the adatoms in the formic acid oxidation mechanism on Pt(111) ELECTRODES. ACS Catal 5:645–654
248. Vielstich W, Yokokawa H, Gasteiger HA (2009) Handbook of fuel cells: fundamentals technology and applications. Wiley, Chichester
249. Chick LA, Marina OA, Coyle CA, Thomsen EC (2013) Effects of temperature and pressure on the performance of a solid oxide fuel cell running on steam reformate of kerosene. J Power Sources 236:341–349
250. Borglum B, Ghezel-Ayagh H (2013) Development of solid oxide fuel cells at versa power systems and FuelCell energy. ECS Trans 57:61–66
251. Blum L, Batfalsky P, de Haart L, Malzbender J, Menzler NH, Peters R, Quadakkers WJ, Remmel J, Tietz F, Stolten D (2013) Overview on the Jülich SOFC development status. ECS Trans 57:23–33
252. Wang SR, Zhan ZL, Wen TL (2013) Introduction of solid oxide fuel cell research in SICCAS. ECS Trans 57:35–41
253. Singhal SC, Kendall K (2003) High-temperature solid oxide fuel cells: fundamentals, design and applications. Elsevier, Oxford
254. Hanifi AR, Torabi A, Etsell TH, Yamarte L, Sarkar P (2011) Porous electrolyte-supported tubular micro-SOFC design. Solid State Ionics 192:368–371
255. Du YH, Sammes NM, Tompsett GA (2000) Optimisation parameters for the extrusion of thin YSZ tubes for SOFC electrolytes. J Eur Ceram Soc 20:959–965
256. Hui S, Yang D, Wang Z, Yick S, Deces-Petit C, Qu W, Tuck A, Maric R, Ghosh D (2007) Metal-supported solid oxide fuel cell operated at 400–600 °C. J Power Sources 167:336–339

257. Leah R, Bone A, Selcuk A, Corcoran D, Lankin M, Dehaney-Steven Z, Selby M, Whalen P (2011) Development of highly robust, volume-manufacturable metal-supported SOFCs for operation below 600 °C. ECS Trans 35:351–367
258. Tucker MC, Lau GY, Jacobson CP, DeJonghe LC, Visco SJ (2007) Performance of metal-supported SOFCs with infiltrated electrodes. J Power Sources 171:477–482
259. Bone A, Postlethwaite O, Leah R, Mukerjee S, Selby M (2016) Validation methodology and results from a ceres power steel cell technology platform. In: 12th European SOFC & SOE Forum, Lucerne/Switzerland 2016, 9–19
260. Christie GM, Huijsmans JPP (1997) State of the art SOFC component development at ECN. In: Proceedings of the Fifth International Symposium on Solid Oxide Fuel Cells (SOFC-V), vol 97, pp 718–726
261. Rotureau D, Viricelle JP, Pijolat C, Caillol N, Pijolat M (2005) Development of a planar SOFC device using screen-printing technology. J Eur Ceram Soc 25:2633–2636
262. Minh NQ (1993) Ceramic Fuel-Cells. J Am Ceram Soc 76:563–588
263. Smeacetto F, Salvo M, Ajitdoss LC, Perero S, Moskalewicz T, Boldrini S, Doubova L, Ferraris M (2010) Yttria-stabilized zirconia thin film electrolyte produced by RF sputtering for solid oxide fuel cell applications. Mater Lett 64:2450–2453
264. Jordan N, Assenmacher W, Uhlenbruck S, Haanappel VAC, Buchkremer HP, Stover D, Mader W (2008) Ce0.8Gd0.2O2-δ protecting layers manufactured by physical va or deposition for IT-SOFC. Solid State Ionics 16. In: Proceedings of the 16th International Conference on Solid State Ionics (SSI-16), Part I, 179, pp 919–923
265. Heiroth S, Lippert T, Wokaun A (2008) Microstructure and electrical conductivity of YSZ thin films prepared by pulsed laser deposition. Appl Phys A 93:639–643
266. Schlupp MVF, Prestat M, Martynczuk J, Rupp JLM, Bieberle-Hutter A, Gauckler LJ (2012) Thin film growth of yttria stabilized zirconia by aerosol assisted chemical vapor deposition. J Power Sources 202:47–55
267. Wang Z, Sun K, Shen S, Zhang N, Qiao J, Xu P (2008) Preparation of YSZ thin films for intermediate temperature solid oxide fuel cells by dip-coating method. J Membr Sci 320:500–504
268. Courtin E, Boy P, Rouhet C, Bianchi L, Bruneton E, Poirot N, Laberty-Robert C, Sanchez C (2012) Optimized sol-gel routes to synthesize yttria-stabilized zirconia thin films as solid electrolytes for solid oxide fuel cells. Chem Mater 24:4540–4548
269. Kesler O (2007) Plasma spray processing of solid oxide fuel cells. In: Materials science forum; Trans Tech Publ, pp 1385–1390
270. Sammes NM, Du Y (2007) Fabrication and characterization of tubular solid oxide fuel cells. Int J Appl Ceram Technol 4:89–102
271. Singhal SC (1999) Recent progress in tubular solid oxide fuel cell technology. In: Proceedings of the International Symposium on Solid Oxide Fuel Cells V, 1999; Electrochemical Society, Pennington, 1999, pp 37–50
272. Hanifi AR, Shinbine A, Etsell TH, Sarkar P (2012) Development of monolithic YSZ porous and dense layers through multiple slip casting for ceramic fuel cell applications. Int J Appl Ceram Technol 9:1011–1021
273. Panthi D, Choi B, Tsutsumi A (2015) Fabrication and evaluation of a micro-tubular solid oxide fuel cell with an inert support using scandia-stabilized zirconia electrolyte. J Electrochem Soc 162:F1555–F1560
274. Singhal SC (2000) Advances in solid oxide fuel cell technology. Solid State Ionics 135:305–313
275. Fergus JW (2006) Electrolytes for solid oxide fuel cells. J Power Sources 162:30–40
276. Nomura K, Mizutani Y, Kawai M, Nakamura Y, Yamamoto O (2000) Aging and Raman scattering study of scandia and yttria doped zirconia. Solid State Ionics 132:235–239
277. Wiik K, Schmidt CR, Faaland S, Shamsili S, Einarsrud MA, Grande T (1999) Reactions between strontium-substituted lanthanum manganite and yttria-stabilized zirconia: I. Powder samples. J Am Ceram Soc 82:721–728
278. Marina OA, Bagger C, Primdahl S, Mogensen M (1999) A solid oxide fuel cell with a gadolinia-doped ceria anode: preparation and performance. Solid State Ionics 123:199–208
279. Yahiro H, Eguchi K, Arai H (1989) Electrical properties and reducibilities of ceria-rare earth oxide systems and their application to solid oxide fuel cell. Solid State Ionics 36:71–75
280. Zhang X, Robertson M, Deces-Petit C, Qu W, Kesler O, Maric R, Ghosh D (2007) Internal shorting and fuel loss of a low temperature solid oxide fuel cell with SDC electrolyte. J Power Sources 164:668–677
281. Wang S, Kobayashi T, Dokiya M, Hashimoto T (2000) Electrical and ionic conductivity of Gd-doped Ceria. J Electrochem Soc 147:3606–3609
282. Kannan R, Singh K, Gill S, Furstenhaupt T, Thangadurai V (2013) Chemically stable proton conducting doped BaCeO3-no more fear to SOFC wastes. Sci Rep 3:2138–2142
283. Liu J, Birss V, Hill J (2010) Electrochemical performance and microstructure characterization of nickel yttrium-stabilized zirconia anode. AIChE J 56:1651–1658
284. Prakash BS, Kumar SS, Aruna ST (2014) Properties and development of Ni/YSZ as an anode material in

solid oxide fuel cell: a review. Renew Sust Energ Rev 36:149–179
285. Jiang SP, Chan SH (2004) A review of anode materials development in solid oxide fuel cells. J Mater Sci 39:4405–4439
286. Sarantaridis D, Atkinson A (2007) Redox cycling of Ni-based solid oxide fuel cell anodes: a review. Fuel Cells 7:246–258
287. Klemenso T, Mogensen M (2007) Ni/YSZ solid oxide fuel cell anode behavior upon redox cycling based on electrical characterization. J Am Ceram Soc 90:3582–3588
288. Young JL, Birss VI (2011) Crack severity in relation to non-homogeneous Ni oxidation in anode-supported solid oxide fuel cells. J Power Sources 196:7126–7135
289. Vedasri V, Young JL, Birss VI (2010) A possible solution to the mechanical degradation of Ni-yttria stabilized zirconia anode-supported solid oxide fuel cells due to redox cycling. J Power Sources 195:5534–5542
290. Young JL, Molero H, Birss VI (2014) The effect of pre-oxidation treatments on the oxidation tolerance of Ni-yttria-stabilized zirconia anodes in solid oxide fuel cells. J Power Sources 271:538–547
291. Cheng Z, Liu M (2007) Characterization of sulfur poisoning of Ni/YSZ anodes for solid oxide fuel cells using in situ Raman microspectroscopy. Solid State Ionics 178:925–935
292. Mirfakhraei B, Paulson S, Thangadurai V, Birss V (2013) Enhanced hydrogen oxidation activity and H2S tolerance of Ni-infiltrated ceria solid oxide fuel cell anodes. J Power Sources 243:95–101
293. Deleebeeck L, Shishkin M, Addo P, Paulson S, Molero H, Ziegler T, Birss V (2014) Activation of H2 oxidation at sulphur-exposed Ni surfaces under low temperature SOFC conditions. Phys Chem Chem Phys 16:9383–9393
294. Singh A, Paulson S, Hill JM, Birss V (2013) Beneficial effects of low ppm levels of H2S on the performance of Ni-YSZ SOFC anodes in syngas fuels. ECS Trans 57:1277–1287
295. Smith TR, Wood A, Birss VI (2009) Effect of hydrogen sulfide on the direct internal reforming of methane in solid oxide fuel cells. Appl Catal A Gen 354:1–7
296. Brett DJL, Atkinson A, Brandon NP, Skinner SJ (2008) Intermediate temperature solid oxide fuel cells. Chem Soc Rev 37:1568–1578
297. Gong M, Liu X, Trembly J, Johnson C (2007) Sulfur-tolerant anode materials for solid oxide fuel cell application. J Power Sources 168:289–298
298. Cowin PI, Petit CTG, Lan R, Irvine JTS, Tao S (2011) Recent progress in the development of anode materials for solid oxide fuel cells. Adv Energy Mater 1:314–332
299. Murray EP, Tsai T, Barnett SA (1999) A direct-methane fuel cell with a ceria-based anode. Nature 400:649–651
300. Gross MD, Vohs JM, Gorte RJ (2007) Recent progress in SOFC anodes for direct utilization of hydrocarbons. J Mater Chem 17:3071–3077
301. Flytzani-Stephanopoulos M, Sakbodin M, Wang Z (2006) Regenerative adsorption and removal of H2S from hot fuel gas streams by rare earth oxides. Science 312:1508–1510
302. Canales-Vazquez J s, Ruiz-Morales JC, Irvine JTS, Zhou W (2005) Sc-substituted oxygen excess titanates as fuel electrodes for SOFCs. J Electrochem Soc 152:A1458–A1465
303. Tsoga A, Gupta A, Naoumidis A, Nikolopoulos P (2000) Gadolinia-doped ceria and yttria stabilized zirconia interfaces: regarding their application for SOFC technology. Acta Mater 48:4709–4714
304. Marina OA, Canfield NL, Stevenson JW (2002) Thermal, electrical, and electrocatalytical properties of lanthanum-doped strontium titanate. Solid State Ionics 149:21–28
305. Hui S, Petric A (2001) Conductivity and stability of SrVO3 and mixed perovskites at low oxygen partial pressures. Solid State Ionics 143:275–283
306. Maffei N, de Silveira G (2003) Interfacial layers in tape cast anode-supported doped lanthanum gallate SOFC elements. Solid State Ionics 159:209–216
307. Tao S, Irvine JTS (2004) Synthesis and Characterization of (La0.75Sr0.25) Cr0.5Mn0.5 O3-δ, a redox-stable, efficient perovskite anode for SOFC. J Electrochem Soc 151:A252–A259
308. Yang L, Zuo C, Liu M (2010) High-performance anode-supported Solid Oxide Fuel Cells based on Ba(Zr0.1Ce0.7Y0.2)O3-δ (BZCY) fabricated by a modified co-pressing process. J Power Sources 195:1845–1848
309. Mirfakhraei B, Ramezanipour F, Paulson S, Birss V, Thangadurai V (2014) Effect of sintering temperature on microstructure, chemical stability, and electrical properties of transition metal or Yb-doped BaZr0.1Ce0.7Y0.1 M0.1O3-δ (M = Fe, Ni, Co, and b). Front Energy Res 2:9
310. Chen M, Paulson S, Thangadurai V, Birss V (2013) Sr-rich chromium ferrites as symmetrical solid oxide fuel cell electrodes. J Power Sources 236:68–79
311. Addo PK, Molero-Sanchez B, Buyukaksoy A, Paulson S, Birss V (2015) Sulfur tolerance of La0.3 M0.7Fe0.7Cr0.3O3-δ (M = Sr, Ca) solid oxide fuel cell anodes. ECS Trans 66:219–228
312. Huang YH, Dass RI, Xing ZL, Goodenough JB (2006) Double perovskites as anode materials for solid-oxide fuel cells. Science 312:254–257
313. Handal HT, Thangadurai V (2014) Electrochemical characterization of multi-element-doped ceria as potential anodes for SOFCs. Solid State Ionics 262:359–364
314. Deleebeeck L, Fournier JL, Birss V (2010) Comparison of Sr-doped and Sr-free La 1-x Sr x Mn 0.5 Cr 0.5 O 3 ± δ SOFC anode. Solid State Ionics 181:1229–1237

315. Neagu D, Tsekouras G, Miller DN, Menard H, Irvine JTS (2013) In situ growth of nanoparticles through control of non-stoichiometry. Nat Chem 5:916–923
316. Sun Y, Li J, Zeng Y, Amirkhiz BS, Wang M, Behnamian Y, Luo J (2015) A-site deficient perovskite: the parent for in situ exsolution of highly active, regenerable nano-particles as SOFC anodes. J Mater Chem A 3:11048–11056
317. Co AC, Birss VI (2006) Mechanistic analysis of the oxygen reduction reaction at (La, Sr) MnO3 cathodes in solid oxide fuel cells. J Phys Chem B 110:11299–11309
318. Ishihara T (2009) Perovskite oxide for solid oxide fuel cells. Springer, Dordrecht
319. Sun C, Hui R, Roller J (2009) Cathode materials for solid oxide fuel cells: a review. J Solid State Electrochem 14:1125–1144
320. Liu J, Co A (2006) C.; Paulson, S. and Birss, V. I., Oxygen reduction at sol-gel derived La 0.8 Sr 0.2 Co 0.8 Fe 0.2 O 3 cathodes. Solid State Ionics 177:377–387
321. Uhlenbruck S, Moskalewicz T, Jordan N, Penkalla HJ, Buchkremer HP (2009) Element interdiffusion at electrolyte-cathode interfaces in ceramic high-temperature fuel cells. Solid State Ionics 180:418–423
322. Mai A, Haanappel VAC, Tietz F, Stover D (2006) Ferrite-based perovskites as cathode materials for anode-supported solid oxide fuel cells: Part II. Influence of the CGO interlayer. Solid State Ionics 177:2103–2107
323. Shao Z, Haile SM (2004) A high-performance cathode for the next generation of solid-oxide fuel cells. Nature 431:170–173
324. Meng X, Lv S, Ji Y, Wei T, Zhang Y (2008) Characterization of Pr1-xSrxCo0.8Fe0.2O3-δ ($0.2 \leq x \leq 0.6$) cathode materials for intermediate-temperature solid oxide fuel cells. J Power Sources 183:581–585
325. Molero-Sanchez B, Prado-Gonjal J, Avila-Brande D, Chen M, Moran E, Birss V (2015) High performance La0.3Ca0.7Cr0.3Fe0.7O3-δ air electrode for reversi le solid oxide fuel cell applications. Int J Hydrog Energy 40:1902–1910
326. Chen M, Paulson S, Kan WH, Thangadurai V, Birss V (2015) Surface and bulk study of strontium-rich chromium ferrite oxide as a robust solid oxide fuel cell cathode. J Mater Chem A 3:22614–22626
327. Molero-Sanchez B, Prado-Gonjal J, Avila-Brande D, Birss V, Moran E (2015) Microwave-assisted synthesis and characterization of new cathodic material for solid oxide fuel cells: La0.3Ca0.7Fe0.7Cr0.3-δ. Ceram Int 41:8411–8416
328. Zhu WZ, Deevi SC (2003) Development of interconnect materials for solid oxide fuel cells. Mater Sci Eng A 348:227–243
329. Fergus JW (2004) Lanthanum chromite-based materials for solid oxide fuel cell interconnects. Solid State Ionics 171:1–15
330. Thyssenkrupp VDM (2010) Material Data Sheet No. 4046 for Crofer 22 APU. Jun-2006. Accessed 28 Feb 2011
331. Jose G-VM, Laurent L, Vladislav K, Harald F, del Mar J-LM (2005) Oxidation of potential SOFC interconnect materials, Crofer 22 APU and Avesta 353 MA, in dry and humid air studied in situ by X-ray diffraction. Mater High Temp 22:245–251
332. Gannon PE, Kayani A, Ramana CV, Deibert MC, Smith RJ, Gorokhovsky VI (2008) Simulated SOFC interconnect performance of crofer 22 APU with and without filtered arc CrAlON coatings. Electrochem Solid-State Lett 11:B54–B58
333. Wang K, Liu Y, Fergus JW (2011) Interactions between SOFC interconnect coating materials and chromia. J Am Ceram Soc 94:4490–4495
334. Yang Z, Xia G-G, Maupin GD, Stevenson JW (2006) Conductive protection layers on oxidation resistant alloys for SOFC interconnect applications. Surf Coat Technol 201:4476–4483
335. Chen X, Hou PY, Jacobson CP, Visco SJ, De Jonghe LC (2005) Protective coating on stainless steel interconnect for SOFCs: oxidation kinetics and electrical properties. Solid State Ionics 176:425–433
336. Yang Z, Xia G, Simner SP, Stevenson JW (2005) Thermal growth and performance of manganese cobaltite spinel protection layers on ferritic stainless steel SOFC interconnects. J Electrochem Soc 152: A1896–A1901
337. Petric A, Huang P, Tietz F (2000) Evaluation of La-Sr-Co-Fe-O perovskites for solid oxide fuel cells and gas separation membranes. Solid State Ionics 135:719–725
338. Gorelov VP, Bronin DI, Sokolova JV, Näfe H, Aldinger F (2001) The effect of doping and processing conditions on properties of La1-xSrxGa1-yMgyO3-α. J Eur Ceram Soc 21:2311–2317
339. Shao Z, Zhou W, Zhu Z (2012) Advanced synthesis of materials for intermediate-temperature solid oxide fuel cells. Prog Mater Sci 57:804–874
340. Bansal NP, Zhong Z (2006) Combustion synthesis of Sm0.5Sr0.5CoO3-x and La0.6Sr0.4CoO3-x nanopowders for solid oxide fuel cell cathodes. J Power Sources 158:148–153
341. Fu Y-P, Wen S-B, Lu C-H (2008) Preparation and characterization of samaria-doped ceria electrolyte materials for solid oxide fuel cells. J Am Ceram Soc 91:127–131
342. Celerier, Laberty C, Ansart F, Lenormand P, Stevens P (2006) New chemical route based on sol-gel process for the synthesis of oxyapatite La9.33Si6O26. Ceram Int 32:271–276
343. Wang JX, Tao YK, Shao J, Wang WG (2009) Synthesis and properties of (La0.75Sr0.25) 0.95MnO3 ± δ nano-powder prepared via Pechini route. J Power Sources 186:344–348
344. Dikmen S, Shuk P, Greenblatt M, Gocmez H (2002) Hydrothermal synthesis and properties of Ce 1 − x

Gd x O 2 − δ solid solutions. Solid State Sci 4:585–590
345. Sholklapper TZ, Kurokawa H, Jacobson CP, Visco SJ, De Jonghe LC (2007) Nanostructured solid oxide fuel cell electrodes. Nano Lett 7:2136–2141
346. Keyvanfar P, Birss V (2014) Optimization of infiltration techniques used to construct Ni/YSZ anodes. J Electrochem Soc 161:F660–F667
347. Torrell M, Hernández E, Slodczyk A, Morata A, Tarancon A (2016) Characterization of solid oxide electrolyser cells nanocomposite electrodes based on mesoporous ceramic scaffolds infiltration. In: 12th European SOFC & SOE Forum, Lucerne/Switzerland, pp 44–53
348. Ouyang MBP, Brandon NP (2016) Controlling TPB length through calcination temperature, and its influence on the microstructure and electrochemical performance of Ni infiltrated CGO anodes. In: 12th European SOFC & SOE Forum, Lucerne/Switzerland, pp 191–199
349. Keyvanfar P, Hanifi AR, Sarkar P, Etsell TH, Birss V (2015) Enhancing the stability of infiltrated Ni/YSZ anodes. ECS Trans 68:1255–1263
350. Buyukaksoy A, Petrovsky V, Dogan F (2012) Stability and performance of solid oxide fuel cells with nanocomposite electrodes. J Electrochem Soc 159: B666–B669
351. Gorte RJ, Vohs JM (2009) Nanostructured anodes for solid oxide fuel cells. Curr Opin Colloid Interface Sci 14:236–244
352. Busawon AN, Sarantaridis D, Atkinson A (2008) Ni infiltration as a possible solution to the redox problem of SOFC anodes. Electrochem Solid-State Lett 11:B186–B189
353. Kurokawa H, Sholklapper TZ, Jacobson CP, De Jonghe LC, Visco SJ (2007) Ceria nanocoating for sulfur tolerant Ni-based anodes of solid oxide fuel cells. Electrochem Solid-State Lett 10:B135–B138
354. Kim G, Lee S, Shin JY, Corre G, Irvine JTS, Vohs JM, Gorte RJ (2009) Investigation of the structural and catalytic requirements for high-performance SOFC anodes formed by infiltration of LSCM. Electrochem Solid-State Lett 12:B48–B52
355. Lee S, Kim G, Vohs JM, Gorte RJ (2008) SOFC anodes based on infiltration of La0.3Sr0.7TiO3. J Electrochem Soc 155:B1179–B1183
356. Huang Y, Vohs JM, Gorte RJ (2006) SOFC cathodes prepared by infiltration with various LSM precursors. Electrochem Solid-State Lett 9:A237–A240
357. Shah M, Voorhees PW, Barnett SA (2011) Time-dependent performance changes in LSCF-infiltrated SOFC cathodes: the role of nano-particle coarsening. Solid State Ionics 187:64–67
358. Nicholas JD, Barnett SA (2010) Measurements and modeling of Sm0. 5Sr0. 5CoO3-x-Ce0. 9Gd0. 1O1 95 SOFC cathodes produced using infiltrate solution additives. J Electrochem Soc 157:B536–B541
359. Haanappel VAC, Rutenbeck D, Mai A, Uhlenbruck S, Sebold D, Wesemeyer H, Rowekamp B, Tropartz C, Tietz F (2004) The influence of noble-metal-containing cathodes on the electrochemical performance of anode-supported SOFCs. J Power Sources 130:119–128
360. Buyukaksoy A, Petrovsky V, Dogan F (2011) Redox stable solid oxide fuel cells with Ni-YSZ cermet anodes prepared by polymeric precursor infiltration. J Electrochem Soc 159:B232–B234
361. Singh CA, Bansal L, Tiwari P, Krishnan VV (2009) Strong metal support interactions of infiltrated Ni with TiO2 in a porous YSZ anode matrix-A possible method for Ni-stabilization. ECS Trans 25:1897–1904
362. Farooque M (2015) WIREs Energy Environ 4:178–188
363. Mehmeti A, Santoni F, Della Pietra M, McPhail SJ (2016) Life cycle assessment of molten carbonate fuel cellls: state of the art and strategies for the future. J Power Sources 308:97–108
364. Frangini S (2010) Celle a combustibile a carbonati fusi per la cattura di CO2 da gas combusti: prospettive e limiti di applicazione in settori industriali soggetti alla direttiva EU-ETS
365. Moreno A, McPhail SJ, Bove R (2008) International status of molten carbonate fuel cell (MCFC) technology
366. Au SF, McPhail SJ, Woudstra N, Hemmes K (2003) The influence of operating temperature on the efficiency of a combined heat and power fuel cell plant. J Power Sources 122:37–46
367. Krause TR, Ahmed S, Kumar R (2006) ASME 2006 Fourth International Conference on Fuel Cell Science, Engineering and Technology, Parts A and B, Irvine, California, USA, ASME Proceedings. Irvine, California, USA, June 19–21, pp 787–792
368. Xuan J, MKH L, DYC L, Ni M (2009) Renew Sust Energ Rev 13:1301–1313
369. Clarke SH, Dicks AL, Pointon K, Smith TA, Swann A (1997) Catal Today 38:411–423
370. Raissi AT, Banerjee A, Sheinkopf KG (1953) IEEE Proceedings of the 1997 32nd Intersociety Energy Conversion Engineering Conference, 3/4
371. Antolini E (2013) The stability of LiAlO2 powders and electrolyte matrices in molten carbonate fuel cell environment. Ceram Int 39:3463–3478
372. Maru HC, Marianowski LG (1976) Composite model of electrode electrolyte pore structure. In: Extended abstracts, vol 76-2. Fall Meeting of the Electrochemical Society, Las Vegas, NV, p 82. 17–22 Oct, 1976, Abstract No. 31
373. Mekhilef S, Saidur R, Safari A (2012) Comparative study of different fuel cell technologies. Renew Sust Energ Rev 16:981–989
374. Mustafa K, Anwar M, Rana MA, Khan ZS (2015) Development of cobalt doped lithiated NiO nanocomposites and hot corrosion testing of LiAlO2

matrices for molten carbonate fuel cell applications. Mater Chem Phys 164:198–205
375. Cheng J, Guo L, Xu S, Zhang R (2014) The optimization of matrix preparation process and performance testing for molten carbonate fuel cell. J Chem 2014:7
376. Lin H, Zhou L, Zhang H (2007) Sintering mechanisms of porous matrix for molten carbonate fuel cell. J Inorg Mater 22:759–764
377. Huijsmans JPP, Kraaij CJ, Makkus RC, Rietveld G, Sitters EF, Reijers HTJ (2000) An analysis of endurance issues for MCFC. J Power Sources 86:117–121
378. Sotouchi H, Watanabe Y, Kobayashi T, Murai M (1992) Mechanism of crystal growth of lithium aluminate particles in molten lithium and potassium carbonates. J Electrochem Soc 139:1127–1130
379. Terada S, Nagashima I, Higaki K, Ito Y (1998) Stability of LiAlO2 as electrolyte matrix for molten carbonate fuel cells. J Power Sources 75:223–229
380. Morita H, Kawase M, Mugikura Y, Asano K (2010) J Power Sources 195:6988–6996
381. Mitsushima S, Matsuzawa K, Kamiya N, Ota KI (2002) Improvement of MCFC cathode stability by additives. Electrochim Acta 47:2823–2830
382. Arendt RM, Curran J (1980) Process of making electrolyte structure for molten carbonate fuel cells. US Patent 4,216,278
383. Bushnell CL, Bregoli LJ, Schroll CR. Electrolyte matrix for molten carbonate fuel cells. US Patent 4,322,482
384. Frangini S, Scaccia S (2014) The role of foreign cations in enhancing the oxygen solubility properties of alkali molten carbonate systems: brief survey of existing data and new results. Int J Hydrog Energy 39:12266–12272
385. Gong Y, Li X, Zhang L, Tharp W, Qin C, Huang K (2013) Molten carbonates as an effective oxygen reduction catalyst for 550 to 650 °C solid oxide fuel cells. J Electrochem Soc 160:F958–F964
386. Frangini S, Scaccia S (2013) Thermal stability and oxidizing properties of mixed alkaline earth-alkali molten carbonates: a focus on the lithium-sodium carbonate eutectic system with magnesium additions. Thermochim Acta 574:55–62
387. Griffiths TR, Volkovic VA, Carper WR (2009) The structures of active intermediates in catalyst-enhanced molten salt oxidation and a new method for the complete destruction chemical warfare arsenals. Struct Chem 21:291–297
388. Hilmi A, Yuh Y, Farooque M (2014) Carbonate fuel cell anode: a review. ECS Trans 61:245–253
389. Hilmi J, Yuh C, Farooque M (2012) US Patent 8,163,437
390. Xie G, Ema GK, Ito Y (1994) J Appl Electrochem 24:360
391. Kim Y, Lee K, Chum H (2001) J Power Sources 99:26
392. Wee J (2006) Materials Chemistry and Physics 98:273
393. Wee J, Lee KY (2006) J Mater Sci 41:3585
394. Sanchez D, Ubertini S, Munoz de Escalona JM, Chacartegui R (2014) Int J Hydrog Energy 39:4081–4088
395. Mugikura Y, Asano K (2002) Performance of several types of fuel cells and factor analysis of performance. Electr Eng Jpn 138:885–892
396. Nguyen QM (1988) Technological status of Nickel oxide cathodes in molten carbonate fuel cells. J Power Sources 24:1–19
397. Hong MZ, Bae SC, Lee HS, Lee HC, Kim YM, Kim K (2003) Electrochim Acta 48:4213–4221
398. Wijayasinghe A, Lagergren C, Bergman B (2002) Fuel Cells 2:181–188
399. Huang B, Li F, Chen G, Zhao BY, Hu KA (2004) Mater Res Bull 39:1359–1366
400. Huang CM, Yuh C (1999) Electrolyte matrix for molten carbonate fuel cells. US Patent 5,869,203
401. Lee I, Kim W, Moon Y, Lim H, Lee D (2001) Influence of aluminum salt addition on in situ sintering of electrolyte matrices for molten carbonate fuel cells. J Power Sources 101:90–95
402. Doyon JD (1996) Fuel cell anode and fuel cell. US Patent 5,558,948
403. Guo L, Calo JM, DiCocco E, Bain EJ (2013) Development of a low temperature, molten hydroxide direct carbon fuel cell. Energy Fuel 27:1712–1719
404. Vu DL, Lee CG (2016) Korean J Chem Eng 33:1606–1611
405. Watanabe H, Furuyama T, Okazaki K (2016) J Chem Eng Jpn 49:237–242
406. Guoyang Liu, A. Z., Jieshan Qiu, Yating Zhang, Jiangtao Cai, Yongqiang Dang, J Hydrogen Energy Int 2016, 41, 8576–8582.
407. Duan NQ, Tan Y, Yan D, Jia L, Chi B, Pu J, Li J (2016) Appl Energy 165:983–989
408. Giddey S, Badwal SPS, Kulkarni A, Munnings C (2012) Prog Energy Combust Sci 38:360–399
409. Rady AC, Giddey S, Kulkarni A, Badwal SPS, Bhattacharya S (2016) Fuel 180:270–277
410. Zelenay P (2012) Fuel cells for portable power 1. Introduction to DMFCs; 2. Advanced materials and concepts for portable power fuel cells. Los Alamos National Laboratory Los Alamos
411. Mai A, Schuler JA, Fleischhauer F, Nerlich V, Schuler A (2015) Hexis and the SOFC system Galileo 1000 N: experiences from lab and field testing. ECS Trans 68:109–116
412. White BM, Lundberg WL, Pierre JF (2015) Accomplishments, status, and road map for the US Department of Energy's Fossil Energy SOFC Program. ECS Trans 68:23–38
413. Wachsman ED, Singhal SC (2010) Solid oxide fuel cell commercialization, research and challenges. Am Ceram Soc Bull 89:22–32